Dual Principal Component Pursuit

Manolis C. Tsakiris and René Vidal M.TSAKIRIS,RVIDAL@JHU.EDU
CENTER FOR IMAGING SCIENCE
JOHNS HOPKINS UNIVERSITY
BALTIMORE, MD, 21218, USA

Editor: TBD

Abstract

We consider the problem of outlier rejection in single subspace learning. Classical approaches work with a direct representation of the subspace, and are thus efficient when the subspace dimension is small. Our approach works with a dual representation of the subspace and hence aims to find its orthogonal complement; as such it is particularly suitable for high-dimensional subspaces. We pose the problem of computing normal vectors to the subspace as a non-convex ℓ_1 minimization problem on the sphere, which we call Dual Principal Component Pursuit (DPCP). We provide theoretical guarantees, under which every global solution of DPCP is a vector in the orthogonal complement of the inlier subspace. Moreover, we relax the non-convex DPCP problem to a recursion of linear programming problems, which, as we show, converges in a finite number of steps to a vector orthogonal to the subspace. In particular, when the inlier subspace is a hyperplane, then the linear programming recursion converges in a finite number of steps to the global minimum of the non-convex DPCP problem. We propose algorithms based on alternating minimization and Iteratively Reweighted Least-Squares, that are suitable for dealing with large-scale data. Extensive experiments on synthetic data show that the proposed methods are able to handle more outliers and higher-dimensional subspaces than the state-of-the-art methods, while experiments with real face and object images show that our DPCP-based methods are competitive to the state-of-the-art.

1. Introduction

Principal Component Analysis (PCA) is one of the oldest (Pearson, 1901; Hotelling, 1933) and most fundamental techniques in data analysis, with ubiquitous applications in engineering (Moore, 1981), economics and sociology (Vyas and Kumaranayake, 2006), chemistry (Ku et al., 1995), physics (Loyd et al., 2014) and genetics (Price et al., 2006) to name a few; see (Jolliffe, 2002) for more applications. Given a data matrix $\boldsymbol{\mathcal{X}} \in \mathbb{R}^{D\times L}$ of L data points of coordinate dimension D, PCA gives a closed form solution to the problem of fitting, in the Euclidean sense, a d-dimensional linear subspace to the columns of $\boldsymbol{\mathcal{X}}$. Even though the optimization problem associated with PCA is non-convex, it does admit a simple solution by means of the Singular Value Decomposition (SVD) of $\boldsymbol{\mathcal{X}}$. In fact, the d-dimensional subspace $\hat{\mathcal{S}}$ of $\mathbb{R}^D$ that is closest to the columns of $\boldsymbol{\mathcal{X}}$ in the Euclidean sense, is precisely the subspace spanned by the first d left singular vectors of $\boldsymbol{\mathcal{X}}$.

Using $\hat{\mathcal{S}}$ as a model for the data is meaningful when the data $\boldsymbol{\mathcal{X}}$ are known to have an approximately linear structure of underlying dimension d, i.e., they lie close to a d-dimensional subspace $\mathcal{S}$. In practice, the principal components of $\boldsymbol{\mathcal{X}}$ are known to be well-behaved under mild levels of noise, i.e., the principal angles between $\hat{\mathcal{S}}$ and $\mathcal{S}$ are relatively small, and in fact, $\hat{\mathcal{S}}$ is optimal when the noise is Gaussian (Jolliffe, 2002). However, very often in applications the dataset is corrupted

by outliers, i.e., it has the form $\tilde{\boldsymbol{\mathcal{X}}} = [\boldsymbol{\mathcal{X}}\, \boldsymbol{\mathcal{O}}]\, \boldsymbol{\Gamma}$, where $\boldsymbol{\mathcal{O}} \in \mathbb{R}^{D \times M}$ are M points of $\mathbb{R}^D$ whose angles from the underlying ground truth subspace $\mathcal{S}$ associated with the inlier points $\boldsymbol{\mathcal{X}}$ are large, and $\boldsymbol{\Gamma}$ is an unknown permutation. In such cases, the principal angles between $\mathcal{S}$ and its estimate $\hat{\mathcal{S}}$ given by PCA will in general be large, even when M is small. This is to be expected since, by definition, the principal components of $\tilde{\boldsymbol{\mathcal{X}}}$ are orthogonal directions of maximal correlation with *all* the points of $\tilde{\boldsymbol{\mathcal{X}}}$. This phenomenon, together with the fact that outliers are almost always present in real datasets, has given rise to the important problem of outlier detection in PCA.

Traditionally, outlier detection has been a major area of study in robust statistics with notable methods being *Influence-based Detection*, *Multivariate Trimming*, M*-Estimators*, *Iteratively Reweighted Least-Squares* and *Random Sampling Consensus* (RANSAC) (Huber, 1981; Jolliffe, 2002). These methods are usually based on non-convex optimization problems, and in practice, converge only to a local minimum. In addition, their theoretical analysis is usually limited and their computational complexity may be large (e.g. in the case RANSAC). Recently, two attractive methods have appeared (Xu et al., 2010; Soltanolkotabi and Candès, 2012) that are directly based on convex optimization, and are inspired by *low-rank representation* (Liu et al., 2010) and *compressed sensing* (Candès and Wakin, 2008). Even though both of these methods admit theoretical guarantees and efficient implementations, they are in principle applicable only in the low-rank regime: the dimension d of the underlying subspace $\mathcal{S}$ associated to the inliers should be small compared to the ambient dimension D. Interestingly, the even more recent method of (Lerman et al., 2015) is a first step towards surpassing this limitation. Indeed, (Lerman et al., 2015) apply a tight convex relaxation to a non-convex problem, and obtain a subspace learning method that is robust to outliers, and whose theorems of correctness do not explicitly require the subspace dimension d to be small.

In this paper we adopt a *dual* approach to the problem of robust PCA in the presence of outliers, which allows us to explicitly transcend the low-rank regime of modern methods such as (Xu et al., 2010) or (Soltanolkotabi and Candès, 2012). The key idea of our approach comes from the fact that, in the absence of noise, the inliers $\boldsymbol{\mathcal{X}}$ lie inside any hyperplane $\mathcal{H}_1 = \mathrm{Span}(\boldsymbol{b}_1)^\perp$ that contains the underlying linear subspace $\mathcal{S}$ associated to the inliers. This suggests that, instead of attempting to fit directly a low-dimensional linear subspace to the entire dataset $\tilde{\boldsymbol{\mathcal{X}}}$, as done e.g. in (Xu et al., 2010), we can search for a *maximal hyperplane* $\mathcal{H}_1$ that contains as many points of the dataset as possible. When the inliers $\boldsymbol{\mathcal{X}}$ are in general position (to be made precise shortly) inside $\mathcal{S}$, and the outliers $\boldsymbol{\mathcal{O}}$ are in general position in $\mathbb{R}^D$, such a maximal hyperplane will contain the entire set of inliers together with possibly a few outliers. Then one may remove all points that lie outside this hyperplane and be left with an easier robust PCA problem that could potentially be addressed by existing methods. Alternatively, one can continue by finding a second maximal hyperplane $\mathcal{H}_2 = \mathrm{Span}(\boldsymbol{b}_2)^\perp$, with the new dual principal component $\boldsymbol{b}_2$ perpendicular to the first one, i.e., $\boldsymbol{b}_2 \perp \boldsymbol{b}_1$, and so on, until $c := D - d$ such maximal hyperplanes $\mathcal{H}_1, \ldots, \mathcal{H}_c$ have been found, leading to a *Dual Principal Component Analysis (DPCA)* of $\tilde{\boldsymbol{\mathcal{X}}}$. In such a case, the inlier subspace is precisely equal to $\bigcap_{i=1}^{c} \mathcal{H}_i$, and a point is an outlier if and only if it lies outside this intersection.

We formalize the problem of searching for maximal hyperplanes with respect to $\tilde{\boldsymbol{\mathcal{X}}}$ as an ℓ_0 cosparsity-type problem (Nam et al., 2013), which we relax to a non-convex ℓ_1 problem on the sphere, referred to as *the DPCP problem*. We provide theoretical guarantees under which every global solution of the DPCP problem is a vector orthogonal to the linear subspace associated to the inliers, i.e., it is a dual principal component. Moreover, we relax the non-convex DPCP problem to a recursion of linear programming problems, which we show that, under mild conditions, it converges to a dual principal component in a finite number of steps. In particular, when the inlier subspace is

a hyperplane, i.e., when it has dimension equal to $D-1$, then the linear programming recursions converge to the global minimum of the non-convex problem in a finite number of steps. Furthermore, we propose algorithms based on alternating minimization and Iteratively Reweighted Least-Squares, that are suitable for dealing with large-scale data. Extensive experiments on synthetic data show that the proposed methods are able to handle more outliers and higher-dimensional subspaces than the state-of-the-art methods (Fischler and Bolles, 1981; Xu et al., 2010; Soltanolkotabi and Candès, 2012; Lerman et al., 2015), while experiments with real face and object images show that our DPCP-based methods are competitive to the state-of-the-art.

Notation. The symbol $\cong$ stands for *isomorphism* in whatever category the objects lying to the left and right of the symbol belong to. For a positive integer n let $[n] := \{1, 2, \ldots, n\}$. For a positive real number α let $\lceil \alpha \rceil$ denote the smallest integer that is greater than α. If $\mathcal{T}_1, \mathcal{T}_2$ are sets, $\mathcal{T}_1 \setminus \mathcal{T}_2$ denotes the elements of $\mathcal{T}_1$ which are not elements of $\mathcal{T}_2$. Moreover, $\mathcal{T}_1 \sqcup \mathcal{T}_2$ represents the union of the $\mathcal{T}_1, \mathcal{T}_2$ and at the same time provides the information that $\mathcal{T}_1 \cap \mathcal{T}_2 = \emptyset$ (disjoint union). $\mathbb{S}^{D-1}$ denotes the unit sphere of $\mathbb{R}^D$. For a vector $\boldsymbol{w} \in \mathbb{R}^D$ we define $\hat{\boldsymbol{w}} := \boldsymbol{w}/\left\|\boldsymbol{w}\right\|_2$, if $\boldsymbol{w} \neq \boldsymbol{0}$, and $\hat{\boldsymbol{w}} := 0$ otherwise. For $\mathcal{S}$ a linear subspace of $\mathbb{R}^D$, $\pi_{\mathcal{S}} : \mathbb{R}^D \to \mathcal{S}$ denotes the orthogonal projection of $\mathbb{R}^D$ onto $\mathcal{S}$, and $\mathcal{S}^\perp$ the orthogonal complement of $\mathcal{S}$. If $\boldsymbol{y}_1, \ldots, \boldsymbol{y}_s$ are elements of $\mathbb{R}^D$, $\mathrm{Span}(\boldsymbol{y}_1, \ldots, \boldsymbol{y}_s)$ is the subspace of $\mathbb{R}^D$ spanned by these elements. With a mild abuse of notation we will be treating on several occasions matrices as sets, e.g., if $\boldsymbol{\mathcal{X}}$ is $D \times N$ and $\boldsymbol{x}$ a point of $\mathbb{R}^D$, the notation $\boldsymbol{x} \in \boldsymbol{\mathcal{X}}$ signifies that $\boldsymbol{x}$ is a column of $\boldsymbol{\mathcal{X}}$. Similarly, if $\boldsymbol{\mathcal{O}}$ is a $D \times M$ matrix, the notation $\boldsymbol{\mathcal{X}} \cap \boldsymbol{\mathcal{O}}$ signifies the points of $\mathbb{R}^D$ that are common columns of $\boldsymbol{\mathcal{X}}$ and $\boldsymbol{\mathcal{O}}$. Sign denotes the sign function $\mathrm{Sign} : \mathbb{R} \to \{-1, 0, 1\}$ defined as

$$\mathrm{Sign}(x) = \begin{cases} x/|x| & \text{if } x \neq 0, \\ 0 & \text{if } x = 0. \end{cases} \tag{1}$$

The subdifferential of the ℓ_1-norm

$$\boldsymbol{z} = (z_1, \ldots, z_D)^\top \mapsto \left\|\boldsymbol{z}\right\|_1 = \sum_{i=1}^{D} |z_i| \tag{2}$$

is a set-valued function on $\mathbb{R}^D$ defined as

$$\mathrm{Sgn}(x) = \begin{cases} \mathrm{Sign}(x) & \text{if } x \neq 0, \\ [-1, 1] & \text{if } x = 0. \end{cases} \tag{3}$$

The shorthand RHS stands for *Right-Hand-Side*, and similarly LHS stands for *Left-Hand-Side*.

2. Prior Art

In this Section we briefly review some state-of-the-art methods for learning a linear subspace from data $\tilde{\boldsymbol{\mathcal{X}}} = [\boldsymbol{\mathcal{X}}\ \boldsymbol{\mathcal{O}}]\,\boldsymbol{\Gamma}$ in the presence of outliers. The literature on this subject is vast, and our account is far from exhaustive; with a few exceptions, we mainly focus on modern methods that are based on convex optimization. For methods from robust statistics see (Huber, 1981; Jolliffe, 2002), for online subspace learning methods see (Balzano et al., 2010; Feng et al., 2013), while for fast and other methods the reader is referred to the excellent literature review of (Lerman and Zhang, 2014).

RANSAC. One of the oldest and most popular outlier detection methods in PCA is *Random Sampling Consensus (RANSAC)* (Fischler and Bolles, 1981). The idea behind RANSAC is simple:

alternate between randomly sampling a small subset of the dataset and computing a subspace model for this subset, until a model is found that maximizes the number of points in the entire dataset that fit to it within some error. RANSAC is usually characterized by high performance. However, it requires a high computational time, since it is often the case that exponentially many trials are required in order to sample outlier-free subsets, and thus obtain reliable models. Additionally, RANSAC requires as input an estimate for the dimension of the subspace as well as a thresholding parameter, which is used to distinguish outliers from inliers; naturally the performance of RANSAC is very sensitive to these two parameters.

$\ell_{2,1}$-RPCA. Contrary to the classic principles that underlie RANSAC, modern methods for outlier detection in PCA are primarily based on convex optimization. One of the earliest and most important such methods, to be referred to as $\ell_{2,1}$-RPCA, is the method of (Xu et al., 2010), which is in turn inspired by the *Robust PCA* algorithm of (Candès et al., 2011). $\ell_{2,1}$-RPCA computes a $(\ell_* + \ell_{2,1})$-norm decomposition[1] of the data matrix, instead of the $(\ell_* + \ell_1)$-decomposition in (Candès et al., 2011). More specifically, $\ell_{2,1}$-RPCA solves the optimization problem

$$\min_{\boldsymbol{L},\boldsymbol{E}:\,\tilde{\boldsymbol{\mathcal{X}}}=\boldsymbol{L}+\boldsymbol{E}} \|\boldsymbol{L}\|_* + \lambda \, \|\boldsymbol{E}\|_{2,1}\,, \tag{4}$$

which attempts to decompose the data matrix $\tilde{\boldsymbol{\mathcal{X}}} = [\boldsymbol{\mathcal{X}}\, \boldsymbol{\mathcal{O}}]\boldsymbol{\Gamma}$ into the sum of a low-rank matrix $\boldsymbol{L}$, and a matrix $\boldsymbol{E}$ that has only a few non-zero columns. The idea is that $\boldsymbol{L}$ is associated with the inliers, having the form $\boldsymbol{L} = [\boldsymbol{\mathcal{X}}\, \mathbf{0}_{D\times M}]\boldsymbol{\Gamma}$, and $\boldsymbol{E}$ is associated with the outliers, having the form $\boldsymbol{E} = [\mathbf{0}_{D\times N}\, \boldsymbol{\mathcal{O}}]\boldsymbol{\Gamma}$. The optimization problem (4) is convex and admits theoretical guarantees and efficient ADMM (Boyd et al., 2010) implementations. However, it is expected to succeed only when the intrinsic dimension d of the inliers is small enough (otherwise $[\boldsymbol{\mathcal{X}}\, \mathbf{0}_{D\times M}]$ will not be low-rank), and the outlier ratio is not too large (otherwise $[\mathbf{0}_{D\times N}\, \boldsymbol{\mathcal{O}}]$ will not be column-sparse). Finally, notice that $\ell_{2,1}$-RPCA does not require as input the subspace dimension d, because it does not directly compute an estimate for the subspace. Rather, the subspace can be obtained subsequently by doing classic PCA on $\boldsymbol{L}$, and now one does need an estimate for d.

SE-RPCA. Another state-of-the-art method, referred to as *SE-RPCA*, is based on the *self-expressiveness* property of the data matrix, a notion popularized by the work of (Elhamifar and Vidal, 2011, 2013) in the area of subspace clustering (Vidal, 2011). More specifically, observe that if a column of $\tilde{\boldsymbol{\mathcal{X}}}$ is an inlier, then it can in principle be expressed as a linear combination of d other columns of $\tilde{\boldsymbol{\mathcal{X}}}$, which are inliers. If the column is instead an outlier, then it will in principle require D other columns to express it as a linear combination. The self expressiveness matrix $\boldsymbol{C}$ can be obtained as the solution to the convex optimization problem

$$\min_{\boldsymbol{C}} \ \|\boldsymbol{C}\|_1 \ \ s.t. \ \tilde{\boldsymbol{\mathcal{X}}} = \tilde{\boldsymbol{\mathcal{X}}}\boldsymbol{C}, \ \operatorname{Diag}(\boldsymbol{C}) = \mathbf{0}. \tag{5}$$

Having computed the matrix of coefficients $\boldsymbol{C}$, and under the hypothesis that d/D is small, a column of $\tilde{\boldsymbol{\mathcal{X}}}$ is declared as an outlier, if the ℓ_1 norm of the corresponding column of $\boldsymbol{C}$ is large; see (Soltanolkotabi and Candès, 2012) for an explicit formula. SE-RPCA admits theoretical guarantees (Soltanolkotabi and Candès, 2012) and efficient ADMM implementations (Elhamifar and Vidal, 2013). However, as is clear from its description, it is expected to succeed only when the relative dimension d/D is sufficiently small. Nevertheless, in contrast to $\ell_{2,1}$-RPCA, which in principle

1. Here ℓ_* denotes the nuclear norm, which is the sum of the singular values of the matrix. Also, $\ell_{2,1}$ is defined as the sum of the euclidean norms of the columns of a matrix.

fails in the presence of a very large number of outliers, SE-RPCA is still expected to perform well, since the existence of sparse *subspace-preserving* self-expressive patterns does not depend on the number of outliers present. Also, similarly to $\ell_{2,1}$-RPCA, SE-RPCA does not directly require an estimate for the subspace dimension d. Nevertheless, knowledge of d is necessary if one wants to furnish an actual subspace estimate. This would entail removing the outliers (a judiciously chosen threshold would also be necessary here) and doing PCA on the remaining points.

REAPER. A recently proposed single subspace learning method that admits an interesting theoretical analysis is the *REAPER* (Lerman et al., 2015), which is conceptually associated with the optimization problem

$$\min_{\boldsymbol{\Pi}} \sum_{j=1}^{L} \|(\boldsymbol{I}_D - \boldsymbol{\Pi})\tilde{\boldsymbol{x}}_j\|_2 , \;\; \text{s.t. } \boldsymbol{\Pi} \text{ is an orthogonal projection}, \;\; \text{Trace}\,(\boldsymbol{\Pi}) = d, \tag{6}$$

where $\tilde{\boldsymbol{x}}_j$ is the j-th column of $\tilde{\boldsymbol{\mathcal{X}}}$. The matrix $\boldsymbol{\Pi}$ appearing in (6) can be thought of as the product $\boldsymbol{\Pi} = \boldsymbol{U}\boldsymbol{U}^\top$, where $\boldsymbol{U} \in \mathbb{R}^{D\times d}$ contains in its columns an orthonormal basis for a d-dimensional linear subspace $\mathcal{S}$. As (6) is non-convex, (Lerman et al., 2015) relaxes it to the convex semi-definite program

$$\min_{\boldsymbol{P}} \sum_{j=1}^{L} \|(\boldsymbol{I}_D - \boldsymbol{P})\tilde{\boldsymbol{x}}_j\|_2 , \;\; \text{s.t. } \boldsymbol{0} \leq \boldsymbol{P} \leq \boldsymbol{I}_D, \;\; \text{Trace}\,(\boldsymbol{P}) = d, \tag{7}$$

whose global solution $\boldsymbol{P}^*$ is subsequently projected in an ℓ_* sense onto the space of rank-d orthogonal projectors. It is shown in (Lerman et al., 2015) that the orthoprojector $\boldsymbol{\Pi}^*$ obtained in this way is within a neighborhood of the orthoprojector corresponding to the true underlying inlier subspace. One advantage of REAPER with respect to $\ell_{2,1}$-RPCA and SE-RPCA, is that its theoretical conditions do not explicitly require the inlier dimension d to be small. On the other hand, contrary to $\ell_{2,1}$-RPCA, REAPER does require a-priori knowledge of the inlier dimension d. Moreover, the semi-definite program (7) may become prohibitively expensive to solve even for moderate values of the ambient dimension D. As a consequence, (Lerman et al., 2015) proposed an *Iteratively Reweighted Least Squares* (IRLS) scheme to obtain a numerical solution of (7). Interestingly, it was shown in (Lerman et al., 2015) that the objective value of this IRLS scheme converges to a neighborhood of the optimal objective value of problem (7); nevertheless no other properties of this scheme seem to be known.

R1-PCA. A related method is R1-PCA (Ding et al., 2006), which attempts to solve the problem

$$\min_{\boldsymbol{U},\boldsymbol{V}} \;\; \left\|\tilde{\boldsymbol{\mathcal{X}}} - \boldsymbol{U}\boldsymbol{V}\right\|_{2,1}, \;\; \text{s.t. } \boldsymbol{U}^\top\boldsymbol{U} = \boldsymbol{I}, \tag{8}$$

where $\boldsymbol{U}$ is an orthonormal basis for the estimated subspace, and $\boldsymbol{V}$ contains in its columns the low-dimensional representations of the points. Besides for alternating minimization with a power iteration scheme that converges to a local minimum, little else is known about how to solve the non-convex problem (8) to global optimality.

L1-PCA*. Finally, the method L1-PCA* of (Brooks et al., 2013) works with the orthogonal complement of the subspace, but it is slightly unusual in that it learns ℓ_1 hyperplanes, i.e., hyperplanes that minimize the ℓ_1 distance to the points, as opposed to the Euclidean distance, e.g., used

by the classic PCA, R1-PCA, or REAPER. More specifically, an ℓ_1 hyperplane learned by the data is a hyperplane with normal vector $\boldsymbol{b}$ that solves the problem

$$\min_{\boldsymbol{b}\in\mathbb{S}^{D-1};\, \boldsymbol{y}_j\in\mathbb{R}^D,\, j\in[L]} \; \sum_{j=1}^{L} \left\|\tilde{\boldsymbol{x}}_j - \boldsymbol{y}_j\right\|_1 \;\; \text{s.t.} \;\; \boldsymbol{y}_j^\top \boldsymbol{b} = 0,\, \forall j \in [L], \tag{9}$$

where $\boldsymbol{y}_j$ is the representation of point $\tilde{\boldsymbol{x}}_j$ in the hyperplane. Overall, no theoretical guarantees seem to be known for L1-PCA*, as far as the subspace learning problem is concerned. In addition, L1-PCA* requires the solution to quadratically many linear programs of size equal to the ambient dimension, which makes it computationally expensive.

3. Problem Formulation

In this Section we describe the problem of interest of this paper. We begin by establishing our data model in Section 3.1, while in Section 3.2 we motivate the problem on a conceptual level. Finally, in Section 3.3 we formulate our problem as an optimization problem.

3.1 Data model

We employ a deterministic noise-free data model, under which the given data is

$$\tilde{\boldsymbol{\mathcal{X}}} = [\boldsymbol{\mathcal{X}} \;\; \boldsymbol{\mathcal{O}}]\boldsymbol{\Gamma} = [\tilde{\boldsymbol{x}}_1, \ldots, \tilde{\boldsymbol{x}}_L] \in \mathbb{R}^{D\times L}, \tag{10}$$

where the inliers $\boldsymbol{\mathcal{X}} = [\boldsymbol{x}_1, \ldots, \boldsymbol{x}_N] \in \mathbb{R}^{D\times N}$ lie in the intersection of the unit sphere $\mathbb{S}^{D-1}$ with an unknown proper subspace $\mathcal{S}$ of $\mathbb{R}^D$ of unknown dimension $1 \leq d \leq D-1$, and the outliers consist of M points $\boldsymbol{\mathcal{O}} = [\boldsymbol{o}_1, \ldots, \boldsymbol{o}_M] \in \mathbb{R}^{D\times M}$ that lie on the sphere $\mathbb{S}^{D-1}$. The unknown permutation $\boldsymbol{\Gamma}$ indicates that we do not know which point is an inlier and which point is an outlier. Finally, we assume that the points $\tilde{\boldsymbol{\mathcal{X}}}$ are in *general position*, in the sense that there are no relations between the columns of $\tilde{\boldsymbol{\mathcal{X}}}$ except the ones implied by the inclusions $\boldsymbol{\mathcal{X}} \subset \mathcal{S}$ and $\tilde{\boldsymbol{\mathcal{X}}} \subset \mathbb{R}^D$. In particular, every D-tuple of columns of $\tilde{\boldsymbol{\mathcal{X}}}$ such that at most d points come frorm $\boldsymbol{\mathcal{X}}$ is linearly independent. Notice that as a consequence every d-tuple of inliers and every D-tuple of outliers are linearly independent, and also $\boldsymbol{\mathcal{X}} \cap \boldsymbol{\mathcal{O}} = \emptyset$. Finally, to avoid degenerate situations we will assume that $N \geq d+1$ and $M \geq D-d$.[2]

3.2 Conceptual formulation

Notice that we have made no assumption on the dimension of $\mathcal{S}$: indeed, $\mathcal{S}$ can be anything from a line to a $(D-1)$-dimensional hyperplane. Ideally, we would like to be able to partition the columns of $\tilde{\boldsymbol{\mathcal{X}}}$ into those that lie in $\mathcal{S}$ and those that don't. But under such generality, this is not a well-posed problem since $\boldsymbol{\mathcal{X}}$ lies inside every subspace that contains $\mathcal{S}$, which in turn may contain some elements of $\boldsymbol{\mathcal{O}}$. In other words, given $\tilde{\boldsymbol{\mathcal{X}}}$ and without any other a priori knowledge, it may be impossible to correctly partition $\tilde{\boldsymbol{\mathcal{X}}}$ into $\boldsymbol{\mathcal{X}}$ and $\boldsymbol{\mathcal{O}}$. Instead, it is meaningful to search for a linear subspace of $\mathbb{R}^D$ that contains all of the inliers and perhaps a few outliers. Since we do not know the intrinsic dimension d of the inliers, a natural choice is to search for a hyperplane of $\mathbb{R}^D$ that contains all the inliers.

2. If the number of outliers is less than $D-d$, then the entire dataset is degenerate, in the sense that it lies in a proper hyperplane of the ambient space. In such a case we can reduce the coordinate representation of the data and eventually satisfy the stated condition.

Problem 1 *Given the dataset* $\tilde{\boldsymbol{\mathcal{X}}} = [\boldsymbol{\mathcal{X}} \;\; \mathcal{O}]\,\boldsymbol{\Gamma}$*, find a hyperplane* $\mathcal{H}$ *that contains all the inliers* $\boldsymbol{\mathcal{X}}$*.*

Notice that hyperplanes that contain all the inliers always exist: any non-zero vector $\boldsymbol{b}$ inside the orthogonal complement $\mathcal{S}^{\perp}$ of the linear subspace $\mathcal{S}$ associated to the inliers defines a hyperplane (with normal vector $\boldsymbol{b}$) that contains all inliers $\boldsymbol{\mathcal{X}}$. Having such a hyperplane $\mathcal{H}_1$ at our disposal, we can partition our dataset as $\tilde{\boldsymbol{\mathcal{X}}} = \tilde{\boldsymbol{\mathcal{X}}}_1 \sqcup \tilde{\boldsymbol{\mathcal{X}}}_2$, where $\tilde{\boldsymbol{\mathcal{X}}}_1$ are the points of $\tilde{\boldsymbol{\mathcal{X}}}$ that lie in $\mathcal{H}_1$ and $\tilde{\boldsymbol{\mathcal{X}}}_2$ are the remaining points. Then by definition of $\mathcal{H}_1$, we know that $\tilde{\boldsymbol{\mathcal{X}}}_2$ will consist purely of outliers, in which case we can safely replace our original dataset $\tilde{\boldsymbol{\mathcal{X}}}$ with $\tilde{\boldsymbol{\mathcal{X}}}_1$ and reconsider the problem of robust PCA on $\tilde{\boldsymbol{\mathcal{X}}}_1$. We emphasize that $\tilde{\boldsymbol{\mathcal{X}}}_1$ will contain all the inliers $\boldsymbol{\mathcal{X}}$ together with at most $D-d-1$ outliers [3], a number which may be dramatically smaller than the original number of outliers. Then one may apply existing methods such as (Xu et al., 2010), (Soltanolkotabi and Candès, 2012) or (Fischler and Bolles, 1981) to finish the task of identifying the remaining outliers, as the following example demonstrates.

Example 1 *Suppose we have* $N = 1000$ *inliers lying in general position inside a* 90*-dimensional linear subspace of* $\mathbb{R}^{100}$*. Suppose that the dataset is corrupted by* $M = 1000$ *outliers lying in general position in* $\mathbb{R}^{100}$*. Let* $\mathcal{H}$ *be a hyperplane that contains all* 1000 *inliers. Since the dimensionality of the inliers is* 90 *and the dimensionality of the hyperplane is* 99*, there are only* $99-90 = 9$ *linearly independent directions left for the hyperplane to fit, i.e.,* $\mathcal{H}$ *will contain at most* 9 *outliers (it can not contain more outliers since this would violate the general position hypothesis). If we remove the points of the dataset that do not lie in* $\mathcal{H}$*, then we are left with* 1000 *inliers and at most* 9 *outliers. Interestingly, a simple application of RANSAC is expected to identify the remaining outliers in only a few trials.*

Alternatively, one may repeat the above process $c = \operatorname{codim} \mathcal{S} = D - d$ times, until c linearly independent maximal hyperplanes $\mathcal{H}_1, \ldots, \mathcal{H}_c$ have been found [4]. Then a point is an inlier if and only if the point lies in the intersection of these c hyperplanes; this is true because it must be the case that $\bigcap_{k=1}^{c} \mathcal{H}_k = \mathcal{S}$.

3.3 Hyperplane pursuit by ℓ_1 minimization

In this Section we propose an optimization framework for the computation of a hyperplane that solves Problem 1, i.e., a hyperplane that contains all the inliers. To proceed, we need a definition.

Definition 2 *A hyperplane* $\mathcal{H}$ *of* $\mathbb{R}^D$ *is called maximal with respect to the dataset* $\tilde{\boldsymbol{\mathcal{X}}}$*, if it contains a maximal number of data points in* $\tilde{\boldsymbol{\mathcal{X}}}$*, i.e., if for any other hyperplane* $\mathcal{H}^{\dagger}$ *of* $\mathbb{R}^D$ *we have that* $\operatorname{Card}(\tilde{\boldsymbol{\mathcal{X}}} \cap \mathcal{H}) \geq \operatorname{Card}(\tilde{\boldsymbol{\mathcal{X}}} \cap \mathcal{H}^{\dagger})$.

In principle, hyperplanes that are maximal with respect to $\tilde{\boldsymbol{\mathcal{X}}}$, always solve Problem 1.

Proposition 3 *Suppose that* $N \geq d+1$ *and* $M \geq D-d$*, and let* $\mathcal{H}$ *be a hyperplane that is maximal with respect to the dataset* $\tilde{\boldsymbol{\mathcal{X}}}$*. Then* $\mathcal{H}$ *contains all the inliers* $\boldsymbol{\mathcal{X}}$*.*

3. This comes from the general position hypothesis.
4. By the hyperplanes being linearly independent we mean their normal vectors being linearly independent.

Proof By the general position hypothesis on $\boldsymbol{\mathcal{X}}$ and $\mathcal{O}$, any hyperplane that does not contain $\boldsymbol{\mathcal{X}}$ can contain at most $D-1$ points from $\tilde{\boldsymbol{\mathcal{X}}}$. We will show that there exists a hyperplane that contains more than $D-1$ points of $\tilde{\boldsymbol{\mathcal{X}}}$. Indeed, take d inliers and $D-d-1$ outliers and let $\mathcal{H}$ be the hyperplane generated by these $D-1$ points. Denote the normal vector to that hyperplane by $\boldsymbol{b}$. Since $\mathcal{H}$ contains d inliers, $\boldsymbol{b}$ will be orthogonal to these inliers. Since $\boldsymbol{\mathcal{X}}$ is in general position, every d-tuple of inliers is a basis for $\mathrm{Span}(\boldsymbol{\mathcal{X}})$. As a consequence, $\boldsymbol{b}$ will be orthogonal to $\mathrm{Span}(\boldsymbol{\mathcal{X}})$, and in particular $\boldsymbol{b} \perp \boldsymbol{\mathcal{X}}$. This implies that $\boldsymbol{\mathcal{X}} \subset \mathcal{H}$ and so $\mathcal{H}$ will contain $N+D-d-1 \geq d+1+D-d-1 > D-1$ points of $\tilde{\boldsymbol{\mathcal{X}}}$. ■

In view of Proposition 3, we may restrict our search for hyperplanes that contain all the inliers $\boldsymbol{\mathcal{X}}$ to the subset of hyperplanes that are maximal with respect to the dataset $\tilde{\boldsymbol{\mathcal{X}}}$. The advantage of this approach is immediate: the set of hyperplanes that are maximal with respect to $\tilde{\boldsymbol{\mathcal{X}}}$ is in principle computable, since it is precisely the set of solutions of the following optimization problem

$$\min_{\boldsymbol{b}} \left\| \tilde{\boldsymbol{\mathcal{X}}}^{\top} \boldsymbol{b} \right\|_0 \quad s.t. \;\; \boldsymbol{b} \neq 0. \tag{11}$$

The idea behind (11) is that a hyperplane $\mathcal{H} = \mathrm{Span}(\boldsymbol{b})^{\perp}$ contains a maximal number of columns of $\tilde{\boldsymbol{\mathcal{X}}}$ if and only if its normal vector $\boldsymbol{b}$ has a maximal *cosparsity* level with respect to the matrix $\tilde{\boldsymbol{\mathcal{X}}}^{\top}$, i.e., the number of non-zero entries of $\tilde{\boldsymbol{\mathcal{X}}}^{\top} \boldsymbol{b}$ is minimal. Since (11) is a combinatorial problem admitting no efficient solution, we consider its natural relaxation

$$\min_{\boldsymbol{b}} \left\| \tilde{\boldsymbol{\mathcal{X}}}^{\top} \boldsymbol{b} \right\|_1 \quad s.t. \;\; \|\boldsymbol{b}\|_2 = 1, \tag{12}$$

which in our context we will be referring to as *Dual Principal Component Pursuit* (DPCP). A major question that arises, to be answered in Theorem 10, is under what conditions every global solution of (12) is orthogonal to the inlier subspace $\mathrm{Span}(\boldsymbol{\mathcal{X}})$. A second major question, raised by the non-convexity of the constraint $\boldsymbol{b} \in \mathbb{S}^{D-1}$, is how to efficiently solve (12) with theoretical guarantees.

We emphasize here that the optimization problem (12) is far from new; interestingly, its earliest appearance in the literature that we are aware of is in (Späth and Watson, 1987), where the authors proposed to solve it by means of the recursion of convex problems given by [5]

$$\boldsymbol{n}_{k+1} := \operatorname*{argmin}_{\boldsymbol{b}^{\top} \hat{\boldsymbol{n}}_k = 1} \left\| \tilde{\boldsymbol{\mathcal{X}}}^{\top} \boldsymbol{b} \right\|_1. \tag{13}$$

Notice that at each iteration of (13) the problem that is solved is computationally equivalent to a linear program; this makes the recursion (13) a very appealing candidate for solving the non-convex (12). Even though (Späth and Watson, 1987) proved the very interesting result that (13) converges to a critical point of (12) in a finite number of steps (see Appendix A), there is no reason to believe that in general (13) converges to a global minimum of (12).

Other works in which optimization problem (12) appears are (Spielman et al., 2013; Qu et al., 2014; Sun et al., 2015c,d,b,a). More specifically, (Spielman et al., 2013) propose to solve (12) by replacing the quadratic constraint $\boldsymbol{b}^{\top}\boldsymbol{b} = 1$ with a linear constraint $\boldsymbol{b}^{\top}\boldsymbol{w} = 1$ for some vector $\boldsymbol{w}$. In (Qu et al., 2014; Sun et al., 2015b) (12) is approximately solved by alternating minimization, while a Riemannian trust-region approach is employed in (Sun et al., 2015a). Finally, we note that

5. Being unaware of the work of (Späth and Watson, 1987), we independently proposed the same recursion in (Tsakiris and Vidal, 2015).

problem (12) is closely related to the non-convex problem (6) associated with REAPER. To see this, suppose that the REAPER orthoprojector $\mathbf{\Pi}$ appearing in (6), represents the orthogonal projection to a hyperplane $\mathcal{U}$ with unit-ℓ_2 normal vector $\boldsymbol{b}$. In such a case $\boldsymbol{I}_D - \mathbf{\Pi} = \boldsymbol{b}\boldsymbol{b}^\top$, and it readily follows that problem (6) becomes identical to problem (12).

4. Theoretical Contributions

In this section we establish our analysis framework and discuss our main theoretical results regarding the non-convex problem (12) as well as the recursion of convex relaxations (13). We begin our theoretical investigation in §4.1 by establishing a connection between the *discrete* problems (12) and (13) and certain underlying *continuous* problems. The continuous problems do not depend on a finite set of inliers and outliers, rather on uniform distributions on the respective inlier and outlier spaces, and as such, are easier to analyze. The analysis reveals that both the continuous analogue of (12) as well the continuous recursion corresponding to (13) are naturally associated with vectors orthogonal to the inlier subspace $\mathcal{S}$. This suggests that under certain conditions on the distribution of the data, the same must be true for the *discrete* problem (12) and recursion (13). Indeed, in §4.2 we obtain discrete analogues of the theorems of §4.1, which in particular show that both (12) and (13) are natural formulations for computing the orthogonal complement of a linear subspace in the presence of outliers.

4.1 The underlying continuous problem

In this section we show that the problems of interest (12) and (13) can be viewed as discrete versions of certain continuous problems, which we analyze. To begin with, consider given outliers $\boldsymbol{\mathcal{O}} = [\boldsymbol{o}_1, \dots, \boldsymbol{o}_M] \subset \mathbb{S}^{D-1}$ and inliers $\boldsymbol{\mathcal{X}} = [\boldsymbol{x}_1, \dots, \boldsymbol{x}_N] \subset \mathcal{S} \cap \mathbb{S}^{D-1}$, and recall the notation $\tilde{\boldsymbol{\mathcal{X}}} = [\boldsymbol{\mathcal{X}}\, \boldsymbol{\mathcal{O}}]\mathbf{\Gamma}$, where $\mathbf{\Gamma}$ is an unknown permutation. Next, for any $\boldsymbol{b} \in \mathbb{S}^{D-1}$ define the function $f_{\boldsymbol{b}} : \mathbb{S}^{D-1} \to \mathbb{R}$ by $f_{\boldsymbol{b}}(\boldsymbol{z}) = \left|\boldsymbol{b}^\top \boldsymbol{z}\right|$. Define also *discrete* measures $\mu_{\boldsymbol{\mathcal{O}}}$ and $\mu_{\boldsymbol{\mathcal{X}}}$ on $\mathbb{S}^{D-1}$ associated with the outliers and inliers respectively, as

$$\mu_{\boldsymbol{\mathcal{O}}}(\boldsymbol{z}) = \frac{1}{M}\sum_{j=1}^{M} \delta(\boldsymbol{z} - \boldsymbol{o}_j) \;\text{ and }\; \mu_{\boldsymbol{\mathcal{X}}}(\boldsymbol{z}) = \frac{1}{N}\sum_{j=1}^{N} \delta(\boldsymbol{z} - \boldsymbol{x}_j), \tag{14}$$

where $\delta(\cdot)$ is the Dirac function on $\mathbb{S}^{D-1}$, satisfying

$$\int_{\boldsymbol{z}\in\mathbb{S}^{D-1}} g(\boldsymbol{z})\delta(\boldsymbol{z} - \boldsymbol{z}_0) d\mu_{\mathbb{S}^{D-1}} = g(\boldsymbol{z}_0), \tag{15}$$

for every $g : \mathbb{S}^{D-1} \to \mathbb{R}$ and every $\boldsymbol{z}_0 \in \mathbb{S}^{D-1}$; $\mu_{\mathbb{S}^{D-1}}$ is the uniform measure on $\mathbb{S}^{D-1}$.

With these definitions, we have that the objective function $\left\|\tilde{\boldsymbol{\mathcal{X}}}^\top \boldsymbol{b}\right\|_1$ appearing in (12) and (13) is the sum of the weighted expectations of the function $f_{\boldsymbol{b}}$ under the measures $\mu_{\boldsymbol{\mathcal{O}}}$ and $\mu_{\boldsymbol{\mathcal{X}}}$, i.e.,

$$\left\|\tilde{\boldsymbol{\mathcal{X}}}^\top \boldsymbol{b}\right\|_1 = \left\|\boldsymbol{\mathcal{O}}^\top \boldsymbol{b}\right\|_1 + \left\|\boldsymbol{\mathcal{X}}^\top \boldsymbol{b}\right\|_1 = \sum_{j=1}^{M}\left|\boldsymbol{b}^\top \boldsymbol{o}_j\right| + \sum_{j=1}^{N}\left|\boldsymbol{b}^\top \boldsymbol{x}_j\right| \tag{16}$$

$$= \sum_{j=1}^{M} \int_{\boldsymbol{z}\in\mathbb{S}^{D-1}} \left|\boldsymbol{b}^\top \boldsymbol{z}\right| \delta(\boldsymbol{z}-\boldsymbol{o}_j) d\mu_{\mathbb{S}^{D-1}} + \sum_{j=1}^{N} \int_{\boldsymbol{z}\in\mathbb{S}^{D-1}} \left|\boldsymbol{b}^\top \boldsymbol{z}\right| \delta(\boldsymbol{z}-\boldsymbol{x}_j) d\mu_{\mathbb{S}^{D-1}} \tag{17}$$

$$= \int_{\boldsymbol{z}\in\mathbb{S}^{D-1}} \left|\boldsymbol{b}^\top \boldsymbol{z}\right| \left(\sum_{j=1}^{M} \delta(\boldsymbol{z}-\boldsymbol{o}_j)\right) d\mu_{\mathbb{S}^{D-1}} + \int_{\boldsymbol{z}\in\mathbb{S}^{D-1}} \left|\boldsymbol{b}^\top \boldsymbol{z}\right| \left(\sum_{j=1}^{N} \delta(\boldsymbol{z}-\boldsymbol{x}_j)\right) d\mu_{\mathbb{S}^{D-1}} \tag{18}$$

$$= M\,\mathbb{E}_{\mu_{\boldsymbol{\mathcal{O}}}}(f_{\boldsymbol{b}}) + N\,\mathbb{E}_{\mu_{\boldsymbol{\mathcal{X}}}}(f_{\boldsymbol{b}}). \tag{19}$$

Hence, the optimization problem (12), which we repeat here for convenience,

$$\min_{\boldsymbol{b}} \left\|\tilde{\boldsymbol{\mathcal{X}}}^\top \boldsymbol{b}\right\|_1 \;\; \text{s.t.} \;\; \boldsymbol{b}^\top \boldsymbol{b} = 1, \tag{20}$$

is equivalent to the problem

$$\min_{\boldsymbol{b}} \left[M\,\mathbb{E}_{\mu_{\boldsymbol{\mathcal{O}}}}(f_{\boldsymbol{b}}) + N\,\mathbb{E}_{\mu_{\boldsymbol{\mathcal{X}}}}(f_{\boldsymbol{b}})\right] \;\; \text{s.t.} \;\; \boldsymbol{b}^\top \boldsymbol{b} = 1. \tag{21}$$

Similarly, the recursion (13), repeated here for convenience,

$$\boldsymbol{n}_{k+1} = \operatorname*{argmin}_{\boldsymbol{b}} \left\|\tilde{\boldsymbol{\mathcal{X}}}^\top \boldsymbol{b}\right\|_1 \;\; \text{s.t.} \;\; \boldsymbol{b}^\top \hat{\boldsymbol{n}}_k = 1, \tag{22}$$

is equivalent to the recursion

$$\boldsymbol{n}_{k+1} = \operatorname*{argmin}_{\boldsymbol{b}} \left[M\,\mathbb{E}_{\mu_{\boldsymbol{\mathcal{O}}}}(f_{\boldsymbol{b}}) + N\,\mathbb{E}_{\mu_{\boldsymbol{\mathcal{X}}}}(f_{\boldsymbol{b}})\right] \;\; \text{s.t.} \;\; \boldsymbol{b}^\top \hat{\boldsymbol{n}}_k = 1. \tag{23}$$

Now, the discrete measures $\mu_{\boldsymbol{\mathcal{O}}}, \mu_{\boldsymbol{\mathcal{X}}}$ of (14), are discretizations of the continuous measures $\mu_{\mathbb{S}^{D-1}}$, and $\mu_{\mathbb{S}^{D-1}\cap\mathcal{S}}$ respectively, where the latter is the uniform measure on $\mathbb{S}^{D-1}\cap\mathcal{S}$. Hence, for the purpose of understanding the properties of the global minimizer of (21) and the limiting point of (23), it is meaningful to replace in (21) and (23) the discrete measures $\mu_{\boldsymbol{\mathcal{O}}}$ and $\mu_{\boldsymbol{\mathcal{X}}}$ by their continuous counterparts $\mu_{\mathbb{S}^{D-1}}$ and $\mu_{\mathbb{S}^{D-1}\cap\mathcal{S}}$, and study the resulting *continuous* problems

$$\min_{\boldsymbol{b}} \left[M\,\mathbb{E}_{\mu_{\mathbb{S}^{D-1}}}(f_{\boldsymbol{b}}) + N\,\mathbb{E}_{\mu_{\mathbb{S}^{D-1}\cap\mathcal{S}}}(f_{\boldsymbol{b}})\right] \;\; \text{s.t.} \;\; \boldsymbol{b}^\top \boldsymbol{b} = 1, \tag{24}$$

$$\boldsymbol{n}_{k+1} = \operatorname*{argmin}_{\boldsymbol{b}} \left[M\,\mathbb{E}_{\mu_{\mathbb{S}^{D-1}}}(f_{\boldsymbol{b}}) + N\,\mathbb{E}_{\mu_{\mathbb{S}^{D-1}\cap\mathcal{S}}}(f_{\boldsymbol{b}})\right] \;\; \text{s.t.} \;\; \boldsymbol{b}^\top \hat{\boldsymbol{n}}_k = 1. \tag{25}$$

It is important to note that if these two continuous problems have the geometric properties of interest, i.e., if every global solution of (24) is a vector orthogonal to the inlier subspace, and similarly, if the sequence of vectors $\{\boldsymbol{n}_k\}$ produced by (25) converges to a vector $\boldsymbol{n}_{k^*}$ orthogonal to the inlier subspace, then this *correctness* of the continuous problems can be viewed as a first theoretical verification of the correctness of the *discrete* formulations (12) and (13). The objective of the rest of this section is to establish that this is precisely the case.

Before discussing our main two results in this direction, we note that the continuous objective function

$$\mathcal{J}(\boldsymbol{b}) = M\,\mathbb{E}_{\mu_{\mathbb{S}^{D-1}}}(f_{\boldsymbol{b}}) + N\,\mathbb{E}_{\mu_{\mathbb{S}^{D-1}\cap\mathcal{S}}}(f_{\boldsymbol{b}}) \tag{26}$$

can be re-written in a simple form. Writing $\boldsymbol{b} = \|\boldsymbol{b}\|_2 \hat{\boldsymbol{b}}$, and letting $\boldsymbol{R}$ be a rotation that takes $\hat{\boldsymbol{b}}$ to the first standard basis vector $\boldsymbol{e}_1$, we see that the first expectation in (26) becomes equal to

$$\begin{aligned}
\mathbb{E}_{\mu_{\mathbb{S}^{D-1}}}(f_{\boldsymbol{b}}) &= \int_{\boldsymbol{z}\in\mathbb{S}^{D-1}} f_{\boldsymbol{b}}(\boldsymbol{z}) d\mu_{\mathbb{S}^{D-1}} && (27)\\
&= \int_{\boldsymbol{z}\in\mathbb{S}^{D-1}} \left|\boldsymbol{b}^\top \boldsymbol{z}\right| d\mu_{\mathbb{S}^{D-1}} && (28)\\
&= \|\boldsymbol{b}\|_2 \int_{\boldsymbol{z}\in\mathbb{S}^{D-1}} \left|\hat{\boldsymbol{b}}^\top \boldsymbol{z}\right| d\mu_{\mathbb{S}^{D-1}} && (29)\\
&= \|\boldsymbol{b}\|_2 \int_{\boldsymbol{z}\in\mathbb{S}^{D-1}} \left|\boldsymbol{z}^\top \boldsymbol{R}^{-1}\boldsymbol{R}\hat{\boldsymbol{b}}\right| d\mu_{\mathbb{S}^{D-1}} && (30)\\
&= \|\boldsymbol{b}\|_2 \int_{\boldsymbol{z}\in\mathbb{S}^{D-1}} |\boldsymbol{z}^\top \boldsymbol{e}_1| d\mu_{\mathbb{S}^{D-1}} && (31)\\
&= \|\boldsymbol{b}\|_2 \int_{\boldsymbol{z}\in\mathbb{S}^{D-1}} |z_1| d\mu_{\mathbb{S}^{D-1}} = \|\boldsymbol{b}\|_2 c_D, && (32)
\end{aligned}$$

where $\boldsymbol{z} = (z_1, \ldots, z_D)^\top$ is the coordinate representation of $\boldsymbol{z}$, and c_D is the mean height of the unit hemisphere of $\mathbb{R}^D$, given in closed form by

$$c_D = \frac{(D-2)!!}{(D-1)!!} \cdot \begin{cases} \frac{2}{\pi} & \text{if } D \text{ even}, \\ 1 & \text{if } D \text{ odd}, \end{cases} \tag{33}$$

where the double factorial is defined as

$$k!! := \begin{cases} k(k-2)(k-4)\cdots 4 \cdot 2 & \text{if } k \text{ even}, \\ k(k-2)(k-4)\cdots 3 \cdot 1 & \text{if } k \text{ odd}. \end{cases} \tag{34}$$

To see what the second expectation in (26) evaluates to, decompose $\boldsymbol{b}$ as $\boldsymbol{b} = \pi_{\mathcal{S}}(\boldsymbol{b}) + \pi_{\mathcal{S}^\perp}(\boldsymbol{b})$, and note that because the support of the measure $\mu_{\mathbb{S}^{D-1}\cap\mathcal{S}}$ is contained in $\mathcal{S}$, we must have that

$$\begin{aligned}
\mathbb{E}_{\mu_{\mathbb{S}^{D-1}\cap\mathcal{S}}}(f_{\boldsymbol{b}}) &= \int_{\boldsymbol{z}\in\mathbb{S}^{D-1}} \left|\boldsymbol{b}^\top \boldsymbol{z}\right| d\mu_{\mathbb{S}^{D-1}\cap\mathcal{S}} && (35)\\
&= \int_{\boldsymbol{z}\in\mathbb{S}^{D-1}\cap\mathcal{S}} \left|\boldsymbol{b}^\top \boldsymbol{z}\right| d\mu_{\mathbb{S}^{D-1}\cap\mathcal{S}} && (36)\\
&= \int_{\boldsymbol{z}\in\mathbb{S}^{D-1}\cap\mathcal{S}} \left|(\pi_{\mathcal{S}}(\boldsymbol{b}))^\top \boldsymbol{z}\right| d\mu_{\mathbb{S}^{D-1}\cap\mathcal{S}} && (37)\\
&= \|\pi_{\mathcal{S}}(\boldsymbol{b})\|_2 \int_{\boldsymbol{z}\in\mathbb{S}^{D-1}\cap\mathcal{S}} \left|\left(\widehat{\pi_{\mathcal{S}}(\boldsymbol{b})}\right)^\top \boldsymbol{z}\right| d\mu_{\mathbb{S}^{D-1}\cap\mathcal{S}}. && (38)
\end{aligned}$$

Writing $\boldsymbol{z}'$ and $\boldsymbol{b}'$ for the coordinate representation of $\boldsymbol{z}$ and $\widehat{\pi_{\mathcal{S}}(\boldsymbol{b})}$ with respect to a basis of $\mathcal{S}$, and noting that $\mu_{\mathbb{S}^{D-1}\cap\mathcal{S}} \cong \mu_{\mathbb{S}^{d-1}}$, we have that

$$\int_{\boldsymbol{z}\in\mathbb{S}^{D-1}\cap\mathcal{S}} \left|\left(\widehat{\pi_{\mathcal{S}}(\boldsymbol{b})}\right)^\top \boldsymbol{z}\right| d\mu_{\mathbb{S}^{D-1}\cap\mathcal{S}} = \int_{\boldsymbol{z}'\in\mathbb{S}^{d-1}} \left|\boldsymbol{z}'^\top \boldsymbol{b}'\right| d\mu_{\mathbb{S}^{d-1}} = c_d, \tag{39}$$

where now c_d is the average height of the unit hemisphere of $\mathbb{R}^d$. Finally, noting that

$$\|\pi_{\mathcal{S}}(\boldsymbol{b})\|_2 = \|\boldsymbol{b}\|_2 \cos(\phi), \tag{40}$$

where ϕ is the principal angle of $\boldsymbol{b}$ from the subspace $\mathcal{S}$, we have that

$$\mathbb{E}_{\mu_{\mathbb{S}^{D-1}\cap\mathcal{S}}}(f_{\boldsymbol{b}}) = \|\boldsymbol{b}\|_2\, c_d \cos(\phi). \tag{41}$$

Putting everything together, we arrive at the final form of our continuous objective function:

$$\mathcal{J}(\boldsymbol{b}) = M\,\mathbb{E}_{\mu_{\mathbb{S}^{D-1}}}(f_{\boldsymbol{b}}) + N\,\mathbb{E}_{\mu_{\mathbb{S}^{D-1}\cap\mathcal{S}}}(f_{\boldsymbol{b}}) = \|\boldsymbol{b}\|_2\,(Mc_D + Nc_d\cos(\phi))\,. \tag{42}$$

We are finally in a position to state our main results about the continuous problems (24) and (25); the proofs can be found in §5.1 and §5.2 respectively.

Theorem 4 *Any global solution to problem* (24) *must be orthogonal to* $\mathcal{S}$.

Theorem 5 *Consider the sequence* $\{\boldsymbol{n}_k\}_{k\geq 0}$ *generated by recursion* (25)*,* $\hat{\boldsymbol{n}}_0 \in \mathbb{S}^{D-1}$*. Let* ϕ_0 *be the principal angle of* $\boldsymbol{n}_0$ *from* $\mathcal{S}$*, and define* $\alpha := Nc_d/Mc_D$*. Then, as long as* $\phi_0 > 0$*, the sequence* $\{\boldsymbol{n}_k\}_{k\geq 0}$ *converges to a unit* ℓ_2*-norm element of* $\mathcal{S}^\perp$ *in a finite number* k^* *of iterations, where* $k^* = 0$ *if* $\phi_0 = \pi/2$*,* $k^* = 1$ *if* $\tan(\phi_0) \geq 1/\alpha$*, and* $k^* \leq \left\lceil \frac{\tan^{-1}(1/\alpha)-\phi_0}{\sin^{-1}(\alpha\sin(\phi_0))} \right\rceil + 1$ *otherwise.*

Notice the remarkable fact that according to Theorem 5, the continuous recursion (25) converges to a vector orthogonal to the inlier subspace $\mathcal{S}$ in a *finite* number of steps. Moreover, if the relation

$$\tan(\phi_0) \geq 1/\alpha, \tag{43}$$

holds true, then this convergence occurs in a single step. One way to interpret (43) is to notice that as long as the angle ϕ_0 of the initial estimate $\hat{\boldsymbol{n}}_0$ from the inlier subspace is positive, and for any arbitrary but fixed number of outliers M, there is always a sufficiently large number N of inliers, such that (43) is satisfied and thus convergence occurs in one step. Conversely, for any fixed number of inliers N and outliers M, there is always a sufficiently large angle ϕ_0 such that (43) is true, and thus (25) again converges in a single step. More generally, even when (43) is not true, the larger ϕ_0, N are, the smaller the quantity

$$\left\lceil \frac{\tan^{-1}(1/\alpha) - \phi_0}{\sin^{-1}(\alpha\sin(\phi_0))} \right\rceil \tag{44}$$

is, and thus according to Theorem 4 the faster (25) converges.

4.2 The discrete problem

In this section we analyze the discrete problem (12) and the associated discrete recursion (13), where the adjective *discrete* refers to the fact that (12) and (13) depend on a finite set of points $\tilde{\boldsymbol{\mathcal{X}}} = [\boldsymbol{\mathcal{X}}\,\boldsymbol{\mathcal{O}}]\boldsymbol{\Gamma}$ sampled from the union of the space of outliers $\mathbb{S}^{D-1}$ and the space of inliers $\mathbb{S}^{D-1}\cap\mathcal{S}$. In §4.1 we showed that these problems are discrete versions of the continuous problems (24) and (25), for which we further showed that they possess the geometric property of interest, i.e., every global minimizer of (24) must be an element of $\mathcal{S}^\perp \cap \mathbb{S}^{D-1}$ (Theorem 4) and the recursion (25) produces a sequence of vectors which converges in a finite number of steps to an element of $\mathcal{S}^\perp \cap \mathbb{S}^{D-1}$ (Theorem 5). In this section we show that under some conditions on the uniformity of $\boldsymbol{\mathcal{X}} = [\boldsymbol{x}_1, \ldots, \boldsymbol{x}_N]$ and $\boldsymbol{\mathcal{O}} = [\boldsymbol{o}_1, \ldots, \boldsymbol{o}_M]$, a similar statement holds for problems (12) and (13).

The heart of our analysis framework is to bound the deviation of some underlying geometric quantities, which we call the *average outlier* and the *average inlier with respect to* $\boldsymbol{b}$, from their continuous counterparts. To begin with, recall our discrete objective function

$$\mathcal{J}_{\text{discrete}}(\boldsymbol{b}) = \left\| \tilde{\boldsymbol{\mathcal{X}}}^\top \boldsymbol{b} \right\|_1 = \left\| \boldsymbol{\mathcal{O}}^\top \boldsymbol{b} \right\|_1 + \left\| \boldsymbol{\mathcal{X}}^\top \boldsymbol{b} \right\|_1 \tag{45}$$

and its continuous counterpart

$$\mathcal{J}_{\text{continuous}}(\boldsymbol{b}) = \|\boldsymbol{b}\|_2 \left(M c_D + N c_d \cos(\phi) \right), \tag{46}$$

the latter derived in §4.1, equation (42). Now, notice that the term of the discrete objective that depends on the outliers $\boldsymbol{\mathcal{O}}$ can be written as

$$\left\| \boldsymbol{\mathcal{O}}^\top \boldsymbol{b} \right\|_1 = \sum_{j=1}^{M} \left| \boldsymbol{o}_j^\top \boldsymbol{b} \right| = \sum_{j=1}^{M} \boldsymbol{b}^\top \operatorname{Sign}(\boldsymbol{o}_j^\top \boldsymbol{b}) \boldsymbol{o}_j = M \, \boldsymbol{b}^\top \boldsymbol{o}_{\boldsymbol{b}}, \tag{47}$$

where $\operatorname{Sign}(\cdot)$ is the sign function and

$$\boldsymbol{o}_{\boldsymbol{b}} := \frac{1}{M} \sum_{j=1}^{M} \operatorname{Sign}(\boldsymbol{b}^\top \boldsymbol{o}_j) \boldsymbol{o}_j \tag{48}$$

is the *average outlier with respect to* $\boldsymbol{b}$. Defining a vector valued function $\boldsymbol{f}_{\boldsymbol{b}} : \mathbb{S}^{D-1} \to \mathbb{R}^D$ by $\boldsymbol{z} \in \mathbb{S}^{D-1} \overset{\boldsymbol{f}_{\boldsymbol{b}}}{\longmapsto} \operatorname{Sign}(\boldsymbol{b}^\top \boldsymbol{z}) \boldsymbol{z}$, we notice that

$$\boldsymbol{o}_{\boldsymbol{b}} = \frac{1}{M} \sum_{j=1}^{M} \boldsymbol{f}_{\boldsymbol{b}}(\boldsymbol{o}_j), \tag{49}$$

and so $\boldsymbol{o}_{\boldsymbol{b}}$ is a discrete approximation to the integral $\int_{\boldsymbol{z} \in \mathbb{S}^{D-1}} \boldsymbol{f}_{\boldsymbol{b}}(\boldsymbol{z}) d\mu_{\mathbb{S}^{D-1}}$. The value of that integral is given by the next Lemma, whose proof can be found in §5.3.

Lemma 6 *For any* $\boldsymbol{b} \in \mathbb{S}^{D-1}$ *we have*

$$\int_{\boldsymbol{z} \in \mathbb{S}^{D-1}} \boldsymbol{f}_{\boldsymbol{b}}(\boldsymbol{z}) d\mu_{\mathbb{S}^{D-1}} = \int_{\boldsymbol{z} \in \mathbb{S}^{D-1}} \operatorname{Sign}(\boldsymbol{b}^\top \boldsymbol{z}) \boldsymbol{z} d\mu_{\mathbb{S}^{D-1}} = c_D \, \boldsymbol{b}, \tag{50}$$

where c_D *is defined in* (33).

We define $\epsilon_{\boldsymbol{\mathcal{O}}}$ to be the maximum among all possible approximation errors as $\boldsymbol{b}$ varies on $\mathbb{S}^{D-1}$, i.e.,

$$\epsilon_{\boldsymbol{\mathcal{O}}} := \max_{\boldsymbol{b} \in \mathbb{S}^{D-1}} \|c_D \, \boldsymbol{b} - \boldsymbol{o}_{\boldsymbol{b}}\|_2, \tag{51}$$

and we establish that the more *uniformly distributed* $\boldsymbol{\mathcal{O}}$ is the smaller $\epsilon_{\boldsymbol{\mathcal{O}}}$ becomes.

The notion of uniformity of $\boldsymbol{\mathcal{O}} = [\boldsymbol{o}_1, \ldots, \boldsymbol{o}_M] \subset \mathbb{S}^{D-1}$ that we employ here is a deterministic one, and is captured by the *spherical cap discrepancy* of the set $\boldsymbol{\mathcal{O}}$, defined as (Grabner et al., 1997; Grabner and Tichy, 1993)

$$\mathfrak{S}_D(\boldsymbol{\mathcal{O}}) := \sup_{\mathcal{C}} \left| \frac{1}{M} \sum_{j=1}^{M} \mathbb{I}_{\mathcal{C}}(\boldsymbol{o}_j) - \mu_{\mathbb{S}^{D-1}}(\mathcal{C}) \right|. \tag{52}$$

In (52) the supremum is taken over all spherical caps $\mathcal{C}$ of the sphere $\mathbb{S}^{D-1}$, where a spherical cap is the intersection of $\mathbb{S}^{D-1}$ with a half-space of $\mathbb{R}^D$, and $\mathbb{I}_{\mathcal{C}}(\cdot)$ is the indicator function of $\mathcal{C}$, which takes the value 1 inside $\mathcal{C}$ and zero otherwise. The spherical cap discrepancy $\mathfrak{S}_D(\boldsymbol{\mathcal{O}})$ is precisely the supremum among all errors in approximating integrals of indicator functions of spherical caps via averages of such indicator functions on the point set $\boldsymbol{\mathcal{O}}$. Intuitively, $\mathfrak{S}_D(\boldsymbol{\mathcal{O}})$ captures how close is the discrete measure $\mu_{\boldsymbol{\mathcal{O}}}$ (see equation (14)) associated with $\boldsymbol{\mathcal{O}}$ to the measure $\mu_{\mathbb{S}^{D-1}}$, and we will be referring to $\boldsymbol{\mathcal{O}}$ as being uniformly distributed on $\mathbb{S}^{D-1}$, when $\mathfrak{S}_D(\boldsymbol{\mathcal{O}})$ is small.

As a consequence, to show that uniformly distributed points $\boldsymbol{\mathcal{O}}$ correspond to small $\epsilon_{\boldsymbol{\mathcal{O}}}$, it suffices to bound the maximum integration error $\epsilon_{\boldsymbol{\mathcal{O}}}$ from above by a quantity proportional to the spherical cap discrepancy $\mathfrak{S}_D(\boldsymbol{\mathcal{O}})$. Inequalities that bound from above the approximation error of the integral of a function in terms of the variation of the function and the discrepancy of a finite set of points (not necessarily the spherical cap discrepancy; there are several types of discrepancies) are widely known as *Koksma-Hlawka inequalites* (Kuipers and Niederreiter, 2012; Hlawka, 1971). Even though such inequalities exist and are well-known for integration of functions on the unit hypercube $[0,1]^D$ (Kuipers and Niederreiter, 2012; Hlawka, 1971; Harman, 2010), similar inequalities for integration of functions on the unit sphere $\mathbb{S}^{D-1}$ seem not to be known in general (Grabner and Tichy, 1993), except if one makes additional assumptions on the distribution of the finite set of points (Grabner et al., 1997; Brauchart and Grabner, 2015). Nevertheless, the function $f_{\boldsymbol{b}} : \boldsymbol{z} \longmapsto |\boldsymbol{b}^\top \boldsymbol{z}|$ that is associated to $\epsilon_{\boldsymbol{\mathcal{O}}}$ is simple enough to allow for a Koksma-Hlawka inequality of its own, as described in the next lemma, whose proof can be found in §5.4.

Lemma 7 *Let $\boldsymbol{\mathcal{O}} = [\boldsymbol{o}_1, \ldots, \boldsymbol{o}_M]$ be a finite subset of $\mathbb{S}^{D-1}$. Then*

$$\epsilon_{\boldsymbol{\mathcal{O}}} = \max_{\boldsymbol{b} \in \mathbb{S}^{D-1}} \|c_D \boldsymbol{b} - \boldsymbol{o}_{\boldsymbol{b}}\|_2 \leq \sqrt{5} \mathfrak{S}_D(\boldsymbol{\mathcal{O}}), \tag{53}$$

where $c_D, \boldsymbol{o}_{\boldsymbol{b}}$ and $\mathfrak{S}_D(\boldsymbol{\mathcal{O}})$ are defined in (33)*,* (48) *and* (52) *respectively.*

We now turn our attention to the inlier term $\left\| \tilde{\boldsymbol{\mathcal{X}}}^\top \boldsymbol{b} \right\|_1$ of the discrete objective function (45), which is slightly more complicated than the outlier term. We have

$$\left\| \boldsymbol{\mathcal{X}}^\top \boldsymbol{b} \right\|_1 = \sum_{j=1}^{N} \left| \boldsymbol{x}_j^\top \boldsymbol{b} \right| = \sum_{j=1}^{N} \boldsymbol{b}^\top \operatorname{Sign}(\boldsymbol{x}_j^\top \boldsymbol{b}) \boldsymbol{x}_j = N \, \boldsymbol{b}^\top \boldsymbol{x}_{\boldsymbol{b}}, \tag{54}$$

where

$$\boldsymbol{x}_{\boldsymbol{b}} := \frac{1}{N} \sum_{j=1}^{N} \operatorname{Sign}(\boldsymbol{b}^\top \boldsymbol{x}_j) \boldsymbol{x}_j = \frac{1}{N} \sum_{j=1}^{N} \boldsymbol{f}_{\boldsymbol{b}}(\boldsymbol{x}_j) \tag{55}$$

is the *average inlier with respect to* $\boldsymbol{b}$. Thus, $\boldsymbol{x}_{\boldsymbol{b}}$ is a discrete approximation of the integral

$$\int_{\boldsymbol{x} \in \mathbb{S}^{D-1} \cap \mathcal{S}} \boldsymbol{f}_{\boldsymbol{b}}(\boldsymbol{x}) d\mu_{\mathbb{S}^{D-1}}, \tag{56}$$

whose value is given by the next lemma, proved in §5.5.

Lemma 8 *For any $\boldsymbol{b} \in \mathbb{S}^{D-1}$ we have*

$$\int_{\boldsymbol{x} \in \mathbb{S}^{D-1} \cap \mathcal{S}} \boldsymbol{f}_{\boldsymbol{b}}(\boldsymbol{x}) d\mu_{\mathbb{S}^{D-1}} = \int_{\boldsymbol{x} \in \mathbb{S}^{D-1} \cap \mathcal{S}} \operatorname{Sign}(\boldsymbol{b}^\top \boldsymbol{x}) \boldsymbol{x} d\mu_{\mathbb{S}^{D-1}} = c_d \, \hat{\boldsymbol{v}}, \tag{57}$$

where c_d is given by (33) *after replacing D with d, and $\boldsymbol{v}$ is the orthogonal projection of $\boldsymbol{v}$ onto $\mathcal{S}$.*

Next, we define $\epsilon_{\boldsymbol{\mathcal{X}}}$ to be the maximum among all possible approximation errors as $\boldsymbol{b}$ varies on $\mathbb{S}^{D-1}$, which is the same as the maximum of all approximation errors as $\boldsymbol{b}$ varies on $\mathbb{S}^{D-1} \cap \mathcal{S}$, i.e.,

$$\epsilon_{\boldsymbol{\mathcal{X}}} := \max_{\boldsymbol{b} \in \mathbb{S}^{D-1}} \left\| c_d \, \widehat{\pi_{\mathcal{S}}(\boldsymbol{b})} - \boldsymbol{x}_{\boldsymbol{b}} \right\|_2 = \max_{\boldsymbol{b} \in \mathbb{S}^{D-1} \cap \mathcal{S}} \left\| c_d \, \boldsymbol{b} - \boldsymbol{x}_{\boldsymbol{b}} \right\|_2 . \tag{58}$$

Then an almost identical argument as the one that established Lemma 7 gives that

$$\epsilon_{\boldsymbol{\mathcal{X}}} \leq \sqrt{5} \mathfrak{S}_d(\boldsymbol{\mathcal{X}}), \tag{59}$$

where now the discrepancy $\mathfrak{S}_d(\boldsymbol{\mathcal{X}})$ of the inliers $\boldsymbol{\mathcal{X}}$ is defined exactly as in (52) with the only difference that the supremum is taken over all spherical caps of $\mathbb{S}^{D-1} \cap \mathcal{S} \cong \mathbb{S}^{d-1}$.

Finally, to state our main two results about the discrete problems (12) and (13) we need a definition.

Definition 9 *Given a set $\boldsymbol{Y} = [\boldsymbol{y}_1, \ldots, \boldsymbol{y}_L] \subset \mathbb{S}^{D-1}$ and an integer K, define $\mathcal{R}_{\boldsymbol{Y},K}$ to be the maximum circumradius among all polytopes $\operatorname{Conv}\left(\left\{\pm \boldsymbol{y}_{j_1} \pm \boldsymbol{y}_{j_2} \pm \cdots \pm \boldsymbol{y}_{j_K}\right\}\right)$, where $j_1, \ldots, j_K$ are distinct integers in $[L]$, $\operatorname{Conv}(\cdot)$ indicates the convex hull operator, and the circumradius of a bounded subset of $\mathbb{R}^D$ is the infimum over the radii of all euclidean balls of $\mathbb{R}^D$ that contain that subset.*

The next theorem, proved in §5.6, says that if both inliers and outliers are sufficiently uniformly distributed, i.e., if the uniformity parameters $\epsilon_{\boldsymbol{\mathcal{X}}}, \epsilon_{\boldsymbol{\mathcal{O}}}$ are sufficiently small, then every global solution of (12) must be orthogonal to the inlier subspace $\mathcal{S}$. More precisely,

Theorem 10 *Suppose that the condition*

$$\gamma := \frac{M}{N} < \min \left\{ \frac{c_d - \epsilon_{\boldsymbol{\mathcal{X}}}}{2 \, \epsilon_{\boldsymbol{\mathcal{O}}}}, \frac{c_d - \epsilon_{\boldsymbol{\mathcal{X}}} - \left(\mathcal{R}_{\boldsymbol{\mathcal{O}},K_1} + \mathcal{R}_{\boldsymbol{\mathcal{X}},K_2}\right)/N}{\epsilon_{\boldsymbol{\mathcal{O}}}} \right\}, \tag{60}$$

holds for all positive integers K_1, K_2 such that $K_1 + K_2 = D - 1, K_2 \leq d - 1$. Then any global solution $\boldsymbol{b}^*$ to (12) *must be orthogonal to* $\operatorname{Span}(\boldsymbol{\mathcal{X}})$.

Towards interpreting Theorem 10, consider first the asymptotic case where we allow N and M to go to infinity, while keeping the ratio γ constant. Assuming that both inliers and outliers are perfectly well distributed in the limit, i.e., under the hypothesis that $\lim_{N \to \infty} \mathfrak{S}_d(\boldsymbol{\mathcal{X}}) = 0$ and $\lim_{M \to \infty} \mathfrak{S}_D(\boldsymbol{\mathcal{O}}) = 0$, Lemma 7 and inequality (59) give that $\lim_{N \to \infty} \epsilon_{\boldsymbol{\mathcal{X}}} = 0$ and $\lim_{M \to \infty} \epsilon_{\boldsymbol{\mathcal{O}}} = 0$, in which case (60) is satisfied. This suggests the interesting fact that (12) is possible to give a normal to the inliers even for arbitrarily many outliers, and irrespectively of the subspace dimension d. Along the same lines, for a given γ and under the point set uniformity hypothesis, we can always increase the number of inliers and outliers (thus decreasing $\epsilon_{\boldsymbol{\mathcal{X}}}$ and $\epsilon_{\boldsymbol{\mathcal{O}}}$), while keeping γ constant, until (60) is satisfied, once again indicating that (12) is possible to yield a normal to the space of inliers irrespectively of their intrinsic dimension. Notice that the intrinsic dimension d of the inliers

manifests itself through the quantity c_d, which we recall is a decreasing function of d. Consequently, the smaller d is the larger the RHS of (60) becomes, and so the easier it is to satisfy (60).

A similar phenomenon holds for the case of the recursion of convex relaxations (13). Notice that according to Theorem 4, the continuous recursion converges in a finite number of iterations to a vector that is orthogonal to $\mathrm{Span}(\boldsymbol{\mathcal{X}}) = \mathcal{S}$, as long as the initialization $\hat{\boldsymbol{n}}_0$ does not lie in $\mathcal{S}$ (equivalently $\phi_0 > 0$). Intuitively, one should expect that in passing to the discrete case, the conditions for the *discrete* recursion (13) to be successful, should be at least as strong as the conditions of Theorem 10, and strictly stronger than the condition $\phi_0 > 0$ of Theorem 5. Our next result, proved in §5.7, formalizes this intuition.

Theorem 11 *Suppose that condition* (60) *holds true and consider the vector sequence* $\{\hat{\boldsymbol{n}}_k\}_{k\geq 0}$ *generated by the recursion* (13)*. Let* ϕ_0 *be the principal angle of* $\hat{\boldsymbol{n}}_0$ *from* $\mathrm{Span}(\boldsymbol{\mathcal{X}})$ *and suppose that*

$$\phi_0 > \cos^{-1}\left(\frac{c_d - \epsilon_{\boldsymbol{\mathcal{X}}} - 2\,\gamma\,\epsilon_{\boldsymbol{\mathcal{O}}}}{c_d + \epsilon_{\boldsymbol{\mathcal{X}}}}\right). \tag{61}$$

Then after a finite number of iterations the sequence $\{\hat{\boldsymbol{n}}_k\}_{k\geq 0}$ *converges to a unit* ℓ_2*-norm vector that is orthogonal to* $\mathrm{Span}(\boldsymbol{\mathcal{X}})$.

First note that if (60) is true, then the expression of (61) always defines an angle between 0 and $\pi/2$. Moreover, Theorem 11 can be interpreted using the same asymptotic arguments as Theorem 10; notice in particular that the lower bound on the angle ϕ_0 tends to zero as M, N go to infinity with γ constant, i.e., the more uniformly distributed inliers and outliers are, the closer $\boldsymbol{n}_0$ is allowed to be to $\mathrm{Span}(\boldsymbol{\mathcal{X}})$.

We also emphasize that Theorem 11 asserts the correctness of the linear programming recursions (13) as far as recovering a vector $\boldsymbol{n}_{k^*}$ orthogonal to $\mathcal{S} := \mathrm{Span}(\boldsymbol{\mathcal{X}})$ is concerned. Even though this was our initial motivation for posing problem (12), Theorem 11 does not assert in general that $\boldsymbol{n}_{k^*}$ is a global minimizer of problem (12). However, this is indeed the case, when the inlier subspace $\mathcal{S}$ is a hyperplane, i.e., $d = D - 1$. This is because, up to a sign, there is a unique vector $\boldsymbol{b} \in \mathbb{S}^{D-1}$ that is orthogonal to $\mathcal{S}$ (the normal vector to the hyperplane), which, under conditions (60) and (61), is the unique global minimizer of (12), as well as the limit point $\boldsymbol{n}_{k^*}$ of Theorem 11.

5. Proofs

In this section we provide the proofs of all lemmas and theorems stated in section 4.

5.1 Proof of Theorem 4

Because of the constraint $\boldsymbol{b}^\top \boldsymbol{b} = 1$ in (24), and using (42), problem (24) can be written as

$$\min_{\boldsymbol{b}} \;\; [Mc_D + Nc_d \cos(\phi)] \;\; \text{s.t. } \boldsymbol{b}^\top \boldsymbol{b} = 1. \tag{62}$$

It is then immediate that the global minimum is equal to Mc_D and it is attained if and only if $\phi = \pi/2$, which corresponds to $\boldsymbol{b} \perp \mathcal{S}$.

5.2 Proof of Theorem 5

At iteration k the optimization problem associated with (25) is

$$\min_{\boldsymbol{b}\in\mathbb{R}^D} \ \mathcal{J}(\boldsymbol{b}) = \|\boldsymbol{b}\|_2 \left(Mc_D + Nc_d \cos(\phi)\right) \ \text{ s.t. } \ \boldsymbol{b}^\top \hat{\boldsymbol{n}}_k = 1, \tag{63}$$

where ϕ is the principal angle of $\boldsymbol{b}$ from the subspace $\mathcal{S}$.

Let ϕ_k be the principal angle of $\hat{\boldsymbol{n}}_k$ from $\mathcal{S}$, and let $\boldsymbol{n}_{k+1}$ be a global minimizer of (63), with principal angle from $\mathcal{S}$ equal to ϕ_{k+1}. We show that $\phi_{k+1} \geq \phi_k$. To see this, note that the decrease in the objective function at iteration k is

$$\begin{aligned}\mathcal{J}(\hat{\boldsymbol{n}}_k) - \mathcal{J}(\boldsymbol{n}_{k+1}) :=& M\, c_D\, \|\hat{\boldsymbol{n}}_k\|_2 + N\, c_d\, \|\hat{\boldsymbol{n}}_k\|_2\, \cos(\phi_k) \\ &- M\, c_D\, \|\boldsymbol{n}_{k+1}\|_2 - N\, c_d\, \|\boldsymbol{n}_{k+1}\|_2\, \cos(\phi_{k+1}).\end{aligned} \tag{64}$$

Since $\boldsymbol{n}_{k+1}^\top \hat{\boldsymbol{n}}_k = 1$, we must have that $\|\boldsymbol{n}_{k+1}\|_2 \geq 1 = \|\hat{\boldsymbol{n}}_k\|_2$. Now if $\phi_{k+1} < \phi_k$, then $\cos(\phi_{k+1}) > \cos(\phi_k)$. But then (64) implies that $\mathcal{J}(\boldsymbol{n}_{k+1}) > \mathcal{J}(\hat{\boldsymbol{n}}_k)$, which is a contradiction on the optimality of $\boldsymbol{n}_{k+1}$. Hence it must be the case that $\phi_{k+1} \geq \phi_k$, and so the sequence $\{\phi_k\}_k$ is non-decreasing. In particular, since $\phi_0 > 0$ by hypothesis, we must also have $\phi_k > 0$, i.e., $\hat{\boldsymbol{n}}_k \notin \mathcal{S}$, $\forall k \geq 0$.

Letting ψ_k be the angle of $\boldsymbol{b}$ from $\hat{\boldsymbol{n}}_k$, the constraint $\boldsymbol{b}^\top \hat{\boldsymbol{n}}_k = 1$ gives $0 \leq \psi_k < \pi/2$ and $\|\boldsymbol{b}\|_2 = 1/\cos(\psi_k)$, and so we can write the optimization problem (63) equivalently as

$$\min_{\boldsymbol{b}\in\mathbb{R}^D} \ \frac{Mc_D + Nc_d \cos(\phi)}{\cos(\psi_k)} \ \text{ s.t. } \ \boldsymbol{b}^\top \hat{\boldsymbol{n}}_k = 1. \tag{65}$$

If $\hat{\boldsymbol{n}}_k$ is orthogonal to $\mathcal{S}$, i.e., $\phi_k = \pi/2$, then $\mathcal{J}(\hat{\boldsymbol{n}}_k) = Mc_D \leq \mathcal{J}(\boldsymbol{b})$, $\forall \boldsymbol{b} : \boldsymbol{b}^\top \hat{\boldsymbol{n}}_k = 1$, with equality only if $\boldsymbol{b} = \hat{\boldsymbol{n}}_k$. As a consequence, $\boldsymbol{n}_{k'} = \hat{\boldsymbol{n}}_k$, $\forall k' > k$, and in particular if $\phi_0 = \pi/2$, then $k^* = 0$.

So suppose that $\phi_k < \pi/2$ and let $\hat{\boldsymbol{n}}_k^\perp$ be the normalized orthogonal projection of $\hat{\boldsymbol{n}}_k$ onto $\mathcal{S}^\perp$. We will prove that every global minimizer of problem (65) must lie in the two-dimensional plane $\mathcal{H} := \text{Span}(\hat{\boldsymbol{n}}_k, \hat{\boldsymbol{n}}_k^\perp)$. To see this, let $\boldsymbol{b}$ have norm $1/\cos(\psi_k)$ for some $\psi_k < \pi/2$. If $\psi_k > \pi/2 - \phi_k$, then such a $\boldsymbol{b}$ can not be a global minimizer of (65), as the feasible vector $\hat{\boldsymbol{n}}_k^\perp / \sin(\phi_k) \in \mathcal{H}$ already gives a smaller objective, since

$$\mathcal{J}(\hat{\boldsymbol{n}}_k^\perp / \sin(\phi_k)) = \frac{Mc_D}{\sin(\phi_k)} = \frac{Mc_D}{\cos(\pi/2 - \phi_k)} < \frac{Mc_D + Nc_d \cos(\phi)}{\cos(\psi_k)} = \mathcal{J}(\boldsymbol{b}). \tag{66}$$

Thus, without loss of generality, we may restrict to the case where $\psi_k \leq \pi/2 - \phi_k$. Denote by $\hat{\boldsymbol{h}}_k$ the normalized projection of $\hat{\boldsymbol{n}}_k$ onto $\mathcal{S}$ and by $\hat{\boldsymbol{n}}^\dagger$ the vector that is obtained from $\hat{\boldsymbol{n}}_k$ by rotating it towards $\hat{\boldsymbol{n}}_k^\perp$ by ψ_k. Note that both $\hat{\boldsymbol{h}}_k$ and $\hat{\boldsymbol{n}}_k^\dagger$ lie in $\mathcal{H}$. Letting $\Psi_k \in [0, \pi]$ be the spherical angle between the spherical arc formed by $\hat{\boldsymbol{n}}_k, \hat{\boldsymbol{b}}$ and the spherical arc formed by $\hat{\boldsymbol{n}}_k, \hat{\boldsymbol{h}}_k$, the spherical law of cosines gives

$$\cos(\angle \boldsymbol{b}, \hat{\boldsymbol{h}}_k) = \cos(\phi_k)\cos(\psi_k) + \sin(\phi_k)\sin(\psi_k)\cos(\Psi_k). \tag{67}$$

Now, Ψ_k is equal to π if and only if $\hat{\boldsymbol{n}}_k, \hat{\boldsymbol{h}}_k, \boldsymbol{b}$ are coplanar, i.e., if and only if $\boldsymbol{b} \in \mathcal{H}$. Suppose that $\boldsymbol{b} \notin \mathcal{H}$. Then $\Psi_k < \pi$, and so $\cos(\Psi_k) > -1$, which implies that

$$\cos(\angle \boldsymbol{b}, \hat{\boldsymbol{h}}_k) > \cos(\phi_k)\cos(\psi_k) - \sin(\phi_k)\sin(\psi_k) = \cos(\phi_k + \psi_k). \tag{68}$$

This in turn implies that the principal angle ϕ of $\boldsymbol{b}$ from $\mathcal{S}$ is strictly smaller than $\phi_k + \psi_k$, and so

$$\mathcal{J}(\boldsymbol{b}) = \frac{Mc_D + Nc_d\cos(\phi)}{\cos(\psi_k)} > \frac{Mc_D + Nc_d\cos(\phi_k+\psi_k)}{\cos(\psi_k)} = \mathcal{J}(\hat{\boldsymbol{n}}_k^\dagger/\cos(\psi_k)), \tag{69}$$

i.e., the feasible vector $\hat{\boldsymbol{n}}_k^\dagger/\cos(\psi_k) \in \mathcal{H}$ gives strictly smaller objective than $\boldsymbol{b}$.

To summarize, for the case where $\phi_k < \pi/2$, we have shown that any global minimizer $\boldsymbol{b}$ of (65) must i) have angle ψ_k from $\hat{\boldsymbol{n}}_k$ less or equal to $\pi/2 - \phi_k$, and ii) it must lie in $\mathrm{Span}(\hat{\boldsymbol{n}}_k, \hat{\boldsymbol{n}}_k^\perp)$. Hence, we can rewrite (65) in the equivalent form

$$\min_{\psi\in[-\pi/2+\phi_k,\pi/2-\phi_k]} \mathcal{J}_k(\psi) := \frac{Mc_D + Nc_d\cos(\phi_k+\psi)}{\cos(\psi_k)}, \tag{70}$$

where now ψ_k takes positive values as $\boldsymbol{b}$ approaches $\hat{\boldsymbol{n}}_k^\perp$ and negative values as it approaches $\hat{\boldsymbol{h}}_k$. The function $\mathcal{J}_k$ is continuous and differentiable in the interval $[-\pi/2+\phi_k, \pi/2-\phi_k]$, with derivative given by

$$\frac{\partial \mathcal{J}_k}{\partial \psi} = \frac{Mc_D\sin(\psi) - Nc_d\sin(\phi_k)}{\cos^2(\psi)}. \tag{71}$$

Setting the derivative to zero gives

$$\sin(\psi) = \alpha\sin(\phi_k). \tag{72}$$

If $\alpha\sin(\phi_k) \geq \sin(\pi/2-\phi_k) = \cos(\phi_k)$, or equivalently $\tan(\phi_k) \geq 1/\alpha$, then $\mathcal{J}_k$ is strictly decreasing in the interval $[-\pi/2+\phi_k, \pi/2-\phi_k]$, and so it must attain its minimum precisely at $\psi = \pi/2-\phi_k$, which corresponds to the choice $\boldsymbol{n}_{k+1} = \hat{\boldsymbol{n}}_k^\perp/\sin(\phi_k)$. Then by an earlier argument we must have that $\hat{\boldsymbol{n}}_{k'} \perp \mathcal{S}$, $\forall k' \geq k+1$. If, on the other hand, $\tan(\phi_k) < 1/\alpha$, then the equation (72) defines an angle

$$\psi_k^* := \sin^{-1}(\alpha\sin(\phi_k)) \in (0, \pi/2-\phi_k), \tag{73}$$

at which $\mathcal{J}_k$ must attain its global minimum, since

$$\frac{\partial^2 \mathcal{J}_k}{\partial \psi^2}(\psi_k^*) = \frac{1}{\cos(\psi_k^*)} > 0. \tag{74}$$

As a consequence, if $\tan(\phi_k) < 1/\alpha$, then

$$\phi_{k+1} = \phi_k + \sin^{-1}(\alpha\sin(\phi_k)) < \pi/2. \tag{75}$$

We then see inductively that as long as $\tan(\phi_k) < 1/\alpha$, ϕ_k increases by a quantity which is bounded from below by $\sin^{-1}(\alpha\sin(\phi_0))$. Thus, ϕ_k will keep increasing until it becomes greater than the solution to the equation $\tan(\phi) = 1/\alpha$, at which point the global minimizer will be the vector $\boldsymbol{n}_{k+1} = \hat{\boldsymbol{n}}_k^\perp/\sin(\phi_k)$, and so $\hat{\boldsymbol{n}}_{k'} = \hat{\boldsymbol{n}}_{k+1}$, $\forall k' \geq k+1$. Finally, under the hypothesis that $\phi_k < \tan^{-1}(1/\alpha)$, we have

$$\phi_k = \phi_0 + \sum_{j=0}^{k-1} \sin^{-1}(\alpha\sin(\phi_j)) \geq \phi_0 + k\sin^{-1}(\alpha\sin(\phi_0)), \tag{76}$$

from where it follows that the maximal number of iterations needed for ϕ_k to become larger than $\tan^{-1}(1/\alpha)$ is $\left\lceil \frac{\tan^{-1}(1/\alpha)-\phi_0}{\sin^{-1}(\alpha\sin(\phi_0))} \right\rceil$, at which point at most one more iteration will be needed to achieve orthogonality to $\mathcal{S}$.

5.3 Proof of Lemma 6

Letting $\boldsymbol{R}$ be a rotation that takes $\boldsymbol{b}$ to the first canonical vector $\boldsymbol{e}_1$, i.e., $\boldsymbol{R}\boldsymbol{b} = \boldsymbol{e}_1$, we have that

$$\int_{\boldsymbol{z}\in\mathbb{S}^{D-1}} \text{Sign}(\boldsymbol{b}^\top \boldsymbol{z})\boldsymbol{z} d\mu_{\mathbb{S}^{D-1}} = \int_{\boldsymbol{z}\in\mathbb{S}^{D-1}} \text{Sign}(\boldsymbol{b}^\top \boldsymbol{R}^\top \boldsymbol{R}\boldsymbol{z})\boldsymbol{z} d\mu_{\mathbb{S}^{D-1}} \tag{77}$$

$$= \int_{\boldsymbol{z}\in\mathbb{S}^{D-1}} \text{Sign}(\boldsymbol{e}_1^\top \boldsymbol{z})\boldsymbol{R}^\top \boldsymbol{z} d\mu_{\mathbb{S}^{D-1}} \tag{78}$$

$$= \boldsymbol{R}^\top \int_{\boldsymbol{z}\in\mathbb{S}^{D-1}} \text{Sign}(z_1)\boldsymbol{z} d\mu_{\mathbb{S}^{D-1}}, \tag{79}$$

where z_1 is the first cartesian coordinate of $\boldsymbol{z}$. Recalling the definition of c_D in equation (33), we see that

$$\int_{\boldsymbol{z}\in\mathbb{S}^{D-1}} \text{Sign}(z_1) z_1 d\mu_{\mathbb{S}^{D-1}} = \int_{\boldsymbol{z}\in\mathbb{S}^{D-1}} |z_1| \, d\mu_{\mathbb{S}^{D-1}} = c_D. \tag{80}$$

Moreover, for any $i > 1$, we have

$$\int_{\boldsymbol{z}\in\mathbb{S}^{D-1}} \text{Sign}(z_1) z_i d\mu_{\mathbb{S}^{D-1}} = 0. \tag{81}$$

Consequently, the integral in (79) becomes

$$\int_{\boldsymbol{z}\in\mathbb{S}^{D-1}} \text{Sign}(\boldsymbol{b}^\top \boldsymbol{z})\boldsymbol{z} d\mu_{\mathbb{S}^{D-1}} = \boldsymbol{R}^\top \int_{\boldsymbol{z}\in\mathbb{S}^{D-1}} \text{Sign}(z_1)\boldsymbol{z} d\mu_{\mathbb{S}^{D-1}} \tag{82}$$

$$= \boldsymbol{R}^\top (c_D \boldsymbol{e}_1) = c_D \boldsymbol{b}. \tag{83}$$

5.4 Proof of Lemma 7

For any $\boldsymbol{b} \in \mathbb{S}^{D-1}$ we can write

$$c_D \boldsymbol{b} - \boldsymbol{o}_{\boldsymbol{b}} = \rho_1 \boldsymbol{b} + \rho_2 \boldsymbol{\zeta}, \tag{84}$$

for some vector $\boldsymbol{\zeta} \in \mathbb{S}^{D-1}$ orthogonal to $\boldsymbol{b}$, and so it is enough to show that $\sqrt{\rho_1^2 + \rho_2^2} \leq \sqrt{5}\mathfrak{S}_D(\boldsymbol{\mathcal{O}})$. Let us first bound from above $|\rho_1|$ in terms of $\mathfrak{S}_D(\boldsymbol{\mathcal{O}})$. Towards that end, observe that

$$\rho_1 = \boldsymbol{b}^\top (c_D \boldsymbol{b} - \boldsymbol{o}_{\boldsymbol{b}}) = c_D - \frac{1}{M}\sum_{j=1}^{M} \left|\boldsymbol{b}^\top \boldsymbol{o}_j\right| \tag{85}$$

$$= \int_{\boldsymbol{z}\in\mathbb{S}^{D-1}} f_{\boldsymbol{b}}(\boldsymbol{z}) d\mu_{\mathbb{S}^{D-1}} - \frac{1}{M}\sum_{j=1}^{M} f_{\boldsymbol{b}}(\boldsymbol{o}_j), \tag{86}$$

where the equality follows from the definition of c_D in (33) and recalling that $f_{\boldsymbol{b}}(\boldsymbol{z}) = \left|\boldsymbol{b}^\top \boldsymbol{z}\right|$. In other words, ρ_1 is the error in approximating the integral of $f_{\boldsymbol{b}}$ on $\mathbb{S}^{D-1}$ by the average of $f_{\boldsymbol{b}}$ on the point set $\boldsymbol{\mathcal{O}}$.

Now, notice that each *super-level set* $\left\{\boldsymbol{z} \in \mathbb{S}^{D-1} : f_{\boldsymbol{b}}(\boldsymbol{z}) \geq \alpha\right\}$ for $\alpha \in [0, 1]$, is the union of two spherical caps, and also that

$$\sup_{\boldsymbol{z}\in\mathbb{S}^{D-1}} f_{\boldsymbol{b}}(\boldsymbol{z}) - \inf_{\boldsymbol{z}\in\mathbb{S}^{D-1}} f_{\boldsymbol{b}}(\boldsymbol{z}) = 1 - 0 = 1. \tag{87}$$

We these in mind, repeating the entire argument of the proof of Theorem 1 in (Harman, 2010) that lead to inequality (9) in (Harman, 2010), but now for a measurable function with respect to $\mu_{\mathbb{S}^{D-1}}$ (that would be $f_{\boldsymbol{b}}$), leads directly to

$$|\rho_1| \leq \mathfrak{S}_D(\boldsymbol{\mathcal{O}}). \tag{88}$$

For ρ_2 we have that

$$\rho_2 = \boldsymbol{\zeta}^\top (c_D \boldsymbol{b}) - \boldsymbol{\zeta}^\top \boldsymbol{o_b} \tag{89}$$

$$= \int_{\boldsymbol{z} \in \mathbb{S}^{D-1}} \text{Sign}\left(\boldsymbol{b}^\top \boldsymbol{z}\right) \boldsymbol{\zeta}^\top \boldsymbol{z} d\mu_{\mathbb{S}^{D-1}} - \frac{1}{M} \sum_{j=1}^{M} \text{Sign}\left(\boldsymbol{b}^\top \boldsymbol{o}_j\right) \boldsymbol{\zeta}^\top \boldsymbol{o}_j \tag{90}$$

$$= \int_{\boldsymbol{z} \in \mathbb{S}^{D-1}} g_{\boldsymbol{b},\boldsymbol{\zeta}}(\boldsymbol{z}) d\mu_{\mathbb{S}^{D-1}} - \frac{1}{M} \sum_{j=1}^{M} g_{\boldsymbol{b},\boldsymbol{\zeta}}(\boldsymbol{o}_j), \tag{91}$$

where $g_{\boldsymbol{b},\boldsymbol{\zeta}} : \mathbb{S}^{D-1} \to \mathbb{R}$ is defined as $g_{\boldsymbol{b},\boldsymbol{\zeta}}(\boldsymbol{z}) = \text{Sign}\left(\boldsymbol{b}^\top \boldsymbol{z}\right) \boldsymbol{\zeta}^\top \boldsymbol{z}$. Then a similar argument as for ρ_1, with the difference that now

$$\sup_{\boldsymbol{z} \in \mathbb{S}^{D-1}} g_{\boldsymbol{b},\boldsymbol{\zeta}}(\boldsymbol{z}) - \inf_{\boldsymbol{z} \in \mathbb{S}^{D-1}} g_{\boldsymbol{b},\boldsymbol{\zeta}}(\boldsymbol{z}) = 1 - (-1) = 2, \tag{92}$$

leads to

$$|\rho_2| \leq 2\mathfrak{S}_D(\boldsymbol{\mathcal{O}}). \tag{93}$$

In view of (88), inequality (93) establishes that $\sqrt{\rho_1^2 + \rho_2^2} \leq \sqrt{5}\mathfrak{S}_D(\boldsymbol{\mathcal{O}})$, which concludes the proof of the lemma.

5.5 Proof of Lemma 8

Since $\boldsymbol{x}$ lies in $\mathcal{S}$, we have $\boldsymbol{f_b}(\boldsymbol{x}) = \boldsymbol{f_v}(\boldsymbol{x}) = \boldsymbol{f_{\hat{v}}}(\boldsymbol{x})$, so that

$$\int_{\boldsymbol{x} \in \mathbb{S}^{D-1} \cap \mathcal{S}} \text{Sign}(\boldsymbol{b}^\top \boldsymbol{x}) \boldsymbol{x} d\mu_{\mathbb{S}^{D-1}} = \int_{\boldsymbol{x} \in \mathbb{S}^{D-1} \cap \mathcal{S}} \text{Sign}(\hat{\boldsymbol{v}}^\top \boldsymbol{x}) \boldsymbol{x} d\mu_{\mathbb{S}^{D-1}}. \tag{94}$$

Now express $\boldsymbol{x}$ and $\hat{\boldsymbol{v}}$ on a basis of $\mathcal{S}$, use Lemma 6 replacing D with d, and then switch back to the standard basis of $\mathbb{R}^D$.

5.6 Proof of Theorem 10

To prove the theorem we need two lemmas.

Lemma 12 *Let $\boldsymbol{b} \in \mathbb{S}^{D-1} \setminus \mathcal{S}^\perp$, and let $\phi < \pi/2$ be its principal angle from $\mathcal{S}$. Then*

$$M(c_D + \epsilon_{\boldsymbol{\mathcal{O}}}) \geq \left\| \boldsymbol{\mathcal{O}}^\top \boldsymbol{b} \right\|_1 \geq M(c_D - \epsilon_{\boldsymbol{\mathcal{O}}}), \tag{95}$$

$$N(c_d + \epsilon_{\boldsymbol{\mathcal{X}}}) \cos(\phi) \geq \left\| \boldsymbol{\mathcal{X}}^\top \boldsymbol{b} \right\|_1 \geq N(c_d - \epsilon_{\boldsymbol{\mathcal{X}}}) \cos(\phi). \tag{96}$$

Proof We only prove the second inequality as the first is even simpler. Let $\boldsymbol{v} \neq \boldsymbol{0}$ be the orthogonal projection of $\boldsymbol{b}$ onto $\mathcal{S}$. By definition of $\epsilon_{\boldsymbol{\mathcal{X}}}$, there exists a vector $\boldsymbol{\xi} \in \mathcal{S}$ of ℓ_2 norm less or equal to $\epsilon_{\boldsymbol{\mathcal{X}}}$, such that

$$\boldsymbol{x}_{\boldsymbol{v}} = \boldsymbol{x}_{\boldsymbol{b}} = \frac{1}{N} \sum_{j=1}^{N} \text{Sign}(\boldsymbol{b}^\top \boldsymbol{x}_j) \boldsymbol{x}_j = c_d \hat{\boldsymbol{v}} + \boldsymbol{\xi}. \tag{97}$$

Taking inner product of both sides with $\boldsymbol{b}$ gives

$$\frac{1}{N} \left\| \boldsymbol{\mathcal{X}}^\top \boldsymbol{b} \right\|_1 = c_d \cos(\phi) + \boldsymbol{b}^\top \boldsymbol{\xi}. \tag{98}$$

Now, the result follows by noting that $\left| \boldsymbol{b}^\top \boldsymbol{\xi} \right| \leq \epsilon_{\boldsymbol{\mathcal{X}}} \cos(\phi)$, since the principal angle of $\boldsymbol{b}$ from $\text{Span}(\boldsymbol{\xi})$ can not be less then ϕ. ■

Lemma 13 *Let $\boldsymbol{y}_1, \ldots, \boldsymbol{y}_K$, be K non-zero points of $\mathbb{R}^D$. Then the set of all points of the form $\sum \alpha_k \boldsymbol{y}_k$, where $\alpha_k \in [-1, 1]$, is precisely the convex hull of all points of the form $\pm \boldsymbol{y}_1 \pm \cdots \pm \boldsymbol{y}_K$, i.e.,*

$$\left\{ \sum_{k=1}^{K} \alpha_k \boldsymbol{y}_k : \alpha_k \in [-1, 1] \right\} = \text{Conv}\left(\{ \pm \boldsymbol{y}_1 \pm \cdots \pm \boldsymbol{y}_K \} \right). \tag{99}$$

Proof Let $\boldsymbol{e}_1, \ldots, \boldsymbol{e}_K$ be the standard basis vectors of $\mathbb{R}^K$. Then the hypercube of $\mathbb{R}^K$ with center the origin is precisely the set $\left\{ \sum_{k=1}^{K} \alpha_k \boldsymbol{e}_k : \alpha_k \in [-1, 1] \right\}$, which is equal to the convex hull of its vertices $\pm \boldsymbol{e}_1 \pm \cdots \pm \boldsymbol{e}_K$. Now, let $\boldsymbol{A} : \mathbb{R}^K \to \mathbb{R}^D$ be the linear transformation that takes $\boldsymbol{e}_k$ to $\boldsymbol{y}_k$. Let $\boldsymbol{y} = \sum_k \alpha_k \boldsymbol{y}_k$, for some $\alpha_k \in [-1, 1]$. Then $\boldsymbol{y} = \boldsymbol{A}\left(\sum_k \alpha_k \boldsymbol{e}_k \right)$. But we already know that

$$\sum_k \alpha_k \boldsymbol{e}_k = \sum_{\substack{\sigma_k \in \{-1,1\} \\ k \in [K]}} \gamma_{\sigma_1, \ldots, \sigma_K} (\sigma_1 \boldsymbol{e}_1 + \cdots + \sigma_K \boldsymbol{e}_K), \tag{100}$$

where

$$\sum_{\substack{\sigma_k \in \{-1,1\} \\ k \in [K]}} \gamma_{\sigma_1, \ldots, \sigma_K} = 1, \;\; \gamma_{\sigma_1, \ldots, \sigma_K} > 0, \tag{101}$$

and so

$$\boldsymbol{y} = \sum_k \alpha_k \boldsymbol{y}_k = \boldsymbol{A} \left(\sum_k \alpha_k \boldsymbol{e}_k \right) \tag{102}$$

$$= \boldsymbol{A} \left(\sum_{\substack{\sigma_k \in \{-1,1\} \\ k \in [K]}} \gamma_{\sigma_1, \ldots, \sigma_K} (\sigma_1 \boldsymbol{e}_1 + \cdots + \sigma_K \boldsymbol{e}_K) \right) \tag{103}$$

$$= \sum_{\substack{\sigma_k \in \{-1,1\} \\ k \in [K]}} \gamma_{\sigma_1, \ldots, \sigma_K} (\sigma_1 \boldsymbol{y}_1 + \cdots + \sigma_K \boldsymbol{y}_K), \tag{104}$$

which proves one direction. The other direction is proved in a similar manner. ■

Now, let $\boldsymbol{b}^*$ be an optimal solution of (12), then $\boldsymbol{b}^*$ must satisfy the first order optimality relation

$$\mathbf{0} \in \tilde{\boldsymbol{\mathcal{X}}} \operatorname{Sgn}(\tilde{\boldsymbol{\mathcal{X}}}^\top \boldsymbol{b}^*) + \lambda \boldsymbol{b}^*, \tag{105}$$

where λ is a scalar Lagrange multiplier parameter, and Sgn is the sub-differential of the ℓ_1 norm. For the sake of contradiction, suppose that $\boldsymbol{b}^* \not\perp \mathcal{S}$. Then by the general position hypothesis as well as Lemma 14, $\boldsymbol{b}^*$ will be orthogonal to precisely $D-1$ points, among which K_1 points belong to $\boldsymbol{\mathcal{O}}$, say $\boldsymbol{o}_1, \ldots, \boldsymbol{o}_{K_1}$, and $0 \leq K_2 \leq d-1$ points belong to $\boldsymbol{\mathcal{X}}$, say $\boldsymbol{x}_1, \ldots, \boldsymbol{x}_{K_2}$. Then there must exist real numbers $-1 \leq \alpha_j, \beta_j \leq 1$, such that

$$\sum_{j=1}^{K_1} \alpha_j \boldsymbol{o}_j + \sum_{j=K_1+1}^{M} \operatorname{Sign}(\boldsymbol{o}_j^\top \boldsymbol{b}^*) \boldsymbol{o}_j + \sum_{j=1}^{K_2} \beta_j \boldsymbol{x}_j + \sum_{j=K_2+1}^{N} \operatorname{Sign}(\boldsymbol{x}_j^\top \boldsymbol{b}^*) \boldsymbol{x}_j + \lambda \boldsymbol{b}^* = \mathbf{0}. \tag{106}$$

Since $\operatorname{Sign}(\boldsymbol{o}_j^\top \boldsymbol{b}^*) = 0, \forall j \leq K_1$ and similarly $\operatorname{Sign}(\boldsymbol{x}_j^\top \boldsymbol{b}^*) = 0, \forall j \leq K_2$, we can equivalently write

$$\sum_{j=1}^{K_1} \alpha_j \boldsymbol{o}_j + \sum_{j=1}^{M} \operatorname{Sign}(\boldsymbol{o}_j^\top \boldsymbol{b}^*) \boldsymbol{o}_j + \sum_{j=1}^{K_2} \beta_j \boldsymbol{x}_j + \sum_{j=1}^{N} \operatorname{Sign}(\boldsymbol{x}_j^\top \boldsymbol{b}^*) \boldsymbol{x}_j + \lambda \boldsymbol{b}^* = \mathbf{0} \tag{107}$$

or more compactly

$$\boldsymbol{\xi}_{\boldsymbol{\mathcal{O}}} + M\, \boldsymbol{o}_{\boldsymbol{b}^*} + \boldsymbol{\xi}_{\boldsymbol{\mathcal{X}}} + N\, \boldsymbol{x}_{\hat{\boldsymbol{v}}^*} + \lambda \boldsymbol{b}^* = \mathbf{0}, \tag{108}$$

where by Lemma 13 we have

$$\boldsymbol{\xi}_{\boldsymbol{\mathcal{O}}} := \sum_{j=1}^{K_1} \alpha_j \boldsymbol{o}_j \in \operatorname{Conv}\left(\{\pm \boldsymbol{o}_1 \pm \cdots \pm \boldsymbol{o}_{K_1}\}\right) \tag{109}$$

$$\boldsymbol{\xi}_{\boldsymbol{\mathcal{X}}} := \sum_{j=1}^{K_2} \beta_j \boldsymbol{x}_j \in \operatorname{Conv}\left(\{\pm \boldsymbol{x}_1 \pm \cdots \pm \boldsymbol{x}_{K_2}\}\right), \tag{110}$$

$\hat{\boldsymbol{v}}^*$ is the normalized projection of $\boldsymbol{b}^*$ onto $\mathcal{S}$ (which is nonzero since $\boldsymbol{b}^* \not\perp \mathcal{S}$ by hypothesis), and

$$\boldsymbol{o}_{\boldsymbol{b}^*} := \frac{1}{M} \sum_{j=1}^{M} \operatorname{Sign}(\boldsymbol{o}_j^\top \boldsymbol{b}^*), \quad \boldsymbol{x}_{\boldsymbol{v}^*} := \frac{1}{N} \sum_{j=1}^{N} \operatorname{Sign}(\boldsymbol{x}_j^\top \boldsymbol{v}^*). \tag{111}$$

Now, from the definitions of $\epsilon_{\boldsymbol{\mathcal{O}}}$ and $\epsilon_{\boldsymbol{\mathcal{X}}}$ in (51) and (58) respectively, we have that

$$\boldsymbol{o}_{\boldsymbol{b}^*} = c_D\, \boldsymbol{b}^* + \boldsymbol{\eta}_{\boldsymbol{\mathcal{O}}}, \;\; ||\boldsymbol{\eta}_{\boldsymbol{\mathcal{O}}}||_2 \leq \epsilon_{\boldsymbol{\mathcal{O}}} \tag{112}$$

$$\boldsymbol{x}_{\hat{\boldsymbol{v}}^*} = c_d\, \hat{\boldsymbol{v}}^* + \boldsymbol{\eta}_{\boldsymbol{\mathcal{X}}}, \;\; ||\boldsymbol{\eta}_{\boldsymbol{\mathcal{X}}}||_2 \leq \epsilon_{\boldsymbol{\mathcal{X}}}, \tag{113}$$

and so (108) becomes

$$\boldsymbol{\xi}_{\boldsymbol{\mathcal{O}}} + M\, c_D\, \boldsymbol{b}^* + M\, \boldsymbol{\eta}_{\boldsymbol{\mathcal{O}}} + \boldsymbol{\xi}_{\boldsymbol{\mathcal{X}}} + N\, c_d\, \hat{\boldsymbol{v}}^* + N\, \boldsymbol{\eta}_{\boldsymbol{\mathcal{X}}} + \lambda \boldsymbol{b}^* = \mathbf{0}. \tag{114}$$

Define $\mathcal{U} := \text{Span}\,(\boldsymbol{b}^*, \hat{\boldsymbol{v}}^*)$ and project (114) onto $\mathcal{U}$ to get

$$\pi_{\mathcal{U}}(\boldsymbol{\xi}_{\boldsymbol{\mathcal{O}}}) + M\, c_D\, \boldsymbol{b}^* + M\, \pi_{\mathcal{U}}(\boldsymbol{\eta}_{\boldsymbol{\mathcal{O}}}) + \pi_{\mathcal{U}}(\boldsymbol{\xi}_{\boldsymbol{\mathcal{X}}}) + N\, c_d\, \hat{\boldsymbol{v}}^* + N\, \pi_{\mathcal{U}}(\boldsymbol{\eta}_{\boldsymbol{\mathcal{X}}}) + \lambda \boldsymbol{b}^* = \boldsymbol{0}. \tag{115}$$

Now suppose that $\boldsymbol{b}^* \in \mathcal{S}$, in which case $\boldsymbol{b}^* = \hat{\boldsymbol{v}}^*$. Then using Lemma 12, we have

$$\begin{aligned} M\, c_D + M\, \epsilon_{\boldsymbol{\mathcal{O}}} &\geq \min_{\boldsymbol{b} \perp \mathcal{S}, \boldsymbol{b}^\top \boldsymbol{b} = 1} \left\| \boldsymbol{\mathcal{O}}^\top \boldsymbol{b} \right\|_1 \geq \left\| \boldsymbol{\mathcal{O}}^\top \boldsymbol{b}^* \right\|_1 + \left\| \boldsymbol{\mathcal{X}}^\top \boldsymbol{b}^* \right\|_1 \\ &\geq M\, c_D - M\, \epsilon_{\boldsymbol{\mathcal{O}}} + N\, c_d - N\, \epsilon_{\boldsymbol{\mathcal{X}}}, \end{aligned} \tag{116}$$

which violates hypothesis (60). Consequently, it must be the case that $\boldsymbol{b}^* \notin \mathcal{S}$, and so there exists a vector $\hat{\boldsymbol{\zeta}} \in \mathcal{U}$ that is orthogonal to $\boldsymbol{b}^*$ but not orthogonal to $\hat{\boldsymbol{v}}^*$.

Notice that every vector $\boldsymbol{u}$ in the image of $\pi_{\mathcal{U}}$ can be written as a linear combination of $\boldsymbol{b}^*$ and $\hat{\boldsymbol{v}}^*$: $\boldsymbol{u} = [\boldsymbol{u}]_{\boldsymbol{b}^*}\, \boldsymbol{b}^* + [\boldsymbol{u}]_{\hat{\boldsymbol{v}}^*}\, \hat{\boldsymbol{v}}^*$. Using this decomposition, we can write (115) as

$$\begin{aligned} &[\pi_{\mathcal{U}}(\boldsymbol{\xi}_{\boldsymbol{\mathcal{O}}})]_{\boldsymbol{b}^*}\, \boldsymbol{b}^* + [\pi_{\mathcal{U}}(\boldsymbol{\xi}_{\boldsymbol{\mathcal{O}}})]_{\hat{\boldsymbol{v}}^*}\, \hat{\boldsymbol{v}}^* + M\, c_D\, \boldsymbol{b}^* \\ &+ M\, [\pi_{\mathcal{U}}(\boldsymbol{\eta}_{\boldsymbol{\mathcal{O}}})]_{\boldsymbol{b}^*}\, \boldsymbol{b}^* + M\, [\pi_{\mathcal{U}}(\boldsymbol{\eta}_{\boldsymbol{\mathcal{O}}})]_{\hat{\boldsymbol{v}}^*}\, \hat{\boldsymbol{v}}^* \\ &+ [\pi_{\mathcal{U}}(\boldsymbol{\xi}_{\boldsymbol{\mathcal{X}}})]_{\boldsymbol{b}^*}\, \boldsymbol{b}^* + [\pi_{\mathcal{U}}(\boldsymbol{\xi}_{\boldsymbol{\mathcal{X}}})]_{\hat{\boldsymbol{v}}^*}\, \hat{\boldsymbol{v}}^* + N\, c_d\, \hat{\boldsymbol{v}}^* \\ &+ N\, [\pi_{\mathcal{U}}(\boldsymbol{\eta}_{\boldsymbol{\mathcal{X}}})]_{\boldsymbol{b}^*}\, \boldsymbol{b}^* + N\, [\pi_{\mathcal{U}}(\boldsymbol{\eta}_{\boldsymbol{\mathcal{X}}})]_{\hat{\boldsymbol{v}}^*}\, \hat{\boldsymbol{v}}^* + \lambda \boldsymbol{b}^* = \boldsymbol{0}. \end{aligned} \tag{117}$$

Projecting the above equation onto the line spanned by $\hat{\boldsymbol{\zeta}}$, we obtain the one-dimensional equation

$$([\pi_{\mathcal{U}}(\boldsymbol{\xi}_{\boldsymbol{\mathcal{O}}})]_{\hat{\boldsymbol{v}}^*} + M\, [\pi_{\mathcal{U}}(\boldsymbol{\eta}_{\boldsymbol{\mathcal{O}}})]_{\hat{\boldsymbol{v}}^*} + [\pi_{\mathcal{U}}(\boldsymbol{\xi}_{\boldsymbol{\mathcal{X}}})]_{\hat{\boldsymbol{v}}^*} + N\, c_d + N\, [\pi_{\mathcal{U}}(\boldsymbol{\eta}_{\boldsymbol{\mathcal{X}}})]_{\hat{\boldsymbol{v}}^*}) \cdot \hat{\boldsymbol{\zeta}}^\top \hat{\boldsymbol{v}}^* = 0. \tag{118}$$

Since $\hat{\boldsymbol{\zeta}}$ is not orthogonal to $\hat{\boldsymbol{v}}^*$, the above equation implies that

$$[\pi_{\mathcal{U}}(\boldsymbol{\xi}_{\boldsymbol{\mathcal{O}}})]_{\hat{\boldsymbol{v}}^*} + M\, [\pi_{\mathcal{U}}(\boldsymbol{\eta}_{\boldsymbol{\mathcal{O}}})]_{\hat{\boldsymbol{v}}^*} + [\pi_{\mathcal{U}}(\boldsymbol{\xi}_{\boldsymbol{\mathcal{X}}})]_{\hat{\boldsymbol{v}}^*} + N\, c_d + N\, [\pi_{\mathcal{U}}(\boldsymbol{\eta}_{\boldsymbol{\mathcal{X}}})]_{\hat{\boldsymbol{v}}^*} = 0, \tag{119}$$

which, together with $\|\boldsymbol{\xi}_{\boldsymbol{\mathcal{O}}}\|_2 \leq \mathcal{R}_{\boldsymbol{\mathcal{O}},K_1}$, $\|\boldsymbol{\xi}_{\boldsymbol{\mathcal{X}}}\|_2 \leq \mathcal{R}_{\boldsymbol{\mathcal{X}},K_2}$, $\|\boldsymbol{\eta}_{\boldsymbol{\mathcal{O}}}\|_2 \leq \epsilon_{\boldsymbol{\mathcal{O}}}$ and $\|\boldsymbol{\eta}_{\boldsymbol{\mathcal{X}}}\|_2 \leq \epsilon_{\boldsymbol{\mathcal{X}}}$, implies that

$$N\, c_d \leq \mathcal{R}_{\boldsymbol{\mathcal{O}},K_1} + M\, \epsilon_{\boldsymbol{\mathcal{O}}} + \mathcal{R}_{\boldsymbol{\mathcal{X}},K_2} + N\, \epsilon_{\boldsymbol{\mathcal{X}}}, \tag{120}$$

which violates the hypothesis (60). Consequently, the initial hypothesis of the proof that $\boldsymbol{b}^* \not\perp \mathcal{S}$ can not be true, and the theorem is proved.

A Geometric View of the Proof of Theorem 10. Let us provide some geometric intuition that underlies the proof of Theorem 10. It is instructive to begin our discussion by considering the case $d = 1, D = 2$, i.e. the inlier space is simply a line and the ambient space is a 2-dimensional plane. Since all points have unit ℓ_2-norm, every column of $\boldsymbol{\mathcal{X}}$ will be of the form $\hat{\boldsymbol{x}}$ or $-\hat{\boldsymbol{x}}$ for a fixed vector $\hat{\boldsymbol{x}} \in \mathcal{S}^1$ that spans the inlier space $\mathcal{S}$. In this setting, let us examine a global solution $\boldsymbol{b}^*$ of the optimization problem (12). We will start by assuming that such a $\boldsymbol{b}^*$ is not orthogonal to $\mathcal{S}$, and intuitively arrive at the conclusion that this can not be the case as long as there are *sufficiently many* inliers.

We will argue on an intuitive level that if $\boldsymbol{b}^* \not\perp \mathcal{S}$, then the principal angle ϕ of $\boldsymbol{b}^*$ from $\mathcal{S}$ needs to be small. To see this, suppose $\boldsymbol{b}^* \not\perp \mathcal{S}$; then $\boldsymbol{b}^*$ will be non-orthogonal to every inlier, and by Lemma 14 orthogonal to $D - 1 = 1$ outlier, say $\boldsymbol{o}_1$. The optimality condition (105) specializes to

$$\alpha_1 \boldsymbol{o}_1 + \underbrace{\sum_{j=1}^{M} \text{Sign}(\boldsymbol{o}_j^\top \boldsymbol{b}^*) \boldsymbol{o}_j}_{M \boldsymbol{o}_{\boldsymbol{b}^*}} + \sum_{j=1}^{N} \text{Sign}(\boldsymbol{x}_j^\top \boldsymbol{b}^*) \boldsymbol{x}_j + \lambda \boldsymbol{b}^* = \boldsymbol{0}, \tag{121}$$

where $-1 \leq \alpha_1 \leq 1$. Notice that the third term is simply $N\ \text{Sign}(\hat{\boldsymbol{x}}^\top \boldsymbol{b}^*)\hat{\boldsymbol{x}}$, and so

$$\alpha_1 \boldsymbol{o}_1 + M\,\boldsymbol{o}_{\boldsymbol{b}^*} + \lambda \boldsymbol{b}^* = -N\ \text{Sign}(\hat{\boldsymbol{x}}^\top \boldsymbol{b}^*)\hat{\boldsymbol{x}}. \tag{122}$$

Now, what (122) is saying is that the point $-N\ \text{Sign}(\hat{\boldsymbol{x}}^\top \boldsymbol{b}^*)\hat{\boldsymbol{x}}$ must lie inside the set

$$\text{Conv}(\pm \boldsymbol{o}_1) + \{M\boldsymbol{o}_{\boldsymbol{b}^*}\} + \text{Span}(\boldsymbol{b}^*) = \{\alpha_1 \boldsymbol{o}_1 + M\boldsymbol{o}_{\boldsymbol{b}^*} + \lambda \boldsymbol{b}^* : |\alpha_1| \leq 1, \lambda \in \mathbb{R}\}, \tag{123}$$

where the $+$ operator on sets is the Minkowski sum. Notice that the set $\text{Conv}(\pm \boldsymbol{o}_1) + M\boldsymbol{o}_{\boldsymbol{b}^*}$ is the translation of the line segment (polytope) $\text{Conv}(\pm \boldsymbol{o}_1)$ by $M\boldsymbol{o}_{\boldsymbol{b}^*}$. Then (122) says that if we draw all affine lines that originate from every point of $\text{Conv}(\pm \boldsymbol{o}_1) + M\boldsymbol{o}_{\boldsymbol{b}^*}$ and have direction $\boldsymbol{b}^*$, then one of these lines must meet the point $-N\ \text{Sign}(\hat{\boldsymbol{x}}^\top \boldsymbol{b}^*)\hat{\boldsymbol{x}}$. Let us illustrate this for the case where $M = N = 5$ and say it so happens that $\boldsymbol{b}^*$ has a rather large angle ϕ from $\mathcal{S}$, say $\phi = 45°$. Recall that $\boldsymbol{o}_{\boldsymbol{b}^*}$ is concentrated around $\boldsymbol{c}_D\, \boldsymbol{b}^*$ and for the case $D = 2$ we have $c_D = \frac{2}{\pi}$. As illustrated in

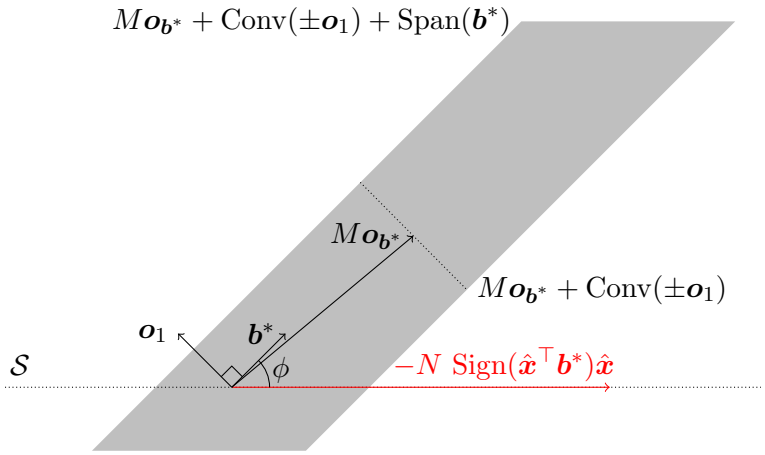

Figure 1: Geometry of the optimality condition (105) and (122) for the case $d = 1, D = 2, M = N = 5$. The polytope $M\boldsymbol{o}_{\boldsymbol{b}^*} + \text{Conv}(\pm \boldsymbol{o}_1) + \text{Span}(\boldsymbol{b}^*)$ misses the point $-N\ \text{Sign}(\hat{\boldsymbol{x}}^\top \boldsymbol{b}^*)\hat{\boldsymbol{x}}$ and so the optimality condition can not be true for both $\boldsymbol{b}^* \not\perp \mathcal{S} = \text{Span}(\hat{\boldsymbol{x}})$ and ϕ large.

Figure 1, because ϕ is large, the unbounded polytope $M\boldsymbol{o}_{\boldsymbol{b}^*} + \text{Conv}(\pm \boldsymbol{o}_1) + \text{Span}(\boldsymbol{b}^*)$ misses the point $-N\ \text{Sign}(\hat{\boldsymbol{x}}^\top \boldsymbol{b}^*)\hat{\boldsymbol{x}}$ thus making the optimality equation (122) infeasible. This indicates that critical vectors $\boldsymbol{b}^* \not\perp \mathcal{S}$ having large angles from $\mathcal{S}$ are unlikely to exist.

On the other hand, critical points $\boldsymbol{b}^* \not\perp \mathcal{S}$ may exist, but their angle ϕ from $\mathcal{S}$ needs to be small, as illustrated in Figure 2. However, such critical points can not be global minimizers, because small angles from $\mathcal{S}$ yield large objective values.[6]

Hence the only possibility that critical points $\boldsymbol{b}^* \not\perp \mathcal{S}$ that are also global minimizers do exist is that the number of inliers is significantly less than the number of outliers, i.e. $N << M$, as illustrated in Figure 3. The precise notion of how many inliers should exist with respect to outliers is captured by condition (60) of Theorem 10.

6. On a more techincal level, it can be verified that if such a critical point is a global minimizer, then its angle ϕ must be large in the sense that $\cos(\phi) \leq 2\epsilon_{\boldsymbol{\mathcal{O}}}$, contradicting the necessary condition that ϕ be small in the first place.

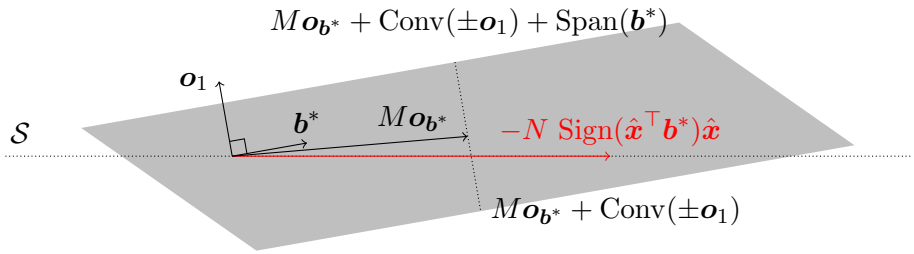

Figure 2: Geometry of the optimality condition (105) and (122) for the case $d = 1, D = 2, M = N = 5$. A critical $\boldsymbol{b}^* \not\perp \mathcal{S}$ exists, but its angle from $\mathcal{S}$ is small, so that the polytope $M\boldsymbol{o}_{\boldsymbol{b}^*} + \mathrm{Conv}(\pm\boldsymbol{o}_1) + \mathrm{Span}(\boldsymbol{b}^*)$ can contain the point $-N\ \mathrm{Sign}(\hat{\boldsymbol{x}}^\top \boldsymbol{b}^*)\hat{\boldsymbol{x}}$. However, $\boldsymbol{b}^*$ can not be a global minimizer, since small angles from $\mathcal{S}$ yield large objective values.

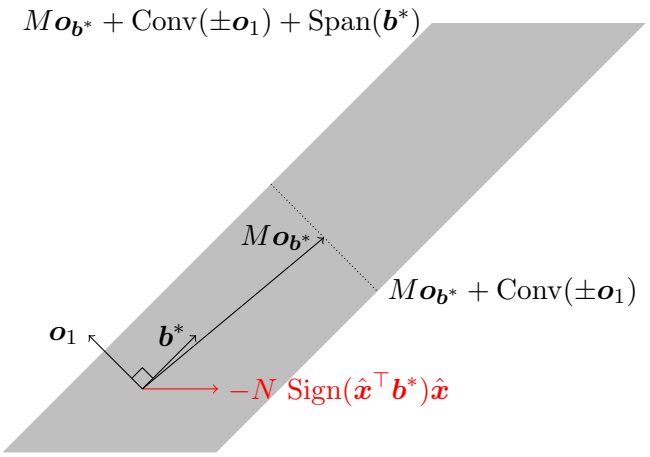

Figure 3: Geometry of the optimality condition (105) and (122) for the case $d = 1, D = 2, N << M$. Critical points $\boldsymbol{b}^* \not\perp \mathcal{S}$ do exist and moreover they can have large angle from $\mathcal{S}$. This is because N is small and so the polytope $M\boldsymbol{o}_{\boldsymbol{b}^*} + \mathrm{Conv}(\pm\boldsymbol{o}_1) + \mathrm{Span}(\boldsymbol{b}^*)$ contains the point $-N\ \mathrm{Sign}(\hat{\boldsymbol{x}}^\top \boldsymbol{b}^*)\hat{\boldsymbol{x}}$. Moreover, such critical points can be global minimizers. Condition (60) of Theorem 10 prevents such cases from occuring.

We should note here that the picture for the general setting is analogous to what we described above, albeit harder to visualize: with reference to equation (107), the optimality condition says that every feasible point $\boldsymbol{b}^* \not\perp \mathcal{S}$ must have the following property: there exist $0 \leq K_2 \leq d-1$ inliers $\boldsymbol{x}_1, \ldots, \boldsymbol{x}_{K_2}$ and $0 \leq K_1 \leq D-1-K_2$ outliers $\boldsymbol{o}_1, \ldots, \boldsymbol{o}_{K_1}$ to which $\boldsymbol{b}^*$ is orthogonal, and two points $\boldsymbol{\xi}_{\mathcal{O}} \in \mathrm{Conv}(\pm\boldsymbol{o}_1 \pm \cdots \pm \boldsymbol{o}_{K_1}) + \boldsymbol{o}_{\boldsymbol{b}^*}$ and $\boldsymbol{\xi}_{\mathcal{X}} \in \mathrm{Conv}(\pm\boldsymbol{x}_1 \pm \cdots \pm \boldsymbol{x}_{K_2}) + \boldsymbol{x}_{\boldsymbol{b}^*}$ that are joined by an affine line that is parallel to the line spanned by $\boldsymbol{b}^*$. In fact in our proof of Theorem 10 we reduced this general case to the case $d = 1, D = 2$ described above: this reduction is precisely taking place in equation (115), where we project the optimality equation onto the 2-dimensional subspace $\mathcal{U}$. The arguments that follow this projection consist of nothing more than a technical treatment of the intuition given above.

5.7 Proof of Theorem 11

We start by establishing that $\hat{\boldsymbol{n}}_k$ does not lie in the inlier space $\mathcal{S}$. For the sake of contradiction suppose that $\hat{\boldsymbol{n}}_k \in \mathcal{S}$ for some $k > 0$. Note that

$$\left\|\tilde{\boldsymbol{\mathcal{X}}}^\top \hat{\boldsymbol{n}}_0\right\|_1 \geq \left\|\tilde{\boldsymbol{\mathcal{X}}}^\top \boldsymbol{n}_1\right\|_1 \geq \left\|\tilde{\boldsymbol{\mathcal{X}}}^\top \hat{\boldsymbol{n}}_1\right\|_1 \geq \cdots \geq \left\|\tilde{\boldsymbol{\mathcal{X}}}^\top \hat{\boldsymbol{n}}_k\right\|_1. \tag{124}$$

Suppose first that $\hat{\boldsymbol{n}}_0 \perp \mathcal{S}$. Then (124) gives

$$\left\|\boldsymbol{\mathcal{O}}^\top \hat{\boldsymbol{n}}_0\right\|_1 \geq \left\|\boldsymbol{\mathcal{O}}^\top \hat{\boldsymbol{n}}_k\right\|_1 + \left\|\boldsymbol{\mathcal{X}}^\top \hat{\boldsymbol{v}}_k\right\|_1, \tag{125}$$

where $\hat{\boldsymbol{v}}_k$ is the normalized projection of $\hat{\boldsymbol{n}}_k$ onto $\mathcal{S}$ (and since $\hat{\boldsymbol{n}}_k \in \mathcal{S}$, these two are equal). Using Lemma 12, we take an upper bound of the LHS and a lower bound of the RHS of (125), and obtain

$$M\, c_D + M\, \epsilon_{\boldsymbol{\mathcal{O}}} \geq M\, c_D - M\, \epsilon_{\boldsymbol{\mathcal{O}}} + N\, c_d - N\, \epsilon_{\boldsymbol{\mathcal{X}}}, \tag{126}$$

or equivalently

$$\gamma \geq \frac{c_d - \epsilon_{\boldsymbol{\mathcal{X}}}}{2\, \epsilon_{\boldsymbol{\mathcal{O}}}}, \tag{127}$$

which contradicts (60). Consequently, $\hat{\boldsymbol{n}}_0 \not\perp \mathcal{S}$. Then (124) implies that

$$\left\|\boldsymbol{\mathcal{O}}^\top \hat{\boldsymbol{n}}_0\right\|_1 + \left\|\boldsymbol{\mathcal{X}}^\top \hat{\boldsymbol{n}}_0\right\|_1 \geq \left\|\boldsymbol{\mathcal{O}}^\top \hat{\boldsymbol{n}}_k\right\|_1 + \left\|\boldsymbol{\mathcal{X}}^\top \hat{\boldsymbol{n}}_k\right\|_1, \tag{128}$$

or equivalently

$$\left\|\boldsymbol{\mathcal{O}}^\top \hat{\boldsymbol{n}}_0\right\|_1 + \cos(\phi_0) \left\|\boldsymbol{\mathcal{X}}^\top \hat{\boldsymbol{v}}_0\right\|_1 \geq \left\|\boldsymbol{\mathcal{O}}^\top \hat{\boldsymbol{n}}_k\right\|_1 + \left\|\boldsymbol{\mathcal{X}}^\top \hat{\boldsymbol{v}}_k\right\|_1, \tag{129}$$

where $\hat{\boldsymbol{v}}_0$ is the normalized projection of $\hat{\boldsymbol{n}}_0$ onto $\mathcal{S}$. Once again, Lemma 12 is used to furnish an upper bound of the LHS and a lower bound of the RHS of (129), and yield

$$M\, c_D + M\, \epsilon_{\boldsymbol{\mathcal{O}}} + (N\, c_d + N\, \epsilon_{\boldsymbol{\mathcal{X}}}) \cos(\phi_0) \geq M\, c_D - M\, \epsilon_{\boldsymbol{\mathcal{O}}} + N\, c_d - N\, \epsilon_{\boldsymbol{\mathcal{X}}}, \tag{130}$$

which contradicts (61).

Now let us complete the proof of the theorem. We know by Lemma 16 that the sequence $\{\boldsymbol{n}_k\}$ converges to a critical point $\boldsymbol{n}_{k^*}$ of problem (12) in a finite number of steps, and we have already shown that $\boldsymbol{n}_{k^*} \notin \mathcal{S}$ (see the beginning of the current proof). Then an identical argument as in the proof of Theorem 10 (with $\boldsymbol{n}_{k^*}$ in place of $\boldsymbol{b}^*$) shows that $\boldsymbol{n}_{k^*}$ must be orthogonal to $\mathcal{S}$.

6. Algorithmic Contributions

In this section we discuss algorithmic formulations based on the ideas presented so far. Specifically, Section 6.1 contains the basic Dual Principal Component Pursuit and Analysis algorithms, which can be implemented by linear programming, while Section 6.2 discusses alternative DPCP algorithms suitable for noisy or high-dimensional data.

Algorithm 1 Relaxed Dual Principal Component Pursuit

procedure DPCP-r($\tilde{\boldsymbol{\mathcal{X}}}, \varepsilon, T_{\max}$)
  $k \leftarrow 0; \Delta\mathcal{J} \leftarrow \infty;$
  $\hat{\boldsymbol{n}}_0 \leftarrow \operatorname{argmin}_{\|\boldsymbol{b}\|_2=1} \left\|\tilde{\boldsymbol{\mathcal{X}}}^\top \boldsymbol{b}\right\|_2;$
  while $k < T_{\max}$ and $\Delta\mathcal{J} > \varepsilon$ **do**
    $k \leftarrow k+1;$
    $\boldsymbol{n}_k \leftarrow \operatorname{argmin}_{\boldsymbol{b}^\top \hat{\boldsymbol{n}}_{k-1}=1} \left\|\tilde{\boldsymbol{\mathcal{X}}}^\top \boldsymbol{b}\right\|_1;$
    $\Delta\mathcal{J} \leftarrow \left(\left\|\tilde{\boldsymbol{\mathcal{X}}}^\top \hat{\boldsymbol{n}}_{k-1}\right\|_1 - \left\|\tilde{\boldsymbol{\mathcal{X}}}^\top \hat{\boldsymbol{n}}_k\right\|_1\right) / \left(\left\|\tilde{\boldsymbol{\mathcal{X}}}^\top \hat{\boldsymbol{n}}_{k-1}\right\|_1 + 10^{-9}\right);$
  end while
  return $\hat{\boldsymbol{n}}_k;$
end procedure

6.1 Relaxed DPCP and DPCA algorithms

Theorem 11 suggests a mechanism for obtaining an element $\boldsymbol{b}_1$ of $\mathcal{S}^\perp$, where $\mathcal{S} = \operatorname{Span}(\boldsymbol{\mathcal{X}})$: run the sequence of linear programs (13) until the sequence $\hat{\boldsymbol{n}}_k$ converges and identify the limit point with $\boldsymbol{b}_1$. Due to computational constraints, in practice one usually terminates the recursions when the objective value $\left\|\tilde{\boldsymbol{\mathcal{X}}}^\top \hat{\boldsymbol{n}}_k\right\|_1$ converges within some small ε, or a maximal number $T_{\max}$ of recursions is reached, and obtains an approximately normal vector $\boldsymbol{b}_1$. The resulting Algorithm 1 is referred to as *DPCP-r*, which stands for *relaxed DPCP*.

We emphasize that step 6 of Algorithm 1 can be canonically solved by linear programming. More specifically, we can rewrite it in the form

$$\min_{\boldsymbol{b},\boldsymbol{u}^+,\boldsymbol{u}^-} \begin{bmatrix}\boldsymbol{1}_{1\times N} & \boldsymbol{1}_{1\times N}\end{bmatrix} \begin{bmatrix}\boldsymbol{u}^+ \\ \boldsymbol{u}^-\end{bmatrix}, \text{ such that} \tag{131}$$

$$\begin{bmatrix}\boldsymbol{I}_N & -\boldsymbol{I}_N & -\tilde{\boldsymbol{\mathcal{X}}}^\top \\ \boldsymbol{0}_{1\times N} & \boldsymbol{0}_{1\times N} & \hat{\boldsymbol{n}}_k^\top\end{bmatrix} \begin{bmatrix}\boldsymbol{u}^+ \\ \boldsymbol{u}^- \\ \boldsymbol{b}\end{bmatrix} = \begin{bmatrix}\boldsymbol{0}_{N\times 1} \\ 1\end{bmatrix}, \ \boldsymbol{u}^+, \boldsymbol{u}^- \geq 0, \tag{132}$$

and solve it efficiently with an optimized general purpose linear programming solver, such as Gurobi (Gurobi Optimization, 2015).

Having computed a $\boldsymbol{b}_1$ with Algorithm 1, there are two possibilities: either V is a hyperplane of dimension $D-1$ or $\dim\mathcal{S} < D-1$. In the first case we can identify our subspace model with the hyperplane defined by the normal $\boldsymbol{b}_1$. If on the other hand $\dim\mathcal{S} < D-1$, we can proceed to find a $\boldsymbol{b}_2 \perp \boldsymbol{b}_1$ that is approximately orthogonal to $\mathcal{S}$, and so on; this naturally leads to the *relaxed Dual Principal Component Analysis* of Algorithm 2.

In Algorithm 2, c is an estimate for the codimension $D-d$ of the inlier subspace $\operatorname{Span}(\mathcal{X})$. If c is rather large, then in the computation of each $\boldsymbol{b}_i$, it is more efficient to be reducing the coordinate representation of the data to $D-(i-1)$ coordinates, by projecting the data orthogonally onto $\operatorname{Span}(\boldsymbol{b}_1,\ldots,\boldsymbol{b}_{i-1})^\perp$ and solving the linear program in the projected space.

Notice further how the algorithm initializes $\boldsymbol{n}_0$: This is precisely the right singular vector of $\tilde{\boldsymbol{\mathcal{X}}}^\top$ that corresponds to the smallest singular value, after projection of $\tilde{\boldsymbol{\mathcal{X}}}$ onto $\operatorname{Span}(\boldsymbol{b}_1,\ldots,\boldsymbol{b}_{i-1})^\perp$. As it will be demonstrated in Section 7, this choice has the effect that the angle of $\boldsymbol{n}_0$ from the inlier

Algorithm 2 Relaxed Dual Principal Component Analysis

procedure DPCA-r($\tilde{\boldsymbol{\mathcal{X}}}, c, \varepsilon, T_{\max}$)
  $\mathcal{B} \leftarrow \emptyset$;
  for $i = 1 : c$ **do**
    $k \leftarrow 0; \Delta\mathcal{J} \leftarrow \infty$;
    $\hat{\boldsymbol{n}}_0 \leftarrow \operatorname{argmin}_{\boldsymbol{b} \perp \mathcal{B}} \left\| \tilde{\boldsymbol{\mathcal{X}}}^\top \boldsymbol{b} \right\|_2$;
    while $k \leq T_{\max}$ and $\Delta\mathcal{J} > \varepsilon$ **do**
      $k \leftarrow k + 1$;
      $\boldsymbol{n}_k \leftarrow \operatorname{argmin}_{\boldsymbol{b}^\top \hat{\boldsymbol{n}}_{k-1} = 1, \boldsymbol{b} \perp \mathcal{B}} \left\| \tilde{\boldsymbol{\mathcal{X}}}^\top \boldsymbol{b} \right\|_1$;
      $\Delta\mathcal{J} \leftarrow \left(\left\| \tilde{\boldsymbol{\mathcal{X}}}^\top \hat{\boldsymbol{n}}_{k-1} \right\|_1 - \left\| \tilde{\boldsymbol{\mathcal{X}}}^\top \hat{\boldsymbol{n}}_k \right\|_1 \right) / \left(\left\| \tilde{\boldsymbol{\mathcal{X}}}^\top \hat{\boldsymbol{n}}_{k-1} \right\|_1 + 10^{-9} \right)$;
    end while
    $\boldsymbol{b}_i \leftarrow \hat{\boldsymbol{n}}_k$;
    $\mathcal{B} \leftarrow \mathcal{B} \cup \{\boldsymbol{b}_i\}$;
  end for
  return $\mathcal{B}$;
end procedure

Algorithm 3 Denoised Dual Principal Component Pursuit

procedure DPCP-d($\tilde{\boldsymbol{\mathcal{X}}}, \varepsilon, T_{\max}, \delta, \tau$)
  Compute a Cholesky factorization $\boldsymbol{L}\boldsymbol{L}^\top = \tilde{\boldsymbol{\mathcal{X}}}\tilde{\boldsymbol{\mathcal{X}}}^\top + \delta \boldsymbol{I}_D$;
  $k \leftarrow 0; \Delta\mathcal{J} \leftarrow \infty$;
  $\boldsymbol{b} \leftarrow \operatorname{argmin}_{\boldsymbol{b} \in \mathbb{R}^D : \|\boldsymbol{b}\|_2 = 1} \left\| \tilde{\boldsymbol{\mathcal{X}}}^\top \boldsymbol{b} \right\|_2$;
  $\mathcal{J}_0 \leftarrow \tau \left\| \tilde{\boldsymbol{\mathcal{X}}}^\top \boldsymbol{b} \right\|_1$;
  while $k < T_{\max}$ and $\Delta\mathcal{J} > \varepsilon$ **do**
    $k \leftarrow k + 1$;
    $\boldsymbol{y} \leftarrow \mathcal{S}_\tau \left(\tilde{\boldsymbol{\mathcal{X}}}^\top \boldsymbol{b} \right)$;
    $\boldsymbol{b} \leftarrow$ solution of $\boldsymbol{L}\boldsymbol{L}^\top \boldsymbol{\xi} = \tilde{\boldsymbol{\mathcal{X}}} \boldsymbol{y}$ by backward/forward propagation;
    $\boldsymbol{b} \leftarrow \boldsymbol{b} / \|\boldsymbol{b}\|_2$;
    $\mathcal{J}_k \leftarrow \tau \|\boldsymbol{y}\|_1 + \frac{1}{2} \left\| \boldsymbol{y} - \tilde{\boldsymbol{\mathcal{X}}}^\top \boldsymbol{b} \right\|_2^2$;
    $\Delta\mathcal{J} \leftarrow (\mathcal{J}_{k-1} - \mathcal{J}_k) / \left(\mathcal{J}_{k-1} + 10^{-9} \right)$;
  end while
  return $(\boldsymbol{y}, \boldsymbol{b})$;
end procedure

subspace is typically large; more precisely, it is often larger than the smallest initial angle (61) required for the success of the linear programming recursions.

Algorithm 4 Dual Principal Component Pursuit via Iteratively Re-weighted Least Squares

procedure DPCP-IRLS($\tilde{\boldsymbol{\mathcal{X}}}, c, \varepsilon, T_{\max}, \delta$)
  $k \leftarrow 0; \Delta\mathcal{J} \leftarrow \infty;$
  $\boldsymbol{B}_0 \leftarrow \operatorname{argmin}_{\boldsymbol{B}\in\mathbb{R}^{D\times c}} \left\|\tilde{\boldsymbol{\mathcal{X}}}^\top \boldsymbol{B}\right\|_2, \ \text{s.t. } \boldsymbol{B}^\top\boldsymbol{B} = \mathcal{I}_c;$
  while $k < T_{\max}$ and $\Delta\mathcal{J} > \varepsilon$ **do**
    $k \leftarrow k+1;$
    $\boldsymbol{B}_k \leftarrow \operatorname{argmin}_{\boldsymbol{B}\in\mathbb{R}^{D\times c}} \sum_{\tilde{\boldsymbol{x}}\in\tilde{\boldsymbol{\mathcal{X}}}} \left\|\boldsymbol{B}^\top\tilde{\boldsymbol{x}}\right\|_2^2 / \max\left\{\delta, \left\|\boldsymbol{B}_{k-1}^\top\tilde{\boldsymbol{x}}\right\|_2\right\} \ \text{s.t. } \boldsymbol{B}^\top\boldsymbol{B} = \mathcal{I}_c;$
    $\Delta\mathcal{J} \leftarrow \left(\left\|\tilde{\boldsymbol{\mathcal{X}}}^\top\boldsymbol{B}_{k-1}\right\|_1 - \left\|\tilde{\boldsymbol{\mathcal{X}}}^\top\boldsymbol{B}_k\right\|_1\right) / \left(\left\|\tilde{\boldsymbol{\mathcal{X}}}^\top\boldsymbol{B}_{k-1}\right\|_1 + 10^{-9}\right);$
  end while
  return $\boldsymbol{B}_k;$
end procedure

6.2 Dealing with noisy or high-dimensional data: Alternative algorithms

DPCP-r-d. When the data are corrupted by noise, one no longer expects the product $\tilde{\boldsymbol{\mathcal{X}}}^\top\boldsymbol{b}$ to be sparse, even if $\boldsymbol{b}$ is orthogonal to the underlying inlier space. Instead, our expectation is that, for such a $\boldsymbol{b}$, $\tilde{\boldsymbol{\mathcal{X}}}^\top\boldsymbol{b}$ should be the sum of a sparse vector with a dense vector of small euclidean norm. This motivates us to replace the optimization problem

$$\min_{\boldsymbol{b}} \left\|\tilde{\boldsymbol{\mathcal{X}}}^\top\boldsymbol{b}\right\|_1, \ \text{s.t. } \boldsymbol{b}^\top\hat{\boldsymbol{n}}_{k-1} = 1, \tag{133}$$

which appears in Algorithm 1, with the *denoised* optimization problem

$$\min_{\boldsymbol{y},\boldsymbol{b}} \left[\tau\|\boldsymbol{y}\|_1 + \frac{1}{2}\left\|\boldsymbol{y} - \tilde{\boldsymbol{\mathcal{X}}}^\top\boldsymbol{b}\right\|_2^2\right], \ \text{s.t. } \boldsymbol{b}^\top\hat{\boldsymbol{n}}_{k-1} = 1, \tag{134}$$

where τ is a positive parameter. Observe, that if the optimal $\boldsymbol{b}$ were known, then $\boldsymbol{y}$ would be given by the element-wise soft thresholding $S_\tau(\tilde{\boldsymbol{\mathcal{X}}}^\top\boldsymbol{b})$, where the function $S_\tau : \mathbb{R} \to \mathbb{R}$ is defined by $S_\tau(\alpha) = \operatorname{Sign}(\alpha)\cdot\max(0, |\alpha| - \tau)$. If on the other hand $\boldsymbol{y}$ were known, then $\boldsymbol{b}$ would be given by $\boldsymbol{b} = \hat{\boldsymbol{n}}_{k-1} + \boldsymbol{U}_{k-1}\boldsymbol{z}$, where $\boldsymbol{U}_{k-1}$ is a $D \times (D-1)$ matrix containing in its columns an orthonormal basis for the orthogonal complement of $\hat{\boldsymbol{n}}_{k-1}$, and $\boldsymbol{z}$ is the solution to the standard least-squares problem

$$\min_{\boldsymbol{z}\in\mathbb{R}^{D-1}} \left\|\boldsymbol{y} - \tilde{\boldsymbol{\mathcal{X}}}^\top\hat{\boldsymbol{n}}_{k-1} - \tilde{\boldsymbol{\mathcal{X}}}^\top\boldsymbol{U}_{k-1}\boldsymbol{z}\right\|_2^2. \tag{135}$$

Observe that solving problem (135) requires solving a linear system of equations with coefficient matrix $\left(\tilde{\boldsymbol{\mathcal{X}}}^\top\boldsymbol{U}_{k-1}\right)^\top\tilde{\boldsymbol{\mathcal{X}}}^\top\boldsymbol{U}_{k-1}$. The dependence of this matrix on the iteration index k, may become a computational issue when D is large. This dependence can be circumvented as follows. First, we treat the computation of $\boldsymbol{b}$ given $\boldsymbol{y}$ as a constrained problem

$$\min_{\boldsymbol{b}} \left\|\boldsymbol{y} - \tilde{\boldsymbol{\mathcal{X}}}^\top\boldsymbol{b}\right\|_2^2 \ \text{, s.t. } \boldsymbol{b}^\top\hat{\boldsymbol{n}}_{k-1} = 1, \tag{136}$$

and thinking in terms of a Lagrange multiplier λ associated to the constraint $\boldsymbol{b}^\top\hat{\boldsymbol{n}}_{k-1} = 1$, we see that $\lambda, \boldsymbol{b}$ must satisfy the relation

$$\tilde{\boldsymbol{\mathcal{X}}}\boldsymbol{y} - \tilde{\boldsymbol{\mathcal{X}}}\tilde{\boldsymbol{\mathcal{X}}}^\top\boldsymbol{b} - \lambda\hat{\boldsymbol{n}}_{k-1} = 0. \tag{137}$$

Noting that $\tilde{\boldsymbol{\mathcal{X}}}\tilde{\boldsymbol{\mathcal{X}}}^\top$ is always invertible under our data model, we must have that

$$\boldsymbol{b} = \left(\tilde{\boldsymbol{\mathcal{X}}}\tilde{\boldsymbol{\mathcal{X}}}^\top\right)^{-1}\boldsymbol{y} - \lambda\left(\tilde{\boldsymbol{\mathcal{X}}}\tilde{\boldsymbol{\mathcal{X}}}^\top\right)^{-1}\hat{\boldsymbol{n}}_{k-1}. \tag{138}$$

Now, multiplying the above equation from the left with $\hat{\boldsymbol{n}}_{k-1}^\top$, we obtain

$$1 = \hat{\boldsymbol{n}}_{k-1}^\top\left(\tilde{\boldsymbol{\mathcal{X}}}\tilde{\boldsymbol{\mathcal{X}}}^\top\right)^{-1}\boldsymbol{y} - \lambda\hat{\boldsymbol{n}}_{k-1}^\top\left(\tilde{\boldsymbol{\mathcal{X}}}\tilde{\boldsymbol{\mathcal{X}}}^\top\right)^{-1}\hat{\boldsymbol{n}}_{k-1}, \tag{139}$$

or equivalently

$$\lambda = \frac{\hat{\boldsymbol{n}}_{k-1}^\top\left(\tilde{\boldsymbol{\mathcal{X}}}\tilde{\boldsymbol{\mathcal{X}}}^\top\right)^{-1}\boldsymbol{y} - 1}{\hat{\boldsymbol{n}}_{k-1}^\top\left(\tilde{\boldsymbol{\mathcal{X}}}\tilde{\boldsymbol{\mathcal{X}}}^\top\right)^{-1}\hat{\boldsymbol{n}}_{k-1}}, \tag{140}$$

which upon substitution into (138) gives our final formula for $\boldsymbol{b}$:

$$\boldsymbol{b} = \left(\tilde{\boldsymbol{\mathcal{X}}}\tilde{\boldsymbol{\mathcal{X}}}^\top\right)^{-1}\boldsymbol{y} - \left(\frac{\hat{\boldsymbol{n}}_{k-1}^\top\left(\tilde{\boldsymbol{\mathcal{X}}}\tilde{\boldsymbol{\mathcal{X}}}^\top\right)^{-1}\boldsymbol{y} - 1}{\hat{\boldsymbol{n}}_{k-1}^\top\left(\tilde{\boldsymbol{\mathcal{X}}}\tilde{\boldsymbol{\mathcal{X}}}^\top\right)^{-1}\hat{\boldsymbol{n}}_{k-1}}\right)\left(\tilde{\boldsymbol{\mathcal{X}}}\tilde{\boldsymbol{\mathcal{X}}}^\top\right)^{-1}\hat{\boldsymbol{n}}_{k-1}. \tag{141}$$

Notice that the quantities $\left(\tilde{\boldsymbol{\mathcal{X}}}\tilde{\boldsymbol{\mathcal{X}}}^\top\right)^{-1}\boldsymbol{y}$ and $\left(\tilde{\boldsymbol{\mathcal{X}}}\tilde{\boldsymbol{\mathcal{X}}}^\top\right)^{-1}\hat{\boldsymbol{n}}_{k-1}$ can be obtained as solutions to linear systems of equations with common coefficient matrix $\tilde{\boldsymbol{\mathcal{X}}}\tilde{\boldsymbol{\mathcal{X}}}^\top$, which themselves can be solved very efficiently by backward and forward substitution, assuming that a pre-computed Cholesky factorization of $\tilde{\boldsymbol{\mathcal{X}}}\tilde{\boldsymbol{\mathcal{X}}}^\top$ is available.

To summarize, we have shown how to approximately solve problem (133) by a very efficient alternating minimization scheme, which involves soft-thresholding and forward-backward substitution; we will be referring to the resulting DPCP algorithm as *DPCP-r-d*, which stands for *relaxed and denoised DPCP*.

DPCP-d. Interestingly, DPCP-r-d is very closely related to the scheme proposed in (Qu et al., 2014), where the authors study problem (12) in the very different context of dictionary learning. To approximately solve (12), the authors of (Qu et al., 2014) solve its *denoised* version

$$\min_{\boldsymbol{b},\boldsymbol{y}:\,\|\boldsymbol{b}\|_2=1}\left[\tau\,\|\boldsymbol{y}\|_1 + \frac{1}{2}\left\|\boldsymbol{y} - \tilde{\boldsymbol{\mathcal{X}}}^\top\boldsymbol{b}\right\|_2^2\right], \tag{142}$$

by alternating minimization. Given $\boldsymbol{b}$, the optimal $\boldsymbol{y}$ is given by $\mathcal{S}_\tau\left(\tilde{\boldsymbol{\mathcal{X}}}^\top\boldsymbol{b}\right)$, where $\mathcal{S}_\tau$ is the soft-thresholding operator applied element-wise on the vector $\tilde{\boldsymbol{\mathcal{X}}}^\top\boldsymbol{b}$. Given $\boldsymbol{y}$ the optimal $\boldsymbol{b}$ is a solution to the quadratically constrained least-squares problem

$$\min_{\boldsymbol{b}\in\mathbb{R}^D}\ \left\|\boldsymbol{y} - \tilde{\boldsymbol{\mathcal{X}}}^\top\boldsymbol{b}\right\|_2^2,\ \text{ s.t. }\ \|\boldsymbol{b}\|_2 = 1. \tag{143}$$

In the context of (Qu et al., 2014), the coefficient matrix of the least-squares problem ($\tilde{\boldsymbol{\mathcal{X}}}^\top$ in our notation) has orthonormal columns. As a consequence, the solution to (143) is obtained in closed

form by projecting the solution of the unconstrained least-squares problem $\min_{\boldsymbol{b}\in\mathbb{R}^D} \ ||\boldsymbol{y}-\tilde{\boldsymbol{\mathcal{X}}}^\top \boldsymbol{b}||_2$ onto the unit sphere. However, in our context the assumption that $\tilde{\boldsymbol{\mathcal{X}}}^\top$ has orthonormal columns is strongly violated, so that the optimal $\boldsymbol{b}$ is no longer available in closed form.

In fact, problem (143) is well known in the literature (Elden, 2002; Golub and Von Matt, 1991; Gander, 1980), and the standard way to solve it is by means of Lagrange multipliers. This involves solving a non-linear equation for the Lagrange multiplier, which is known to be challenging (Elden, 2002). For this reason we leave exact approaches for solving (143) to future investigations, and we instead propose to obtain an approximate $\boldsymbol{b}$ as in (Qu et al., 2014). We will call the resulting Algorithm 3 *DPCP-d*, which stands for *denoised DPCP*.

Notice that DPCP-d is very efficient, since the least-squares problems that appear in the various iterations have the same coefficient matrix $\tilde{\boldsymbol{\mathcal{X}}}\tilde{\boldsymbol{\mathcal{X}}}^\top$, a factorization of which can be precomputed [7]. As we will see in Section 7, the performance of DPCP-d is remarkably close to that of DPCP-r, for which we have guarantees of global optimality, suggesting that DPCP-d converges to a global minimum. We leave theoretical investigations of DPCP-d to future research.

Finally, notice that Algorithm 3 computes a single normal vector $\boldsymbol{b}_1$. As with DPCP-r, it is trivial to adjust Algorithm 3 to compute a second normal vector $\boldsymbol{b}_2$, since one only needs to incorporate the linear constraint $\boldsymbol{b}^\top \boldsymbol{b}_1 = 0$, and so on. We will again refer to such an algorithm that computes $c \geq 1$ normals as DPCP-d.

DPCP-IRLS. Even though DPCP-d and DPCP-r-d are very attractive from a computational point of view, they only produce approximate normal vectors (even in the absence of noise), and have the additional disadvantage that their performance depends on the parameter τ, whose tuning is not well understood. On the other hand, DPCP-r was shown to produce exact normal vectors, yet solving linear programs of the form (131)-(132) can be inefficient when the data are high-dimensional. This motivates us to propose a direct IRLS algorithm for solving the DPCP problem (12). In fact, since we are interested in obtaining an orthonormal basis for the orthogonal complement of the inlier subspace, we propose an *Iteratively Reweighted Least-Squares (IRLS)* scheme for solving problem

$$\min_{\boldsymbol{B}\in\mathbb{R}^{D\times c}} \left\|\tilde{\boldsymbol{\mathcal{X}}}^\top \boldsymbol{B}\right\|_{1,2}, \ \text{s.t.} \ \boldsymbol{B}^\top\boldsymbol{B} = \boldsymbol{I}_c, \tag{144}$$

which is a generalization of the DPCP problem for multiple normal vectors. More specifically, given a $D \times c$ orthonormal matrix $\boldsymbol{B}_{k-1}$, we define for each point $\tilde{\boldsymbol{x}}_j$ a weight

$$w_{j,k} := \frac{1}{\max\left\{\delta, \left\|\boldsymbol{B}_{k-1}^\top \tilde{\boldsymbol{x}}_j\right\|_2\right\}}, \tag{145}$$

where $\delta > 0$ is a small constant that prevents division by zero. Then we obtain $\boldsymbol{B}_k$ as the solution to the quadratic problem

$$\min_{\boldsymbol{B}\in\mathbb{R}^{D\times c}} \sum_{j=1}^{L} w_{j,k} \left\|\boldsymbol{B}^\top \tilde{\boldsymbol{x}}_j\right\|_2^2, \ \text{s.t.} \ \boldsymbol{B}^\top\boldsymbol{B} = \boldsymbol{I}_c, \tag{146}$$

which is readily seen to be the c right singular vectors corresponding to the c smallest singular values of the weighted data matrix $\boldsymbol{W}_k\tilde{\boldsymbol{\mathcal{X}}}^\top$, where $\boldsymbol{W}$ is a diagonal matrix with $\sqrt{w_{j,k}}$ at position (j,j).

7. The parameter δ in Algorithm 3 is a small positive number, typically 10^{-6}, which helps avoiding solving ill-conditioned linear systems.

We refer to the resulting Algorithm 4 as *DPCP-IRLS*; a study of its theoretical properties is deferred to future work. We note here that the technique of solving an optimization problem (convex or non-convex) through IRLS is a common one. In fact, REAPER (Lerman et al., 2015) solves through IRLS a convex relaxation of precisely problem (144). Other prominent instances of IRLS schemes from compressed sensing are (Candès et al., 2008; Daubechies et al., 2010; Chartrand and Yin, 2008).

7. Experiments

In this Section we evaluate the proposed algorithms experimentally. In Section 7.1 we investigate the performance of our principal algorithmic proposal, i.e., DPCP-r, described in Algorithm 1. In Section 7.2 we compare DPCP-r, DPCP-d, DPCP-r-d [8] and DPCP-IRLS with state-of-the-art robust PCA algorithms using synthetic data, and similarly in Section 7.3 using real images.

7.1 Computing a single dual principal component

We begin by investigating the behavior of the DPCP-r Algorithm 1 in the absence of noise, for random subspaces $\mathcal{S}$ of varying dimensions $d = 1 : 1 : 29$ and varying outlier percentages $R := M/(M+N) = 0.1 : 0.1 : 0.9$. We fix the ambient dimension $D = 30$, sample $N = 200$ inliers uniformly at random from $\mathcal{S} \cap \mathbb{S}^{D-1}$ and M outliers uniformly at random from $\mathbb{S}^{D-1}$. We set $\epsilon = 10^{-3}$ and $T_{\max} = 10$ in Algorithm 1. Our main interest is in examining the ability of DPCP-r in recovering a single normal vector to the subspace ($c = 1$). The results over 10 independent trials are shown in Fig. 4, in which the vertical axis denotes the *relative dimension* of the subspace, defined as d/D.

Fig. 4(a) shows whether the theoretical condition (60) is satisfied (white) or not (black). In checking this condition, we estimate the abstract quantities $\epsilon_{\boldsymbol{\mathcal{O}}}, \epsilon_{\boldsymbol{\mathcal{X}}}, \mathcal{R}_{\boldsymbol{\mathcal{O}},K_1}, \mathcal{R}_{\boldsymbol{\mathcal{X}},K_2}$ by Monte-Carlo simulation. Whenever the condition is true, we choose $\hat{\boldsymbol{n}}_0$ in a controlled fashion, so that its angle ϕ_0 from the subspace is larger than the minimal angle ϕ_0^* of (61); then we run DPCP-r. If on the other hand (60) is not true, we do not run DPCP-r and report a 0 (black). Fig 4(b) shows the angle of $\hat{\boldsymbol{n}}_{10}$ from the subspace. We see that whenever (60) is true, DPCP-r returns a normal after only 10 iterations. Fig 4(c) shows that if we initialize randomly $\hat{\boldsymbol{n}}_0$, then its angle ϕ_0 from the subspace tends to become less than the minimal angle ϕ_0^*, as d increases. Even so, Fig. 4(d) shows that DPCP-r still yields a numerical normal, except for the regime where both d and R are very high. Notice that this is roughly the regime where we have no theoretical guarantees, according to Fig. 4(a). Fig. 4(e) shows that if we initialize $\hat{\boldsymbol{n}}_0$ as the right singular vector of $\tilde{\boldsymbol{\mathcal{X}}}^\top$ corresponding to the smallest singular value, then $\phi_0 > \phi_0^*$ is true for most cases, and the corresponding performance of DPCP-r in Fig. 4(f) improves further. Finally, Fig. 4(g) plots $\phi_0 *$. We see that for very low d this angle is almost zero, i.e. DPCP-r does not depend on the initialization, even for large R. As d increases though, so does ϕ_0^*, and in the extreme case of the upper rightmost regime, where d and R are very high, ϕ_0^* is close to 90^o, verifying our expectation that DPCP-r will succeed only if $\hat{\boldsymbol{n}}_0$ is very close to $\mathcal{S}^\perp$.

8. To avoid confusion, we will slightly abuse our terminology and refer to DPCA-r (DPCA-d, DPCA-r-d) as DPCP-r (DPCP-d, DPCP-r-d), even when $c > 1$. The distinction of whether a single versus multiple dual principal components are being computed will be clear from the context.

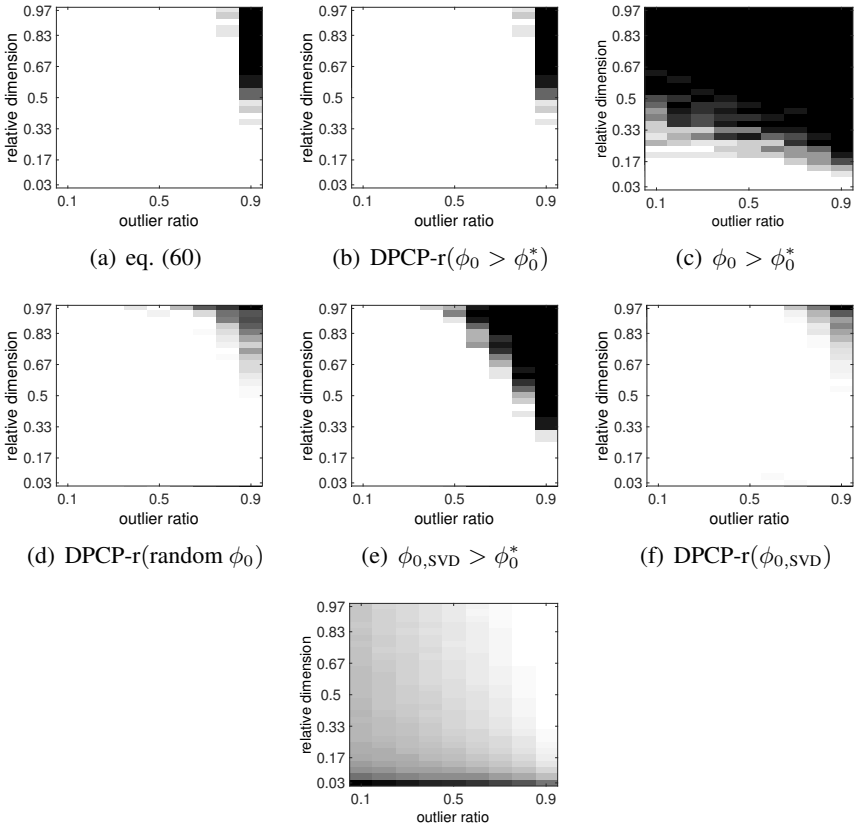

(a) eq. (60) (b) DPCP-r($\phi_0 > \phi_0^*$) (c) $\phi_0 > \phi_0^*$

(d) DPCP-r(random ϕ_0) (e) $\phi_{0,\text{SVD}} > \phi_0^*$ (f) DPCP-r($\phi_{0,\text{SVD}}$)

(g) ϕ_0^*

Figure 4: Various quantities associated to the performance of DPCP-r. Fig. 4(a) shows whether the sufficient condition (60) is true (white) or not (black). Fig. 4(b) shows the angle from $\mathcal{S}$ of the vector $\hat{\boldsymbol{n}}_{10}$ produced after 10 iterations of DPCP-r for the cases where (60) is true; the other cases are mapped to black. Fig. 4(c) shows whether $\hat{\boldsymbol{n}}_0$, when chosen uniformly at random, satisfies the sufficient condition $\phi_0 > \phi_0^*$, where ϕ_0^* is the minimal angle appearing in Theorem 11. Fig. 4(d) shows the angle from $\mathcal{S}$ of $\hat{\boldsymbol{n}}_{10}$ for randomly chosen $\hat{\boldsymbol{n}}_0$. Fig. 4(e) shows the angle from $\mathcal{S}$ of the right singular vector of $\tilde{\boldsymbol{\mathcal{X}}}$ corresponding to the smallest singular value, and Fig. 4(f) shows the corresponding angle of $\hat{\boldsymbol{n}}_{10}$. Finally, Fig. 4(g) plots ϕ_0^*. For more details see Section 7.2.

7.2 Comparative Analysis Using Synthetic Data

In this Section we begin by using the same synthetic experimental set-up as in Section 7.1 (except that now $N = 300$) to demonstrate the behavior of several methods relative to each other under uniform conditions, in the context of outlier rejection in single subspace learning. In particular, we test DPCP-r, DPCP-d, DPCP-r-d, DPCP-IRLS, the IRLS version of REAPER (Lerman et al., 2015), RANSAC (Fischler and Bolles, 1981), SE-RPCA (Soltanolkotabi and Candès, 2012), and ℓ_{21}-RPCA (Xu et al., 2010); see Section 2 for details on existing methods.

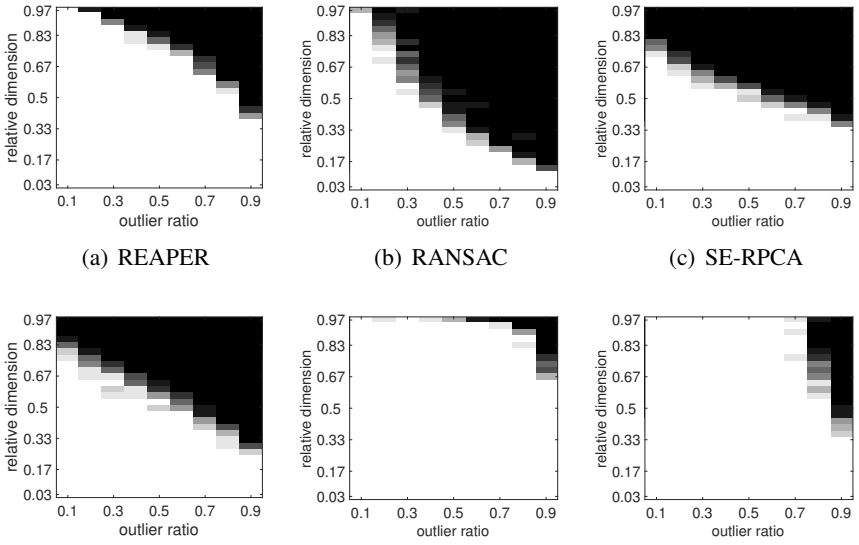

(a) REAPER (b) RANSAC (c) SE-RPCA

(d) ℓ_{21}-RPCA (e) DPCP-IRLS (f) DPCP-r

Figure 5: Outlier/Inlier separation in the absence of noise over 10 independent trials. The horizontal axis is the outlier ration defined as $M/(N+M)$, where M is the number of outliers and N is the number of inliers. The vertical axis is the relative inlier subspace dimension d/D; the dimension of the ambient space is $D = 30$. Success (white) is declared by the existence of a threshold that, when applied to the output of each method, perfectly separates inliers from outliers.

For the methods that require an estimate of the subspace dimension d, such as REAPER, RANSAC, and all DPCP variants, we provide as input the true subspace dimension. The convergence accuracy of all methods is set to 10^{-3}. For REAPER we set the regularization parameter δ equal to 10^{-6} and the maximal number of iterations equal to 100. For DPCP-r we set $\tau = 1/\sqrt{N+M}$ as suggested in Qu et al. (2014) and maximal number of iterations 1000. For RANSAC we set its thresholding parameter equal to 10^{-3}, and for fairness, we do not let it terminate earlier than the running time of DPCP-r. Both SE-RPCA and ℓ_{21}-RPCA are implemented with ADMM, with augmented Lagrange parameters 1000 and 100 respectively. For ℓ_{21}-RPCA λ is set to $3/(7\sqrt{M})$, as suggested in (Xu et al., 2010). DPCP variants are given the same initialization, as in Algorithm 2, and the parameters of DPCP-r are as in Section 7.1.

Absence of Noise. We investigate the potential of each of the above methods to perfectly distinguish outliers from inliers in the absence of noise [9]. Note that each method returns a *signal* $\boldsymbol{\alpha} \in \mathbb{R}_+^{N+M}$, which can be thresholded for the purpose of declaring outliers and inliers. For SE-RPCA, $\boldsymbol{\alpha}$ is the ℓ_1-norm of the columns of the coefficient matrix $\boldsymbol{C}$, while for ℓ_{21}-RPCA it is the ℓ_2-norm of the columns of $\boldsymbol{E}$. Since REAPER, RANSAC, DPCP-r and DPCP-IRLS directly return subspace models, for these methods $\boldsymbol{\alpha}$ is simply the distances of all points to the estimated subspace.

9. We do not include the results of DPCP-d and DPCP-r-d for this experiment, since they only approximately solve the DPCP optimization problem, and hence they can not be expected to perfectly separate inliers from outliers, even when there is no noise.

In Fig. 5 we depict success (white) versus failure (black), where success is interpreted as the existence of a threshold on $\boldsymbol{\alpha}$ that perfectly separates outliers and inliers. First observe that, as expected, SE-RPCA and ℓ_{21}-RPCA succeed only when the subspace dimension d is small. In particular, the more outliers are present the lower the dimension of the subspace needs to be for the methods to succeed. The same is true for RANSAC, except when there are only very few outliers (10%), in which case the probability of sampling outlier-free points is high. Finally notice that SE-RPCA is the best method among these three in dealing with large percentages of outliers ($> 70\%$). This is not a surprise, because the theoretical guarantees of SE-RPCA do not place an explicit upper bound on the number of outliers, in contrast to ℓ_{21}-RPCA and RANSAC. Next, notice that REAPER performs uniformly better than RANSAC, SE-RPCA and ℓ_{21}-RPCA. In particular REAPER can handle higher dimensions and higher outlier percentages; for example it succeeds over all trials for hyperplanes when there are 10% outliers.

In summary, none of REAPER, RANSAC, SE-RPCA, and ℓ_{21}-RPCA can deal with hyperplanes with more than 20% outliers or with subspaces of medium relative dimension ($d > 13$) for as many as 90% outliers. This gap is filled by the two proposed methods DPCP-r and DPCP-IRLS. Notice that DPCP-r is the only method that succeeds irrespectively of subspace dimension with almost 70% outliers, while DPCP-IRLS is the only method that succeeds when $d \leq 19$ and $R = 90\%$.

Presence of Noise. Next, we keep $D = 30$ and investigate the performance of the methods, adding DPCP-d and DPCP-r-d in the mix, in the presence of varying levels of noise and outliers for two cases of high-dimensional subspaces, i.e., $d = 25$ and $d = 29$. The inliers are corrupted by additive white gaussian noise of zero mean and standard deviation $\sigma = 0.02, 0.06, 0.1$, with support in the orthogonal complement of the inlier subspace. Finally, the percentage of outliers varies as $R = 20\%, 33\%, 50\%$. For ADM methods we set $\tau = \max\left\{\sigma, 1/\sqrt{N+M}\right\}$, while for RANSAC we set its threshold equal to σ.

We evaluate the performance of each method by its corresponding ROC curve. Each point of an ROC curve corresponds to a certain value of a threshold, with the vertical coordinate of the point giving the percentage of inliers being correctly identified as inliers (True Positives), and the horizontal coordinate giving the number of outliers erroneously identified as inliers (False Positives). As a consequence, an ideal ROC curve should be concentrated to the top left of the first quadrant, i.e., the area over the curve should be zero.

The ROC curves for the case $d = 25$ are given in Fig. 6, where for each curve we also report the area over the curve. As expected, the low-rank methods RANSAC, SE-RPCA and ℓ_{21}-RPCA perform poorly with RANSAC being the worst method for 50% outliers and SE-RPCA being the weakest method otherwise. On the other hand REAPER, DPCP-d, DPCP-IRLS, DPCP-r-d and DPCP-r perform almost perfectly well, with DPCP-IRLS actually giving zero error across all cases. Notice the interesting fact that DPCP-r performs slightly better across all cases than both DPCP-d and DPCP-r-d, despite the fact that DPCP-d and DPCP-r-d are intuitively more suitable for noisy data than DPCP-r.

The ROC curves for the case $d = 29$ are given in Fig. 7. As expected, the low-rank methods RANSAC, SE-RPCA and ℓ_{21}-RPCA fail even for low noise ($\sigma = 0.02$) and moderate outliers (20%). Notice that for 50% outliers and for any threshold, there is roughly an equal chance of identifying a point as inlier or as outlier, i.e., the performance of the methods is almost the same as that of a random guess. On the other hand, DPCP-r, DPCP-d, and DPCP-IRLS are very robust to variations of the noise level and outlier percentages and are the best methods. DPCP-r-d performs almost identically with these methods, except in the case of 50% outliers, where it performs less

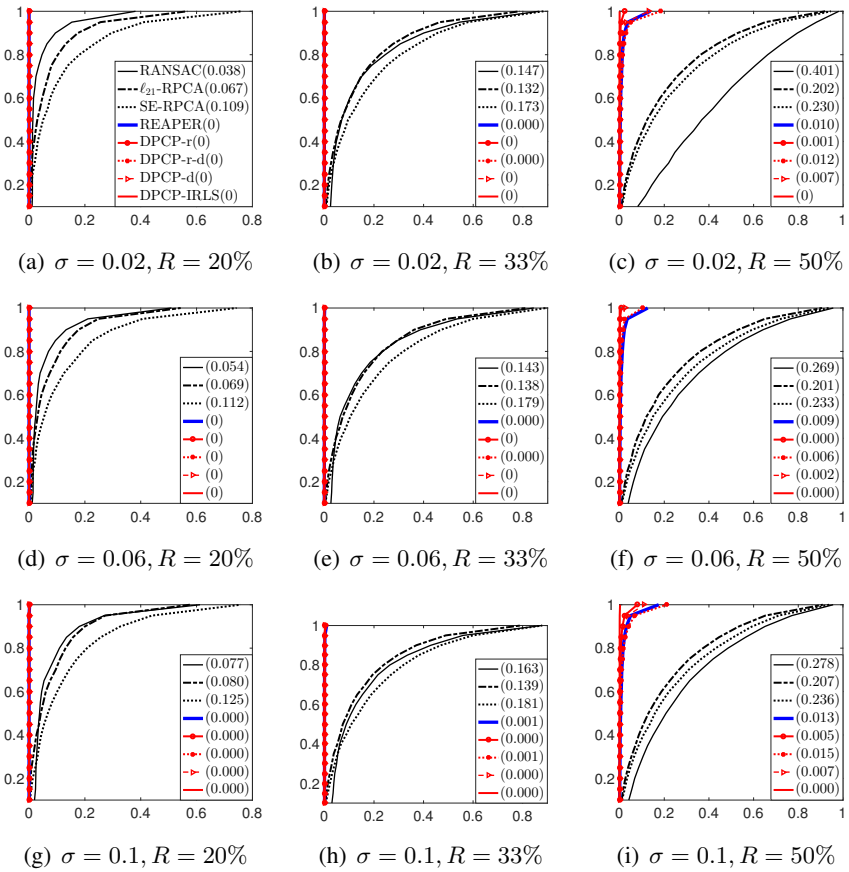

(a) $\sigma = 0.02, R = 20\%$ (b) $\sigma = 0.02, R = 33\%$ (c) $\sigma = 0.02, R = 50\%$

(d) $\sigma = 0.06, R = 20\%$ (e) $\sigma = 0.06, R = 33\%$ (f) $\sigma = 0.06, R = 50\%$

(g) $\sigma = 0.1, R = 20\%$ (h) $\sigma = 0.1, R = 33\%$ (i) $\sigma = 0.1, R = 50\%$

Figure 6: ROC curves as a function of noise standard deviation σ and outlier percentage R, for subspace dimension $d = 25$ in ambient dimension $D = 30$. The horizontal axis is False Positives ratio and the vertical axis is True Positives ratio. The number associated with each curve is the area above the curve; smaller numbers reflect more accurate performance.

accurately. Finally, notice that the performance of REAPER degrades significantly as soon as the outlier percentage exceeds 20%, indicating that REAPER is not the best method for subspaces of very low codimension.

7.3 Comparative Analysis Using Real Data

In this section we use the Extended-Yale-B real face dataset (Georghiades et al., 2001) as well as the real image dataset Caltech101 (Fei-Fei et al., 2007) to compare the proposed algorithms DPCP-r, DPCP-d, DPCP-r-d and DPCP-IRLS to REAPER, RANSAC, ℓ_{21}-RPCA, and SE-RPCA. We recall that the Extended-Yale-B dataset contains 64 face images for each of 38 distinct individuals. We use the first 19 individuals from the Extended-Yale-B dataset and the first half images of each category in Caltech101 for gaining intuition and tuning the parameters of each method (training set), while the remaining part of the datasets serve as a test set.

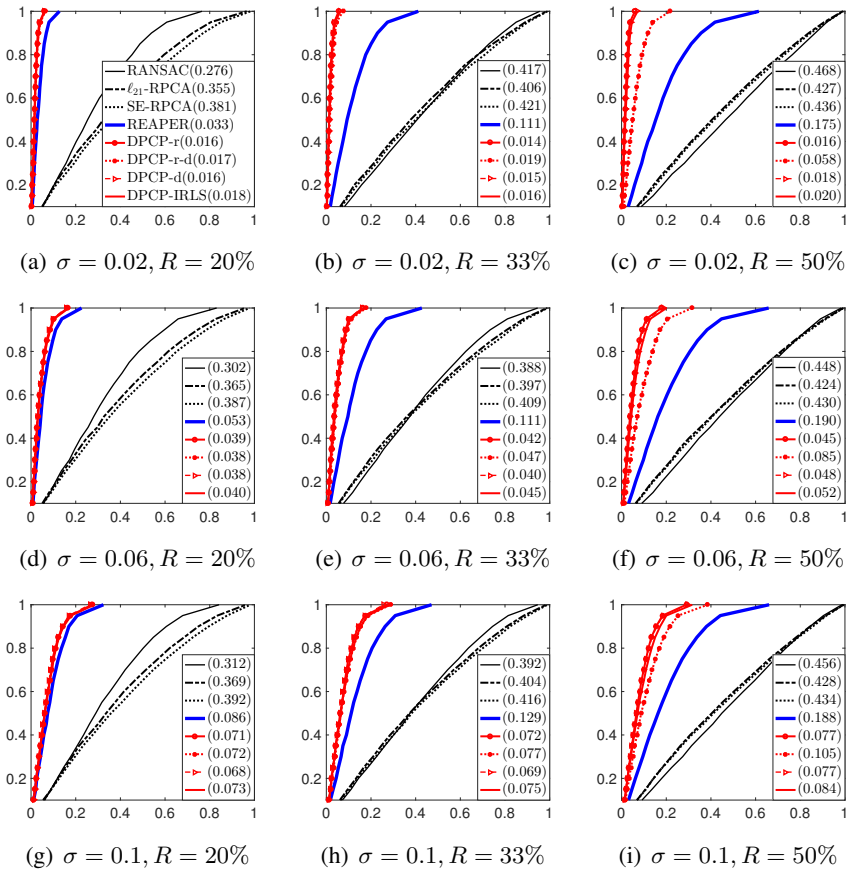

(a) $\sigma = 0.02, R = 20\%$ (b) $\sigma = 0.02, R = 33\%$ (c) $\sigma = 0.02, R = 50\%$

(d) $\sigma = 0.06, R = 20\%$ (e) $\sigma = 0.06, R = 33\%$ (f) $\sigma = 0.06, R = 50\%$

(g) $\sigma = 0.1, R = 20\%$ (h) $\sigma = 0.1, R = 33\%$ (i) $\sigma = 0.1, R = 50\%$

Figure 7: ROC curves as a function of noise standard deviation σ and outlier percentage R, for subspace dimension $d = 29$ in ambient dimension $D = 30$. The horizontal axis is False Positives ratio and the vertical axis is True Positives ratio. The number associated with each curve is the area above the curve; smaller numbers reflect more accurate performance.

In the Extended-Yale-B dataset, all face images correspond to the same fixed pose, while the illumination conditions vary. Such images are known to lie in a 9-dimensional linear subspace, with each individual having its own corresponding subspace (Basri and Jacobs, 2003). In this experiment we use the 42×48 cropped images that were also used in (Elhamifar and Vidal, 2013). Thus, the images of each individual lie approximately in a 9-dimensional linear subspace of $\mathbb{R}^{42\times 48} \cong \mathbb{R}^{2016}$. It is then natural to take as inliers all the images of one individual. For outliers, we consider two possibilities: either the outliers consist of images randomly chosen from the rest of the individuals, or they consist of images randomly chosen from Caltech101; we recall here that Caltech101 is a database of 101 image categories, such as images of airplanes or images of brains. We will consider three different levels of outliers: 20%, 33% and 50%.

There are three important preprocessing steps that one may or may not chose to perform. The first such step is dimensionality reduction. In our case, we choose to use projection of the data

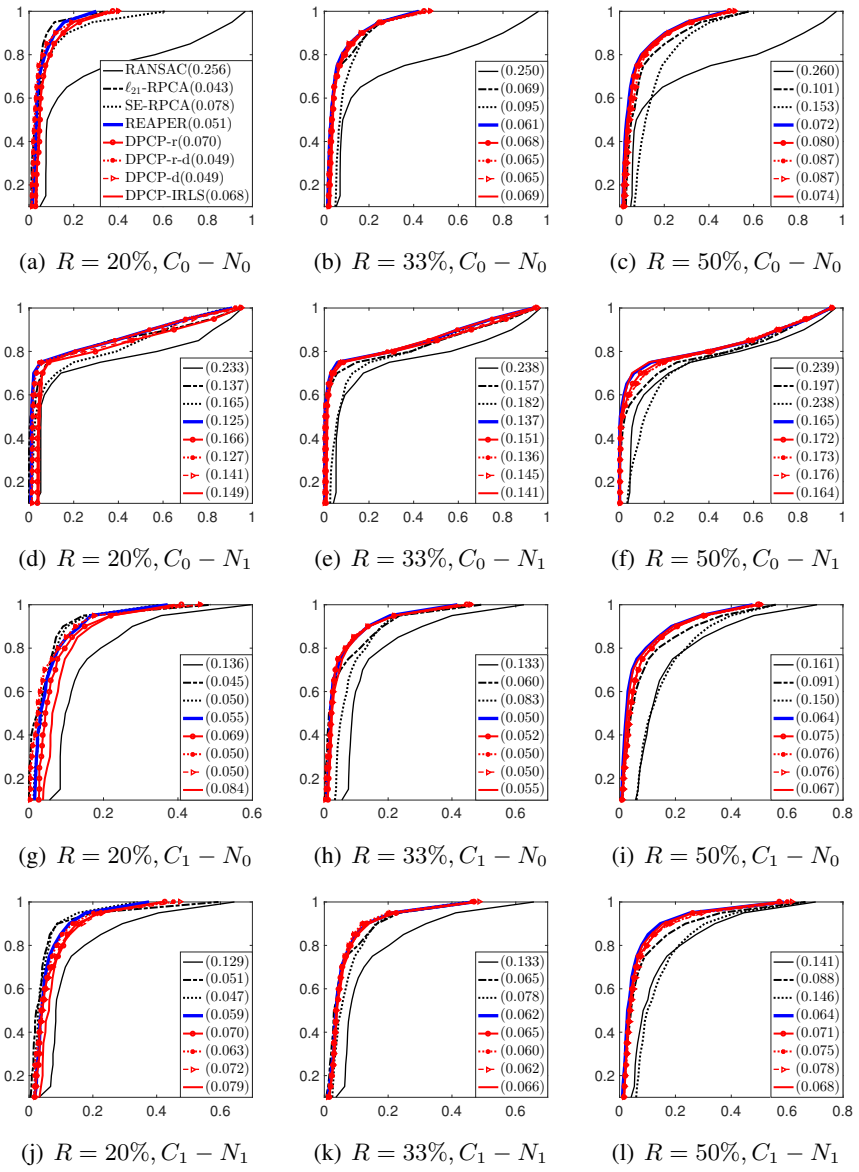

(a) $R = 20\%, C_0 - N_0$ (b) $R = 33\%, C_0 - N_0$ (c) $R = 50\%, C_0 - N_0$

(d) $R = 20\%, C_0 - N_1$ (e) $R = 33\%, C_0 - N_1$ (f) $R = 50\%, C_0 - N_1$

(g) $R = 20\%, C_1 - N_0$ (h) $R = 33\%, C_1 - N_0$ (i) $R = 50\%, C_1 - N_0$

(j) $R = 20\%, C_1 - N_1$ (k) $R = 33\%, C_1 - N_1$ (l) $R = 50\%, C_1 - N_1$

Figure 8: For each experimental trial the inliers consist of all 64 images of some individual in the test set, while the outliers are randomly chosen images from the remaining 18 individuals of the test set. The notation C_0 means that the data are centered (C_0 for non-centered), while N_1 means that they are normalized to unit ℓ_2-norm (N_0 indicates no such normalization takes place). Average ROC curves and average areas over the curves are reported for different percentages R of outliers.

matrix $\tilde{\boldsymbol{\mathcal{X}}}$ onto its first $D = 50$ principal components. This choice is justified by noting that, since the inliers and outliers are each at most 64, the data matrix is at most of rank 128. The choice $d = 50$ avoids situations where the entire data matrix is of low-rank to begin with, or cases where the outliers

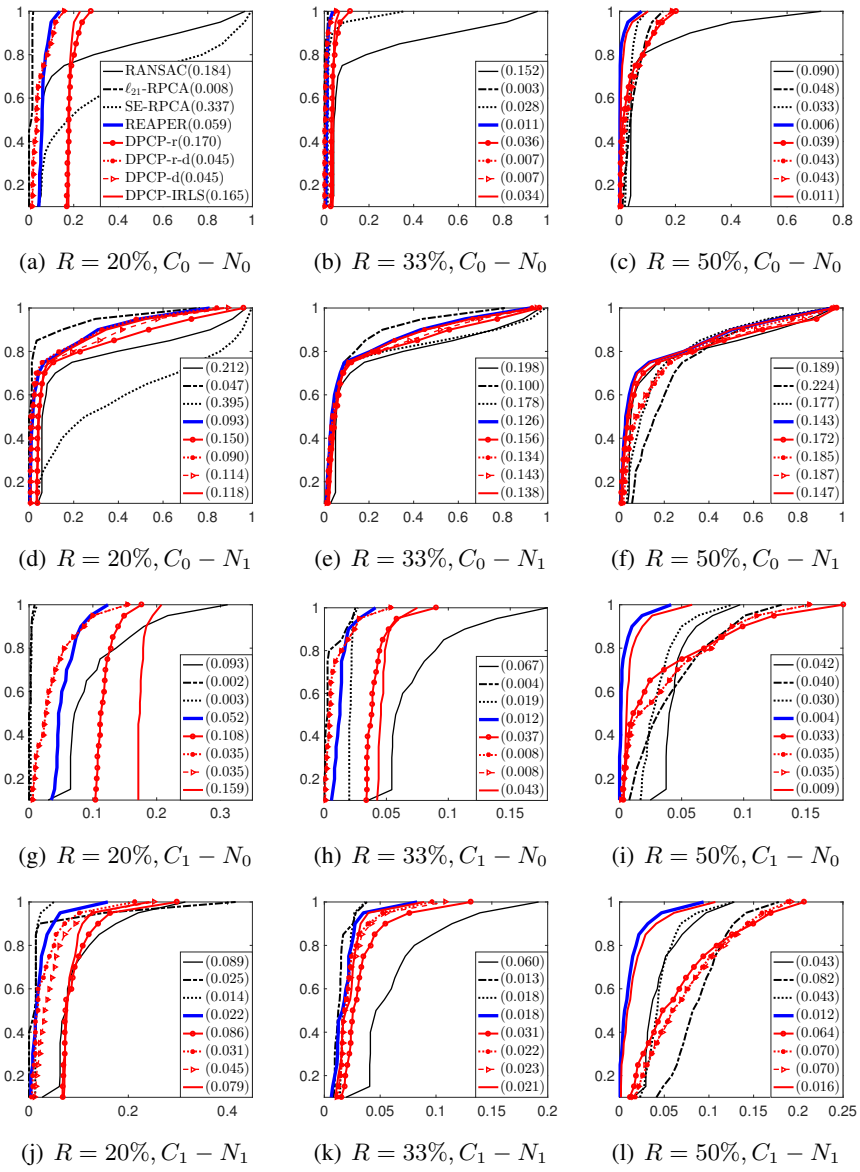

(a) $R = 20\%, C_0 - N_0$ (b) $R = 33\%, C_0 - N_0$ (c) $R = 50\%, C_0 - N_0$

(d) $R = 20\%, C_0 - N_1$ (e) $R = 33\%, C_0 - N_1$ (f) $R = 50\%, C_0 - N_1$

(g) $R = 20\%, C_1 - N_0$ (h) $R = 33\%, C_1 - N_0$ (i) $R = 50\%, C_1 - N_0$

(j) $R = 20\%, C_1 - N_1$ (k) $R = 33\%, C_1 - N_1$ (l) $R = 50\%, C_1 - N_1$

Figure 9: For each experimental trial the inliers consist of all 64 images of some individual in the test set, while the outliers are randomly chosen images from the second half of the images in each category in Caltech101. The notation C_0 means that the data are centered (C_0 for non-centered), while N_1 means that they are normalized to unit ℓ_2-norm (N_0 indicates no such normalization takes place). Average ROC curves and average areas over the curves are reported for different percentages R of outliers.

themselves span a low-dimensional subspace; e.g., this would be true if we were working with the original dimensionality of 2016. These instances would be particularly unfavorable for methods such as SE-RPCA and ℓ_{21}-RPCA. On the other hand, methods such as REAPER, DPCP-IRLS,

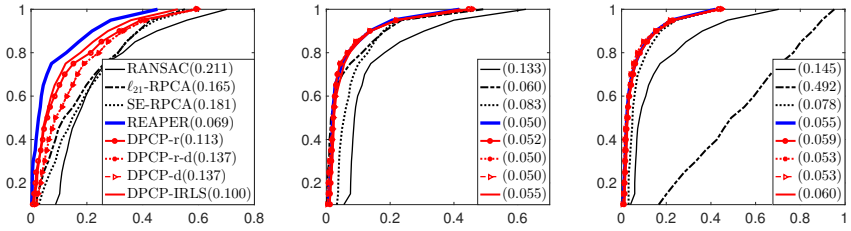

(a) $D = 15$ (b) $D = 50$ (c) $D = 150$

Figure 10: ROC curves for three different projection dimensions, when there are 33% face outliers; data are centered but not normalized ($C_1 - N_0$).

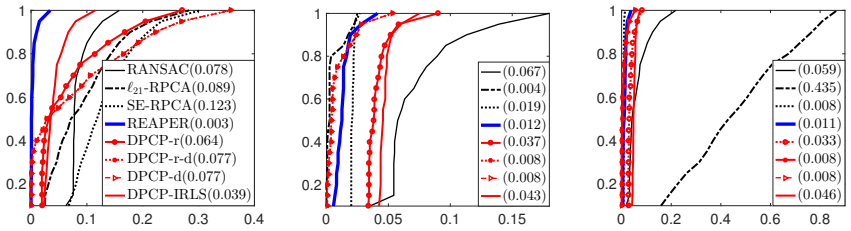

(a) $D = 15$ (b) $D = 50$ (c) $D = 150$

Figure 11: ROC curves for three different projection dimensions, when there are 33% outliers from Caltech101; data are centered but not normalized ($C_1 - N_0$).

DPCP-d, DPCP-r-d and DPCP-r work with the orthogonal complement of the subspace, and so the lower the codimension the more efficient these methods are. We will shortly see how the methods behave for varying projection dimensions.

Another pre-processing step is that of centering the data, i.e., forcing the entire dataset $\tilde{\boldsymbol{\mathcal{X}}}$ to have zero mean; we will be writing C_0 to denote that no centering takes place and C_1 otherwise. Note here that we do not consider centering the inliers separately, as was done in (Lerman et al., 2015); this is unrealistic, since it requires knowledge of the ground truth, i.e., which image is an inlier and which is an outlier. Finally, one may normalize the columns of $\tilde{\boldsymbol{\mathcal{X}}}$ to have unit norm or not. We will denote these two possibilities as N_1 and N_0 respectively.

Various possibilities for the parameters of all algorithms were considered by experimenting with the training set, and the ones that minimize the average area under the corresponding ROC curves were chosen, for the case of 33% outliers, for 50 independent experimental instances (which individual plays the role of the inlier subspace is a random event). The results for the two different choices of outliers and all four pre-processing $C_0 - N_0, C_0 - N_1, C_1 - N_0$ and $C_1 - N_1$, over 50 independent trials on the test set, are reported in Figs. 8 and 9.

Our first observation is on the average all methods perform about the same, with REAPER being the best method and RANSAC the worse. Evidently, normalizing the data without centering them, leads to uniform performance degradation for all methods, for both outlier scenarios. On the other hand, all methods seem to be robust to the remaining three combinations of centering and normal-

ization, with perhaps $C_1 - N_0$ being the best for this experiment. A second observation is that the ROC curves are better for all methods, when the outliers come from Caltech101. This is indeed expected, since, in that case, not only the inliers and outliers live in different datasets, but their content is on the average very different. On the other hand, when the outliers are face images themselves, it is intuitively expected that the inlier/outlier separation problem becomes harder, simply because the outliers are of similar content with the inliers.

Notice also the interesting phenomenon of all methods behaving worse when the outliers are minimal. For example, when $R = 20\%$, the area over the curves for all methods in Fig. 9(a) is bigger than when $R = 33\%$ (Fig. 9(b)). In fact, REAPER, RANSAC and DPCP-IRLS are becoming better as the number of outliers increases from 20% to 50% (Figs. 9(a)-9(c)). This phenomenon is partially explained by our theory: separating inliers from outliers is easier when the outliers are uniformly distributed in the ambient space, and this latter condition is more easily achieved when the outliers are large in number.

Finally, figures 10 and 11 show how the methods behave if we vary the projection dimension to $D = 15$ or $D = 150$, without adjusting any parameters. Evidently, REAPER is once again the most robust method, while ℓ_{21}-RPCA is the least robust. Interestingly, when going from $D = 50$ to $D = 150$ for the case of face outliers, only SE-RPCA shows a slight improvement; the rest of the methods become slightly worse.

8. Conclusions

We presented and studied a solution to the problem of robust principal component analysis in the presence of outliers, called *Dual Principal Component Pursuit (DPCP)*. The heart of the proposed method consisted of a non-convex ℓ_1 optimization problem on the sphere, for which a solution strategy based on a recursion of linear programs was analyzed. Rigorous mathematical analysis revealed that DPCP is a natural method for detecting outliers, particularly when both the number of outliers and the subspace dimension are large. In fact, experiments on synthetic data showed that DPCP was the only method that could handle 70% outliers inside a 30-dimensional ambient space, irrespectively of the subspace dimension. Moreover, experiments with real data showed that DPCP and related variants are competitive with state-of-the-art robust PCA methods. Future research will be concerned with extending the theory and algorithms of DPCP to multiple subspaces as well as investigating big-data applications.

Acknowledgement

This work was supported by grant NSF 1447822. The first author is thankful to Prof. Daniel P. Robinson of the Applied Mathematics and Statistics department of the Johns Hopkins University for many comments that helped improve this manuscript, as well to Prof. Glyn Harman for pointing out the proof of Lemma 7.

Appendix A. Results on Problems (12) and (13) following (Späth and Watson, 1987)

In this Section we state three results that are important for our mathematical analysis, already known in (Späth and Watson, 1987). For the sake of clarity and convenience, we have also taken the liberty

of writing complete proofs of the statements, as not all of them can be found in (Späth and Watson, 1987).

Lemma 14 *Any global solution $\boldsymbol{b}^*$ to $\min_{\boldsymbol{b}^\top \boldsymbol{b}=1} \left\|\boldsymbol{\mathcal{X}}^\top \boldsymbol{b}\right\|_1$, must be orthogonal to $(D-1)$ linearly independent points of $\boldsymbol{\mathcal{X}}$.*

Proof Suppose that $\boldsymbol{b}^*$ is orthogonal to elements $\boldsymbol{\xi}_1, \ldots, \boldsymbol{\xi}_K \subset \boldsymbol{\mathcal{X}}$, whose span is of dimension less than $D-1$. Then there exists a unit norm vector $\boldsymbol{\zeta} \in \mathbb{S}^{D-1}$ that is orthogonal to all $\boldsymbol{\xi}_1, \ldots, \boldsymbol{\xi}_K, \boldsymbol{b}^*$. Moreover, we can choose $\boldsymbol{\zeta}$ such that

$$\sum_{j:\, \boldsymbol{b}^* \not\perp \boldsymbol{x}_j} \operatorname{Sign}(\boldsymbol{x}_j^\top \boldsymbol{b}^*) \boldsymbol{\zeta}^\top \boldsymbol{x}_j \leq 0. \tag{147}$$

Furthermore, we can choose a sufficiently small $\varepsilon > 0$, such that

$$\operatorname{Sign}(\boldsymbol{x}_j^\top \boldsymbol{b}^* + \varepsilon \boldsymbol{x}_j^\top \boldsymbol{\zeta}) = \operatorname{Sign}(\boldsymbol{x}_j^\top \boldsymbol{b}^*), \;\; \forall j \in [N]. \tag{148}$$

Consequently, we can write

$$\left|\boldsymbol{x}_j^\top (\boldsymbol{b}^* + \varepsilon \boldsymbol{\zeta})\right| = \left|\boldsymbol{x}_j^\top \boldsymbol{b}^*\right| + \varepsilon \operatorname{Sign}(\boldsymbol{x}_j^\top \boldsymbol{b}^*) \boldsymbol{x}_j^\top \boldsymbol{\zeta}, \tag{149}$$

and so

$$\left\|\boldsymbol{\mathcal{X}}^\top (\boldsymbol{b}^* + \varepsilon \boldsymbol{\zeta})\right\|_1 = \left\|\boldsymbol{\mathcal{X}}^\top \boldsymbol{b}^*\right\|_1 + \varepsilon \sum_{j:\, \boldsymbol{b}^* \not\perp \boldsymbol{x}_j} \operatorname{Sign}(\boldsymbol{x}_j^\top \boldsymbol{b}^*) \boldsymbol{\zeta}^\top \boldsymbol{x}_j \leq \left\|\boldsymbol{\mathcal{X}}^\top \boldsymbol{b}^*\right\|_1. \tag{150}$$

However,

$$\|\boldsymbol{b}^* + \varepsilon \boldsymbol{\zeta}\|_2 = \sqrt{1 + \varepsilon^2} > 0, \tag{151}$$

and normalizing $\boldsymbol{b}^* + \varepsilon \boldsymbol{\zeta}$ to have unit ℓ_2 norm, we get a contradiction on $\boldsymbol{b}^*$ being a global solution. ■

Lemma 15 *Problem $\min_{\boldsymbol{b}^\top \hat{\boldsymbol{n}}_k=1} \left\|\boldsymbol{\mathcal{X}}^\top \boldsymbol{b}\right\|_1$ admits a computable solution $\boldsymbol{n}_{k+1}$ that is orthogonal to $(D-1)$ linearly independent points of $\boldsymbol{\mathcal{X}}$.*

Proof Let $\boldsymbol{n}_{k+1}$ be a solution to $\min_{\boldsymbol{b}^\top \hat{\boldsymbol{n}}_k=1} \left\|\boldsymbol{\mathcal{X}}^\top \boldsymbol{b}\right\|_1$ that is orthogonal to less than $D-1$ linearly independent points of $\boldsymbol{\mathcal{X}}$. Then we can find a unit norm vector $\boldsymbol{\zeta}$ that is orthogonal to the same points of $\boldsymbol{\mathcal{X}}$ that $\boldsymbol{n}_{k+1}$ is orthogonal to, and moreover $\boldsymbol{\zeta} \perp \boldsymbol{n}_{k+1}$. In addition, we can find a sufficiently small $\varepsilon > 0$ such that

$$\left\|\boldsymbol{\mathcal{X}}^\top (\boldsymbol{n}_{k+1} + \varepsilon \boldsymbol{\zeta})\right\|_1 = \left\|\boldsymbol{\mathcal{X}}^\top \boldsymbol{n}_{k+1}\right\|_1 + \varepsilon \sum_{j:\, \boldsymbol{n}_{k+1} \not\perp \boldsymbol{x}_j} \operatorname{Sign}(\boldsymbol{x}_j^\top \boldsymbol{n}_{k+1}) \boldsymbol{\zeta}^\top \boldsymbol{x}_j, \tag{152}$$

where

$$\sum_{j:\, \boldsymbol{n}_{k+1} \not\perp \boldsymbol{x}_j} \operatorname{Sign}(\boldsymbol{x}_j^\top \boldsymbol{n}_{k+1}) \boldsymbol{\zeta}^\top \boldsymbol{x}_j \leq 0. \tag{153}$$

Since $\boldsymbol{n}_{k+1}$ is optimal, it must be the case that

$$\sum_{j:\, \boldsymbol{n}_{k+1} \not\perp \boldsymbol{x}_j} \operatorname{Sign}(\boldsymbol{x}_j^\top \boldsymbol{n}_{k+1}) \boldsymbol{\zeta}^\top \boldsymbol{x}_j = 0, \tag{154}$$

and so

$$\left\| \boldsymbol{\mathcal{X}}^\top (\boldsymbol{n}_{k+1} + \varepsilon \boldsymbol{\zeta}) \right\|_1 = \left\| \boldsymbol{\mathcal{X}}^\top \boldsymbol{n}_{k+1} \right\|_1 . \tag{155}$$

By (155) we see that as we vary ε the objective remains unchanged. Notice also that varying ε preserves all zero entries appearing in the vector $\boldsymbol{\mathcal{X}}^\top \boldsymbol{n}_{k+1}$. Furthermore, because of (154), it is always possible to either decrease or increase ε until an additional zero is achieved, i.e., until $\boldsymbol{n}_{k+1} + \varepsilon \boldsymbol{\zeta}$ becomes orthogonal to a point of $\boldsymbol{\mathcal{X}}$ that $\boldsymbol{n}_{k+1}$ is not orthogonal to. Then we can replace $\boldsymbol{n}_{k+1}$ with $\boldsymbol{n}_{k+1} + \varepsilon \boldsymbol{\zeta}$ and repeat the process, until we get some $\boldsymbol{n}_{k+1}$ that is orthogonal to $D-1$ linearly independent points of $\boldsymbol{\mathcal{X}}$. ■

Lemma 16 *Suppose that for each problem* $\min_{\boldsymbol{b}^\top \hat{\boldsymbol{n}}_k = 1} \left\| \boldsymbol{\mathcal{X}}^\top \boldsymbol{b} \right\|_1$*, a solution* $\boldsymbol{n}_{k+1}$ *is chosen such that* $\boldsymbol{n}_{k+1}$ *is orthogonal to* $D-1$ *linearly independent points of* $\boldsymbol{\mathcal{X}}$*, in accordance with Proposition 15. Then the sequence* $\{\boldsymbol{n}_k\}$ *converges to a critical point of problem* $\min_{\boldsymbol{b}^\top \boldsymbol{b} = 1} \left\| \boldsymbol{\mathcal{X}}^\top \boldsymbol{b} \right\|_1$ *in a finite number of steps.*

Proof If $\boldsymbol{n}_{k+1} = \hat{\boldsymbol{n}}_k$, then inspection of the first order optimality conditions of the two problems, reveals that $\hat{\boldsymbol{n}}_k$ is a critical point of $\min_{\boldsymbol{b}^\top \boldsymbol{b} = 1} \left\| \boldsymbol{\mathcal{X}}^\top \boldsymbol{b} \right\|_1$. If $\boldsymbol{n}_{k+1} \neq \hat{\boldsymbol{n}}_k$, then $\|\boldsymbol{n}_{k+1}\|_2 > 1$, and so $\left\| \boldsymbol{\mathcal{X}}^\top \hat{\boldsymbol{n}}_{k+1} \right\|_1 < \left\| \boldsymbol{\mathcal{X}}^\top \hat{\boldsymbol{n}}_k \right\|_1$. As a consequence, if $\boldsymbol{n}_{k+1} \neq \hat{\boldsymbol{n}}_k$, then $\hat{\boldsymbol{n}}_k$ can not arise as a solution for some $k' > k$. Now, because of Proposition 15, for each k, there is a finite number of candidate directions $\boldsymbol{n}_{k+1}$. These last two observations imply that the sequence $\{\boldsymbol{n}_k\}$ must converge in a finite number of steps to a critical point of $\min_{\boldsymbol{b}^\top \boldsymbol{b} = 1} \left\| \boldsymbol{\mathcal{X}}^\top \boldsymbol{b} \right\|_1$. ■

References

L. Balzano, R. Nowak, and B. Recht. Online identification and tracking of subspaces from highly incomplete information. In *Communication, Control, and Computing (Allerton), 2010 48th Annual Allerton Conference on*, pages 704–711. IEEE, 2010.

R. Basri and D. W. Jacobs. Lambertian reflectance and linear subspaces. *IEEE transactions on pattern analysis and machine intelligence*, 25(2):218–233, 2003.

S. Boyd, N. Parikh, E. Chu, B. Peleato, and J. Eckstein. Distributed optimization and statistical learning via the alternating direction method of multipliers. *Foundations and Trends in Machine Learning*, 3(1):1–122, 2010.

J. S. Brauchart and P. J. Grabner. Distributing many points on spheres: minimal energy and designs. *Journal of Complexity*, 31(3):293–326, 2015.

J.P. Brooks, J.H. Dulá, and E.L. Boone. A pure l1-norm principal component analysis. *Computational statistics & data analysis*, 61:83–98, 2013.

E. Candès and M. Wakin. An introduction to compressive sampling. *IEEE Signal Processing Magazine*, 25(2):21–30, 2008.

E. Candès, M. Wakin, and S. Boyd. Enhancing sparsity by reweighted ℓ_1 minimization. *Journal of Fourier Analysis and Applications*, 14(5):877–905, 2008.

E. Candès, X. Li, Y. Ma, and J. Wright. Robust principal component analysis? *Journal of the ACM*, 58(3), 2011.

R. Chartrand and W. Yin. Iteratively reweighted algorithms for compressive sensing. In *2008 IEEE International Conference on Acoustics, Speech and Signal Processing*, pages 3869–3872. IEEE, 2008.

I. Daubechies, R. DeVore, M. Fornasier, and C. S. Güntürk. Iteratively reweighted least squares minimization for sparse recovery. *Communications on Pure and Applied Mathematics*, 63(1): 1–38, 2010.

C. Ding, D. Zhou, X. He, and H. Zha. R_1-pca: rotational invariant l_1-norm principal component analysis for robust subspace factorization. In *Proceedings of the 23rd international conference on Machine learning*, pages 281–288. ACM, 2006.

L. Elden. Solving quadratically constrained least squares problems using a differential-geometric approach. *BIT Numerical Mathematics*, 42(2):323–335, 2002.

E. Elhamifar and R. Vidal. Robust classification using structured sparse representation. In *IEEE Conference on Computer Vision and Pattern Recognition*, 2011.

E. Elhamifar and R. Vidal. Sparse subspace clustering: Algorithm, theory, and applications. *IEEE Transactions on Pattern Analysis and Machine Intelligence*, 35(11):2765–2781, 2013.

L. Fei-Fei, R. Fergus, and P. Perona. Learning generative visual models from few training examples: An incremental bayesian approach tested on 101 object categories. *Comput. Vis. Image Underst.*, 106(1):59–70, April 2007. ISSN 1077-3142. doi: 10.1016/j.cviu.2005.09.012. URL `http://dx.doi.org/10.1016/j.cviu.2005.09.012`.

J. Feng, H. Xu, and S. Yan. Online robust pca via stochastic optimization. In *Advances in Neural Information Processing Systems*, pages 404–412, 2013.

M. A. Fischler and R. C. Bolles. RANSAC random sample consensus: A paradigm for model fitting with applications to image analysis and automated cartography. *Communications of the ACM*, 26: 381–395, 1981.

W. Gander. Least squares with a quadratic constraint. *Numerische Mathematik*, 36(3):291–307, 1980.

A.S. Georghiades, P.N. Belhumeur, and D.J. Kriegman. From few to many: Illumination cone models for face recognition under variable lighting and pose. *IEEE Trans. Pattern Anal. Mach. Intelligence*, 23(6):643–660, 2001.

G. H. Golub and U. Von Matt. Quadratically constrained least squares and quadratic problems. *Numerische Mathematik*, 59(1):561–580, 1991.

P. J. Grabner and R.F. Tichy. Spherical designs, discrepancy and numerical integration. *Math. Comp.*, 60(201):327–336, 1993. ISSN 0025-5718. doi: 10.2307/2153170. URL http://dx.doi.org/10.2307/2153170.

P. J. Grabner, B. Klinger, and R.F. Tichy. Discrepancies of point sequences on the sphere and numerical integration. *Mathematical Research*, 101:95–112, 1997.

Inc. Gurobi Optimization. Gurobi optimizer reference manual, 2015. URL http://www.gurobi.com.

G. Harman. Variations on the koksma-hlawka inequality. *Uniform Distribution Theory*, 5(1):65–78, 2010.

E. Hlawka. Discrepancy and riemann integration. *Studies in Pure Mathematics*, pages 121–129, 1971.

H. Hotelling. Analysis of a complex of statistical variables into principal components. *Journal of Educational Psychology*, 24:417–441, 1933.

P. Huber. *Robust Statistics*. John Wiley & Sons, New York, 1981.

I. Jolliffe. *Principal Component Analysis*. Springer-Verlag, 2nd edition, 2002.

W. Ku, R. H. Storer, and C. Georgakis. Disturbance detection and isolation by dynamic principal component analysis. *Chemometrics and Intelligent Laboratory Systems*, 30:179–196, 1995.

L. Kuipers and H. Niederreiter. Uniform distribution of sequences. *Courier Corporation*, 2012.

G. Lerman and T. Zhang. ℓ_p-recovery of the most significant subspace among multiple subspaces with outliers. *Constructive Approximation*, 40(3):329–385, 2014.

G. Lerman, M. B. McCoy, J. A. Tropp, and T. Zhang. Robust computation of linear models by convex relaxation. *Foundations of Computational Mathematics*, 15(2):363–410, 2015.

G. Liu, Z. Lin, and Y. Yu. Robust subspace segmentation by low-rank representation. In *International Conference on Machine Learning*, pages 663–670, 2010.

S. Loyd, M. Mohseni, and P. Rebentrost. Quantum principal component analysis. *Nature Physics*, (10):631–633, 2014.

B. C. Moore. Principal component analysis in linear systems: Controllability, observability, and model reduction. *IEEE Transactions on Automatic Control*, 26(1):17–32, 1981.

S. Nam, M.E. Davies, M. Elad, and R. Gribonval. The cosparse analysis model and algorithms. *Applied and Computational Harmonic Analysis*, 34(1):30–56, 2013.

K. Pearson. On lines and planes of closest fit to systems of points in space. *The London, Edinburgh and Dublin Philosphical Magazine and Journal of Science*, 2:559–572, 1901.

A. Price, N. Patterson, R. M. Plenge, M. E. Weinblatt, N. A. Shadick, and D. Reich. Principal components analysis corrects for stratification in genome-wide association studies. *Nature Genetics*, (38):904–909, 2006.

Q. Qu, J. Sun, and J. Wright. Finding a sparse vector in a subspace: Linear sparsity using alternating directions. In *Advances in Neural Information Processing Systems*, pages 3401–3409, 2014.

M. Soltanolkotabi and E. J. Candès. A geometric analysis of subspace clustering with outliers. *Annals of Statistics*, 40(4):2195–2238, 2012.

H. Späth and G.A. Watson. On orthogonal linear ℓ_1 approximation. *Numerische Mathematik*, 51 (5):531–543, 1987.

D.A. Spielman, H. Wang, and J. Wright. Exact recovery of sparsely-used dictionaries. In *Proceedings of the 23d international joint conference on Artificial Intelligence*, pages 3087–3090. AAAI Press, 2013.

J. Sun, Q. Qu, and J. Wright. Complete dictionary recovery over the sphere ii: Recovery by riemannian trust-region method. *arXiv preprint arXiv:1511.04777*, 2015a.

J. Sun, Q. Qu, and J. Wright. Complete dictionary recovery over the sphere i: Overview and the geometric picture. *arXiv preprint arXiv:1511.03607*, 2015b.

J. Sun, Q. Qu, and J. Wright. Complete dictionary recovery using nonconvex optimization. In *Proceedings of the 32nd International Conference on Machine Learning (ICML-15)*, pages 2351–2360, 2015c.

J. Sun, Q. Qu, and J. Wright. Complete dictionary recovery over the sphere. In *Sampling Theory and Applications (SampTA), 2015 International Conference on*, pages 407–410. IEEE, 2015d.

M. C. Tsakiris and R. Vidal. Dual principal component pursuit. In *ICCV Workshop on Robust Subspace Learning and Computer Vision*, pages 10–18, 2015.

R. Vidal. Subspace clustering. *IEEE Signal Processing Magazine*, 28(3):52–68, March 2011.

S. Vyas and L. Kumaranayake. Constructing socio-economic status indices: how to use principal components analysis. *Health Policy and Planning*, 21:459–468, 2006.

H. Xu, C. Caramanis, and S. Sanghavi. Robust pca via outlier pursuit. In *Advances in Neural Information Processing Systems*, pages 2496–2504, 2010.